SHAPE AND STABILITY OF TWO-DIMENSIONAL UNIFORM VORTICITY REGIONS

Thesis by
James Russell Kamm

In Partial Fulfillment of the Requirements
for the Degree of
Doctor of Philosophy

California Institute of Technology
Pasadena, California
1987

Submitted 28 April 1987

Acknowledgements

I would like to thank Professor Philip G. Saffman for his knowedgeable guidance of my investigations. His mathematical and physical understanding yielded critical insights into the most difficult aspects of this work; his enthusiasm often provided crucial motivation. I gratefully acknowledge the outstanding facilities he put at my disposal and am thankful for the opportunity to have worked with him and learned from him.

I wish to express my appreciation for each of the following grants, which helped support my graduate studies:

1. National Science Foundation Graduate Fellowship under grants # SPI-81-66306, # SPE-82-64146, and # SPE-83-50009;
2. Caltech Graduate Research Assistantships and Teaching Assistantship, funded by NASA Lewis Research Center Grant # NAG 3-179, ONR Contracts # N00014-79-C-0412 and # N00014-85-K-0205, and DOE Contract # DE-AA03-76SF00767; and
3. Deutscher Akademischer Austauschdienst Jahresstipendium # 315-402-093-6, undertaken at the Max-Planck-Institut für Strömungsforschung in Göttingen, Federal Republic of Germany.

The computations for my investigations were carried out primarily on the Caltech Applied Mathematics DEC VAX 11/750. Additional computations were performed on the following computers:

1. National Magnetic Fusion Energy Computer Center Cray X/MP and Cray 2, and
2. Gesellschaft für wissenschaftliche Datenverarbeitung m.b.H. Göttingen DEC VAX 11/750, DEC VAX 11/780, and Sperry UNIVAC 1180.

Penultimately, I want to thank fellow student/good friend/erstwhile trickster Tim "X" Colvin for making the time at Caltech truly enjoyable.

Finally, my studies would have been neither undertaken nor completed without the tremendous support, encouragement, and understanding of my parents. Their contributions exceeded any that could rationally have been expected of them. This is a small gift to them for their great gifts to me.

Abstract

The steady shapes, linear stability, and energetics of regions of uniform, constant vorticity in an incompressible, inviscid fluid are investigated. The method of Schwarz functions as introduced by Meiron, Saffman & Schatzman [1984] is used in the mathematical formulation of these problems.

Numerical and analytical analyses are provided for several configurations. For the single vortex in strained and rotating flow fields, we find new solutions that bifurcate from the branch of steady elliptical solutions. These nonelliptical steady states are determined to be linearly unstable. We examine the corotating vortex pair and numerically confirm the theoretical results of Saffman & Szeto [1980], relating linear stability characteristics to energetics. The stability properties of the infinite single array of vortices are quantified. The pairing instability is found to be the most unstable subharmonic disturbance, and the existence of an area-dependent superharmonic instability (Saffman & Szeto [1981]) is numerically confirmed. These results are exhibited qualitatively by an elliptical vortex model. Lastly, we study the effects of unequal area on the stability of the the infinite staggered double array of vortices. We numerically verify the results of the perturbation analysis of Jiménez [1986b] by showing that the characteristic subharmonic stability "cross" persists for vortex streets of finite but unequal areas.

Table of Contents

Acknowledgements ii

Abstract iv

Table of Contents v

List of Figures vii

List of Tables viii

Chapter 1 Theory and Numerical Methods 1

Section 1.1 Introduction 1

Section 1.2 Shape Calculations 3

Section 1.3 Stability Calculations 10

Section 1.4 Energy Calculations 16

Chapter 2 The Single Vortex 23

Section 2.1 Introduction 23

Section 2.2 Formulation 24

Section 2.3 The Single Vortex in Unstrained Fluid 32

Section 2.4 The Single Vortex in Strained Fluid 40

Chapter 3 The Vortex Pair 45

Section 3.1 Introduction 45

Section 3.2 Formulation 46

Section 3.3 The Corotating Vortex Pair 58

Chapter 4 The Single Infinite Row 67

Section 4.1 Introduction 67

Section 4.2 Formulation 68

Section 4.3 Elliptically Desingularized Model 75

Section 4.4 Results 81

Chapter 5 The Double Infinite Row 86

Section 5.1 Introduction 86

Section 5.2 Formulation 87

Section 5.3 Results 93

Appendix A Kinematic Constraints for Vortices 98

Appendix B An Energy Integral for Vortices 104

Appendix C Analytic Formulae for Vortex Configurations 105

Appendix D Stream Function Formulation for Corotating Vortices 111

Appendix E Sum Formulae for Infinite Vortex Arrays 118

Appendix F Elliptically Desingularized Double Infinite Array 121

References 130

List of Figures

Figure 1.1 General Vortex Configuration 6

Figure 2.1 Single Rotating Vortex 32

Figure 2.2 Single Rotating Vortex Solution Path 34

Figure 2.3 Single Rotating Bifurcated Vortices 36

Figure 2.4 Single Vortex Energy vs. Angular Momentum 39

Figure 2.5 Single Strained Vortex 40

Figure 2.6 Single Strained Vortex Solution Path 42

Figure 2.7 Single Strained Bifurcated Vortices 43

Figure 3.1 Corotating Vortex Pair 47

Figure 3.2 Counterrotating Vortex Pair 48

Figure 3.3 Corotating Vortex Pair Solution Shapes 59

Figure 3.4 Corotating Vortex Pair Rotation Rate versus Area 60

Figure 3.5 Corotating Vortex Pair Area versus Angular Momentum 61

Figure 3.6 Corotating Vortex Pair Energy versus Angular Momentum 63

Figure 3.7 Corotating Vortex Pair Eigenvalues versus Angular Momentum ... 64

Figure 4.1 Single Vortex Array 69

Figure 4.2 Single Vortex Array Solution Path 82

Figure 4.3 Single Vortex Array Superharmonic Eigenvalues versus Area 83

Figure 4.4 Single Vortex Array Subharmonic Eigenvalues versus Wavenumber 84

Figure 5.1 Double Vortex Array 88

Figure 5.2 Double Vortex Array Stability Boundary 93

Figure 5.3 Double Vortex Array Stability Boundary versus Area Difference ... 96

List of Tables

Table 2.1 Single Rotating Elliptical Vortex Bifurcation Points 35

Table 2.2 Single Rotating Bifurcated Vortices Energy Data 38

Table 2.3 Single Strained Elliptical Vortex Bifurcation Points 42

Table 3.1 Corotating Vortex Pair Solution Data 65

Table 5.1 Double Vortex Array Neutral Stability Points 95

Chapter 1

Theory and Numerical Methods for Calculation of Constant Vorticity Regions

1.1 Introduction

We consider the problem of describing the form and linear stability characteristics of steady states of an unbounded two-dimensional, inviscid, incompressible fluid that contains distinct, simply connected regions of uniform, constant vorticity. This situation arises in the modeling of fluid systems in which relatively isolated regions of vorticity are present, e.g., (1) the aerodynamic trailing-vortex problem (Spreiter & Sacks [1951], Moore & Saffman [1971], Pierrehumbert [1980]), (2) the two-dimensional shear layer (Pierrehumbert & Widnall [1981], Saffman & Szeto [1981]), and (3) the Kármán vortex street (Saffman & Schatzman [1981], [1982], Kida [1982], Meiron, Saffman & Schatzman [1984], Jiménez [1986a,b], MacKay [1986]). Furthermore, knowledge of the interaction of vortex regions is of general fluid mechanical interest.

The analysis of regions of uniform vorticity embedded in an otherwise irrotational fluid has been undertaken using many methods, the most notable of which are the point vortex method and the method of contour dynamics. The simplest application of the point vortex method models vortex regions as single point vortices, the dynamics of which is easily and elegantly formulated (Kirchhoff [1877]). Many results of this basic analysis are covered by Lamb [1945]. In more complicated applications, vortex regions are modeled as large collections of either point vortices or vortex blobs. Many researchers have used these methods to study isolated regions of vorticity, as well as models of developed shear layers

and wake flows. These efforts are reviewed by Saffman & Baker [1979], Leonard [1980] and Aref [1983]. The stability analysis of large collections of point vortices is based upon solutions of the time-dependent evolution equations of the problem. The contour dynamics or boundary-integral method consists of using the Green's function solution of the two-dimensional Laplace equation to obtain an integral relation that determines the shapes of the constant vorticity regions. This was formulated for time-dependent flows by Zabusky *et al.* [1979], and applied in various forms by several authors, as reviewed by Leonard [1980]. This approach is easily formulated, but suffers from the fact that solutions do not readily admit spectral stability analysis.

Recently, Meiron, Saffman & Schatzman [1984] (hereinafter referred to as MSS) employed the method of Schwarz functions to analyze a constant vortex region model of the Kármán vortex street. We extend this technique, which is based upon a complex variable representation similar to that used by Landau [1981] and Burbea [1982], to consider a variety of vortex configurations. This method offers an analytically appealing approach to analyzing general two-dimensional flows in unbounded domains and provides a basis for direct linear stability and energy analyses. In the sections of this chapter we provide an overview of the formulation of the problems to be considered. A single vortex region is analyzed in Chapter 2, and the vortex pair is examined in Chapter 3. The final two chapters contain analyses of configurations with infinitely many vortices: the single infinite array in Chapter 4, and the staggered double array in Chapter 5. We are able to confirm previous solutions, obtain new results for these vortex geometries, and verify a relationship relating energetics and stability in certain cases.

1.2 Shape Calculations

We take the two-dimensional (x, y) plane as the physical plane of the inviscid, incompressible flows considered. In all calculations, we normalize the constant density to one. We describe the boundary and exterior of a simply connected region of constant vorticity in the physical $z = x + iy$ plane as the exterior conformal mapping of the boundary and exterior of the unit circle in the $\zeta = \xi + i\eta$ plane given by

$$z = a_0\zeta\,(1 + a_1/\zeta + \cdots + a_n/\zeta^n + \cdots)\,. \tag{1.2.1}$$

We seek to describe the velocity field induced by the region of constant vorticity ω_1 and area A_1 in terms of the coefficients of this expansion. To do so, we follow the development of MSS, who used the method of Schwarz functions. A Schwarz function is defined as an analytic function of z that assumes the value z^* on a given contour; in the cases we consider, this contour is the vortex boundary. The conjugate of z is expanded as

$$z^* = (a_0^*/\zeta)(1 + a_1^*\zeta + \cdots + a_n^*\zeta^n + \cdots)\,, \tag{1.2.2}$$

where $|\zeta| = 1$ corresponds to the vortex boundary. We assume that the starred coefficients a_n^* are independent of the actual corresponding complex conjugates. We expand the Schwarz function as a Taylor-Laurent series in z on this contour:

$$z^* = g_0/z + g_1/z^2 + \cdots + f_0 + f_1 z + f_2 z^2 + \cdots\,, \tag{1.2.3}$$

where g_n and f_n are currently undetermined. The equation for the stream function in the neighborhood of this vortex is

$$\frac{\partial^2\psi}{\partial x^2} + \frac{\partial^2\psi}{\partial y^2} = \begin{cases} 0 & \text{outside the vortex, and} \\ -\omega_1 & \text{inside the vortex.} \end{cases} \tag{1.2.4}$$

As a consequence of the Cauchy-Riemann equations this implies that

$$\begin{aligned} &u - iv \text{ is analytic outside contour C, and} \\ &u - iv + \frac{i\omega_1}{2}z^* \text{ is analytic inside contour C.} \end{aligned} \tag{1.2.5}$$

The choice

$$u - iv = -\frac{i\omega_1}{2}\left\{\frac{g_0}{z} + \frac{g_1}{z^2} + \cdots\right\} \tag{1.2.6}$$

satisfies these conditions, since this expression is analytic outside the vortex and

$$u - iv + \frac{i\omega_1}{2}z^* = \frac{i\omega_1}{2}\left\{f_0 + f_1 z + f_2 z^2 + \cdots\right\} \tag{1.2.7}$$

is analytic inside the vortex. Similarly, the independent conjugate velocity is obtained as

$$u + iv = \frac{i\omega_1}{2}\left\{\frac{g_0^*}{z^*} + \frac{g_1^*}{z^{*2}} + \cdots\right\}. \tag{1.2.8}$$

To obtain the induced velocity in terms of the mapping coeffients of Equation (1.2.1), we relate the coefficients g_n to the coefficients a_n. From Equation (1.2.3), by Cauchy's integral formula,

$$g_n = \frac{1}{2\pi i}\oint_C z^* z^n \frac{dz}{d\zeta}\, d\zeta\ , \tag{1.2.9}$$

where the contour C is the vortex boundary. Thus, we see that

$$g_n = \text{ the coefficient of } \zeta^{-1} \text{ in } z^* z^n \frac{dz}{d\zeta}. \tag{1.2.10}$$

For the conjugate coefficients we find

$$g_n^* = - \text{ the coefficient of } \zeta^{-1} \text{ in } z\ z^{*n}\frac{dz^*}{d\zeta}; \tag{1.2.11}$$

the minus sign comes from traversing the contour in the opposite direction. As shown by MSS, similar representations can be obtained for the coefficients f_n, f_n^*.

An alternate and useful interpretation of the g_n is as follows: from elementary potential theory the velocity external to the vortex is

$$u - iv = \frac{\omega_1}{2\pi i}\iint_V \frac{dx'\, dy'}{z - z'}. \tag{1.2.12}$$

For $|z'/z| < 1$ we expand the integrand and equate this series with the expression for the velocity (1.2.6) to obtain

$$g_n = \frac{1}{\pi} \iint_V z'^n \, dx' \, dy'; \tag{1.2.13}$$

i.e., g_n is the nth moment about the origin. Specifically, we see that

$$g_0 = A_1/\pi, \qquad \text{and} \tag{1.2.14}$$

$$g_1 = \text{ coordinate of the vortex centroid relative to the origin.} \tag{1.2.15}$$

Expressions such as (1.2.6) for the induced velocity field can be developed for each of the vortices in a given configuration. In a coordinate frame in which the coordinate z is taken with respect to the center of the lth vortex, we write the general induced velocity at a point P external to each vortex for a configuration of N_v vortices as (see Figure 1.1):

$$(u - iv)_{l,\ ind} = \sum_{m=1}^{N_v} \left(\frac{-i\omega_m}{2} \right) \sum_{n=0}^{\infty} \frac{g_n^{(m)}}{(z + z_l - z_m)^{n+1}} \tag{1.2.16}$$

where

$$\begin{aligned} z &= \text{coordinate with respect to the center of the } l\text{th vortex region;} \\ z_m &= \text{coordinate of the center of the } m\text{th vortex region with respect} \\ &\qquad \text{to an absolute origin } O\text{; and} \\ g_n^{(m)} &= n\text{th Schwarz coefficient for the } m\text{th vortex region.} \end{aligned} \tag{1.2.17}$$

Expressions for the lth induced conjugate velocity $(u + iv)_{l,\ ind}$ may be obtained by substituting $-i$ for i, z^* for z, z_m^* for z_m, and $g_n^{*(m)}$ for $g_n^{(m)}$ into (1.2.16). For multiple vortex configurations, the denominator of the infinite sum in the velocity representation is expanded in a series in a length scale of the problem; the details

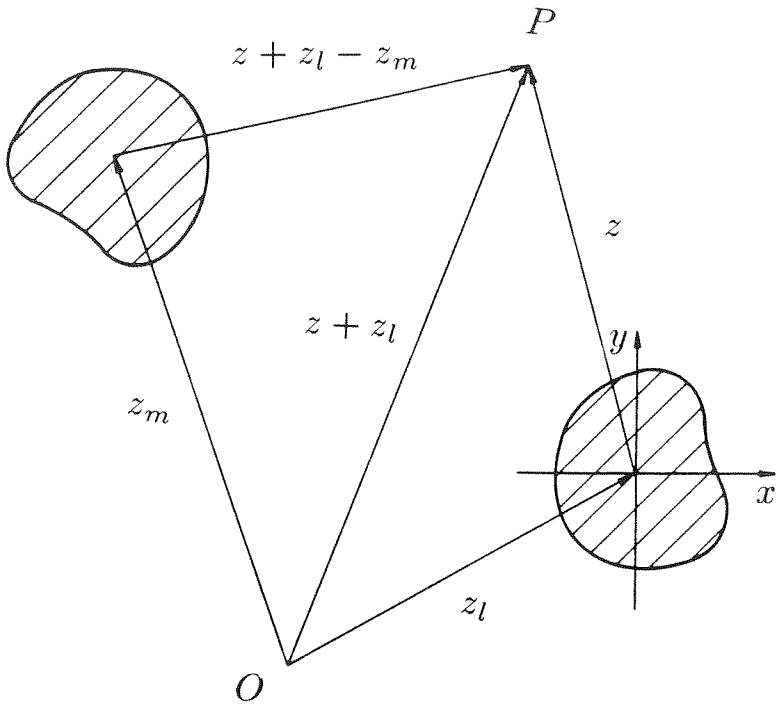

Figure 1.1 General vortex configuration.

of this process, which is equivalent to an expansion in a nondimensionalized area parameter, will be described in later sections.

For the calculation of the steady vortex shapes we prescribe an external velocity that balances any self-induced motion and thereby brings the vortices to rest; this velocity depends upon the geometric configuration of the vortices. This and any other external velocity we denote collectively as $(u - iv)_{l,\ ext}$ with respect to the lth vortex region; $(u + iv)_{l,\ ext}$ denotes the conjugate quantity.

Thus, we have the total velocity field in this coordinate frame as

$$(u - iv)_l = (u - iv)_{l,\ ind} + (u - iv)_{l,\ ext}, \tag{1.2.18}$$

with a similar expression for the conjugate velocity.

To obtain an equation that defines the region to which the vorticity is restricted, we consider the boundary condition at the surface of the vortex. The boundary condition for steady vortices is that the velocity normal to the surface

of each vortex is zero. On the boundary of the vortex, $|dz| = |ds|$, so without loss of generality we parameterize the boundary of the vortex by

$$dz/ds = -e^{i\varphi}, \qquad 0 \le \varphi \le 2\pi. \tag{1.2.19}$$

Here, φ is the clockwise external angle between the counterclockwise tangent and the left-directed horizontal axis. The condition that the normal velocity is zero then becomes

$$u \sin\varphi - v \cos\varphi = 0 \iff (u - iv)\, dz/ds - (u + iv)\, dz^*/ds = 0. \tag{1.2.20}$$

On the vortex boundary, z is the image of $|\zeta| = 1$; choosing the ζ plane parameterization $\zeta = \exp i\theta$ implies $d\zeta/d\theta = i\zeta$, which allows evaluation of the derivatives in (1.2.20) as

$$\frac{dz}{ds} = \frac{dz}{d\zeta}\frac{d\zeta}{d\theta}\frac{d\theta}{ds} = i\zeta\frac{dz}{d\zeta}\frac{d\theta}{ds}\ , \qquad \frac{dz^*}{ds} = \frac{dz^*}{d\zeta}\frac{d\zeta}{d\theta}\frac{d\theta}{ds} = i\zeta\frac{dz^*}{d\zeta}\frac{d\theta}{ds}\ . \tag{1.2.21}$$

The boundary condition (1.2.20) becomes

$$R(\zeta) = (u - iv)\,\zeta\, dz/d\zeta - (u + iv)\,\zeta\, dz^*/d\zeta = 0 \tag{1.2.22}$$

on $|\zeta| = 1$, with $u - iv$, $u + iv$, z, and z^* as described above.

To compute the solutions for the shapes, we choose a positive integer N and truncate the expressions for z and z^* up to and including the terms a_N and a_N^* . Similarly, we truncate the expressions for $u - iv$ and $u + iv$ to include up to g_N and g_N^* . We treat the coefficients and their conjugates as independent variables; this choice allows one check of the calculations. We substitute these expressions into the governing Equation (1.2.22) and obtain the following equation on the boundary of the mth vortex:

$$\sum_{k=-N}^{N} R_m(k)\,\zeta^k = 0; \tag{1.2.23}$$

this equation is consistent in each power of ζ retained. For each vortex we equate to zero each of the coefficients of ζ^k, $-N \leq k \leq N$. For N_v vortices, this truncation provides $N_v \cdot (2N+1)$ complex equations for the $N_v \cdot (2N+2)$ complex shape coefficients.

We eliminate N_v of these unknowns by setting

$$a_0 = a_0^* \tag{1.2.24}$$

for each vortex; this equation effectively specifies the the phase of ζ. The system, however, remains underdetermined. We see that the coefficient of ζ^0 is perforce zero by considering the equation of continuity, as shown in Appendix A. Depending upon the configuration of the vortices, other equations prove to be dependent, and further conditions must be derived to obtain a nonsingular system; these considerations will be described in the sections with the details of the individual cases.

There are two further conditions used in many of the calculations. First, we require that the vortices have prescribed areas. From Equations (1.2.10) and (1.2.14), we define the area of a given vortex as

$$A \equiv \pi a_0 a_0^* (1 - a_2 a_2^* - \cdots - (N-1) a_N a_N^*); \tag{1.2.25}$$

this equation is exact in the limit of infinite N when the starred quantities are the complex conjugates of their unstarred counterparts. Using this expression in the area relation (1.2.14) provides a further equation for each vortex. Second, we stipulate that the centroids of the vortex regions coincide with the local origins. From (1.2.15) we require this by specifying

$$g_1 = g_1^* = 0. \tag{1.2.26}$$

For each problem we have a system of M equations obtained from the boundary condition (1.2.22) and auxiliary conditions, (1.2.24)–(1.2.26), for the M unknowns that determine the shape (i.e., the a_n coefficients) and other properties of the system (e.g., the external velocity). Here, M depends upon N and the specific vortex system being described. We write this nonlinear system of equations as

$$\mathbf{F}(\mathbf{x}) = \mathbf{0}, \tag{1.2.27}$$

where $\mathbf{F}$ represents the M-vector of equations and $\mathbf{x}$ represents the M-vector of unknowns, and obtain solutions using the Newton iteration scheme

$$\mathbf{x}^{\nu+1} = \mathbf{x}^{\nu} - \boldsymbol{\delta}\mathbf{x}^{\nu}. \tag{1.2.28}$$

Here,

$$\boldsymbol{\delta}\mathbf{x}^{\nu} = \{\mathbf{F}'(\mathbf{x}^{\nu})\}^{-1}\mathbf{F}(\mathbf{x}^{\nu}), \tag{1.2.29}$$

where $\mathbf{F}'(\mathbf{x}^{\nu})$ denotes the derivative $\partial\mathbf{F}/\partial\mathbf{x}$ evaluated at $\mathbf{x} = \mathbf{x}^{\nu}$. An initial solution to begin the Newton iteration is often taken as the circular vortex solution, which, for a vortex with area A, is given by

$$a_0 = \sqrt{A/\pi}\ , \quad a_n = a_n^* = 0\ , \qquad n = -N, \ldots, -1, 1, \ldots, N. \tag{1.2.30}$$

Subsequent solutions are obtained using previous solutions as initial data. The convergence criterion of the Newton iteration is taken as requirement that the error in the solution, given by $\| \mathbf{F}(\mathbf{x}^{\nu}) \|$, plus the change in the residuals, given by $\| \boldsymbol{\delta}\mathbf{x}^{\nu} \|$, be less than a prescribed tolerance ϵ; in computations, ϵ was taken as 10^{-12}. The nonsingularity of the Jacobian is taken as verification of the independence of the equations involved. Furthermore, the Newton iteration formulation provides a framework for the application of path-following techniques and indicates possible bifurcation phenomena.

The steady-state solutions for the vortex shapes are taken as the basis for linear stabilty analysis, which is described in the next section.

1.3 Stability Calculations

For a given computed steady shape vortex configuration, we study the linear spectral stability of this solution to two-dimensional disturbances. In some cases to be considered, analytical linear stability analyses have been carried out; however, for the more complicated configurations, numerical linear stability analysis is required. Following the procedure of MSS, we introduce infinitesimal time-dependent deformations to the vortex boundaries, and assume that the vorticity of each region remains constant. By linearizing the resulting governing equations and prescribing an exponential form for the perturbation quantities, we obtain a generalized eigenvalue problem for the eigenmodes of the disturbance. From the solution of this problem we infer the spectral stability properties of the given configuration. In this section we offer an overview of the development of this analysis; details for specific configurations are discussed in subsequent sections.

To begin, we note that the steady boundary condition yields the governing equation in the steady shape calculations; similarly, in the stability calculations the corresponding unsteady boundary condition governs the behavior. The requirement that the vortex boundary move with the fluid is given by

$$(u - \partial x/\partial t)\sin\varphi - (v - \partial y/\partial t)\cos\varphi = 0, \tag{1.3.1}$$

where the vortex boundary $z = x + iy$ is no longer assumed steady; i.e., $x = x(t)$, $y = y(t)$. In analogy with Equation (1.2.20), this condition is written

$$\frac{\partial z^*}{\partial t}\frac{\partial z}{\partial s} - (u - iv)\frac{\partial z}{\partial s} - \frac{\partial z}{\partial t}\frac{\partial z^*}{\partial s} + (u + iv)\frac{\partial z^*}{\partial s} = 0. \tag{1.3.2}$$

In the unsteady case we write

$$z = Z + z', \qquad u - iv = U - iV + u' - iv', \tag{1.3.3}$$

where capitalized quantities are the known steady solution values and primed quantities are time-dependent infinitesimal perturbations.

Introducing these relations into the boundary condition (1.3.2) implies the following equation to leading order:

$$(U - iV)\frac{\partial Z}{\partial s} - (U + iV)\frac{\partial Z^*}{\partial s} = 0. \tag{1.3.4}$$

This relation is the requirement that the steady solution values satisfy the steady-state boundary condition. To first order in the perturbed quantities we obtain

$$\frac{\partial z^{*\prime}}{\partial t}\frac{\partial Z}{\partial s} - (U - iV)\frac{\partial z'}{\partial s} - (u' - iv')\frac{\partial Z}{\partial s} - \frac{\partial z'}{\partial t}\frac{\partial Z^*}{\partial s} + (U + iV)\frac{\partial z^{*\prime}}{\partial s} + (u' + iv')\frac{\partial Z^*}{\partial s} = 0. \tag{1.3.5}$$

Exponential time dependence is assumed for all primed quantities; e.g.,

$$z' = z'(s)e^{\sigma t}, \qquad u' - iv' = [u'(s) - iv'(s)]e^{\sigma t}, \tag{1.3.6}$$

so that Equation (1.3.5) becomes

$$\begin{aligned}(U - iV)\frac{\partial z'}{\partial s} + (u' - iv')\frac{\partial Z}{\partial s} - (U + iV)\frac{\partial z^{*\prime}}{\partial s} - (u' + iv')\frac{\partial Z^*}{\partial s} \\ = \sigma\left\{z'^*\frac{\partial Z}{\partial s} - z'\frac{\partial Z^*}{\partial s}\right\}.\end{aligned} \tag{1.3.7}$$

Using relationship $\partial/\partial s = (\partial\theta/\partial s)\,\partial/\partial\theta$ on the vortex boundary and canceling the common $\partial\theta/\partial s$ factor, we obtain the equation governing linear stability:

$$\begin{aligned}(U - iV)\frac{\partial z'}{\partial \theta} + (u' - iv')\frac{\partial Z}{\partial \theta} - (U + iV)\frac{\partial z^{*\prime}}{\partial \theta} - (u' + iv')\frac{\partial Z^*}{\partial \theta} \\ = \sigma\left\{z^{*\prime}\frac{\partial Z}{\partial \theta} - z'\frac{\partial Z^*}{\partial \theta}\right\}.\end{aligned} \tag{1.3.8}$$

This boundary condition is to be satisfied on every vortex; symmetry assumptions in the infinite array configurations imply that this equation needs to be satisfied on only one vortex (for the single array) or on only one vortex in each row (for the

double arrays). The eigensolution of this problem is the shape perturbation z', which appears both explicitly and implicitly (in the velocity perturbation $u' - iv'$) in this equation.

The shape perturbation z' is defined as follows. The boundary of a steady solution vortex is described by the mapping of the unit circle in the ζ plane given by

$$Z = a_0\zeta(1 + a_1/\zeta + \cdots + a_n/\zeta^n + \cdots); \tag{1.3.9}$$

a similar expression exists for Z^*. Perturbing each of the coefficients of the expansion, i.e., letting $a_n \to a_n + a'_n$, and linearizing yields the following expansion for the shape perturbation:

$$z' = a'_0\zeta(1 + a_1/\zeta + \cdots + a_n/\zeta^n + \cdots) + a_0\zeta(a'_1/\zeta + \cdots + a'_n/\zeta^n + \cdots). \tag{1.3.10}$$

Similarly, the perturbation $z^{*\prime}$ is given by

$$z^{*\prime} = (\tilde{a}'_0/\zeta)(1 + a_1^*\zeta + \cdots + a_n^*\zeta^n + \cdots) + (a_0^*/\zeta)(\tilde{a}'_1\zeta + \cdots + \tilde{a}'_n\zeta^n + \cdots). \tag{1.3.11}$$

Here we do *not* require the coefficient $\tilde{a}'_n$ to equal the complex conjugate of a'_n; i.e., the perturbations to the coefficients a_n and a_n^* are taken to be independent, since a_n and a_n^* are treated as independent quantities. With the assumption that a_0 is real (as used in the shape calculations) we *do* assume that $a'_0 = \tilde{a}'_0$ for each vortex.

From the steady-state solution we have series expansions for Z and Z^*, with which we explicitly evaluate the tangential derivatives required in the right side of Equation (1.3.9). On the vortex boundary, $\partial/\partial\theta = (\partial\zeta/\partial\theta)\,\partial/\partial\zeta$; also, $\zeta = \exp i\theta$, so $\partial\zeta/\partial\theta = i\zeta$. Differentiating the shape expansion thus implies

$$\partial Z/\partial\theta = ia_0\,\zeta(1 - (1-1)\frac{a_1}{\zeta} - (2-1)\frac{a_2}{\zeta^2} - \cdots - (n-1)\frac{a_n}{\zeta^n} - \cdots); \tag{1.3.12}$$

a similar result is obtained for $\partial Z^*/\partial\theta$. Using these representations, the right side of Equation (1.3.8) is expanded explicitly as a power series in ζ for the perturbations to each of the shape coefficients of each vortex.

The evaluation of the left side of Equation (1.3.8) is less direct. The complication lies in the evaluation of the perturbation velocity $u' - iv'$ as a power series in ζ in which the perturbed shape coefficients are easily identified. The implementations vary with the geometry of the configuration and the nature of the stability problem, which differs between finite vortex systems and infinite vortex arrays: in the former, the self-oscillations (i.e., shape modes) of the system are studied, while in the latter, in addition to the shape modes, the cooperative modes corresponding to a perturbation of a prescribed wavelength are analyzed. In the subsequent discussion we outline the underlying concepts employed in the evaluation of the left side of Equation (1.3.8); the details for the different configurations are explained in the following chapters. Let $(u - iv)_l$ denote the velocity induced by the lth vortex, and consider the contribution of the perturbation to the nth shape coefficient of the lth vortex. This perturbation implies the linearized velocity perturbation given by

$$(u' - iv')_l = \frac{d(u - iv)}{da'^{(l)}_n} a'^{(l)}_n . \tag{1.3.13}$$

We approximate the derivative in (1.3.13) with central differences as follows. The nth shape coefficient, $a^{(l)}_n$, of this vortex is incremented by a small quantity ε, and the expansion of the resulting perturbed boundary condition at each vortex is obtained using the relationship (1.2.10) between the Schwarz velocity coefficients and the shape coefficients. The tangential velocity at the boundary of each vortex is then evaluated as a power series in ζ. Schematically, we represent this effect on

the boundary condition at the mth vortex as

$$\left\{\left[(u-iv)\frac{\partial z}{\partial\theta}-(u+iv)\frac{\partial z^*}{\partial\theta}\right]_{a_n^{(l)}+\varepsilon}\right\}\Bigg|_{\partial V_m}=\sum_{k=-\infty}^{\infty}R_m(k;a_n^{(l)}+\varepsilon)\,\zeta^k. \quad (1.3.14)$$

We represent the analogous effect for the nth shape coefficient decremented by ε as

$$\left\{\left[(u-iv)\frac{\partial z}{\partial\theta}-(u+iv)\frac{\partial z^*}{\partial\theta}\right]_{a_n^{(l)}-\varepsilon}\right\}\Bigg|_{\partial V_m}=\sum_{k=-\infty}^{\infty}R_m(k;a_n^{(l)}-\varepsilon)\,\zeta^k. \quad (1.3.15)$$

The effect of the perturbation on the boundary condition at the mth vortex is approximated by the expansion

$$\left\{(U-iV)\frac{\partial z'}{\partial\theta}+(u'-iv')\frac{\partial Z}{\partial\theta}-(U+iV)\frac{\partial z^{*\prime}}{\partial\theta}-(u'+iv')\frac{\partial Z^*}{\partial\theta}\right\}_n^{(l)}\Bigg|_{\partial V_m}$$
$$=\sum_{k=-\infty}^{\infty}\frac{1}{2\varepsilon}\left[R_m(k;a_n^{(l)}+\varepsilon)-R_m(k;a_n^{(l)}-\varepsilon)\right]\zeta^k. \quad (1.3.16)$$

The error in this approximation is $O(\varepsilon^2)$. Linearization of the velocity description given in (1.2.18) (with (1.2.16)) shows that perturbation of the nth shape coefficient induces two contributions to the velocity perturbation $u'-iv'$: (1) that given by the perturbed vortex shape in the steady velocity field (described by the unperturbed Schwarz coefficients), and (2) that caused by the induced perturbed velocity field (determined by the perturbed Schwarz coefficients) in which the vortex retains its steady shape. We denote this by

$$u'-iv'=(u'-iv')_{vortex}+(u'-iv')_{velocity}. \quad (1.3.17)$$

As a result of this decomposition, the evaluation of the coefficients R_m in (1.3.16) is divided into two terms; the details of these calculations depend on the vortex configuration and are described in the following chapters. This evaluation procedure is repeated for all shape coefficients of each vortex to obtain the left side of

(1.3.8). Symmetry assumptions imply that this computation needs to be made on only a single vortex for the single infinite array, and on only one vortex in each row for the double array; however, the influence of the other vortices requires careful analysis in these cases.

All terms in the governing stability Equation (1.3.8) can now be evaluated. Equating the coefficients of like powers of ζ in the power series expansions for each side of Equation (1.3.8) yields infinitely many equations in the infinitely many unknown shape perturbations. We write this system as the generalized eigenvalue problem

$$\mathbf{M}\ \mathbf{v} = \sigma\, \mathbf{N}\ \mathbf{v}. \tag{1.3.18}$$

The matrix elements are functions of the steady shapes and other geometry-dependent parameters (e.g., for the infinite arrays, the wavenumber of the perturbation), and the components of the eigenvector $\mathbf{v}$ are the perturbed shape coefficients $\{a'_n, \tilde{a}'_n\}$ of all vortices on which the boundary condition (1.3.8) is imposed.

To solve this problem numerically, we truncate all series to the order used in obtaining the steady shapes. For a general configuration of N_v ($< \infty$) vortices, each vortex contributes $2N + 1$ eigenvector elements, so the system is of order $N_v \cdot (2N + 1)$; by symmetry assumptions the matrices are of order $2N + 1$ for the single infinite array and of order $4N + 2$ for the double infinite array. In the actual solution of these problems, standard eigenvalue routines were used, with no difficulties.

The stability data obtained contain different information depending upon the configuration considered. The results, their differences, and their implications are presented in the subsequent chapters.

1.4 Energy Calculations

To better understand the dynamics of a vortex configuration, we study the energetics of the system. Specifically, we analyze the angular momentum and kinetic energy of vortices so that we can compare our findings with those of other researchers as well as further develop the theory for vortex systems for which there are conflicting results. In addition, energy analyses provide a means to check our results for the simple cases that permit explicit analytic analyses. Our analyses of vortex energetics extend only to systems of finitely many vortices.

The angular momentum of a vortex system is defined with respect to an absolute origin as

$$H = -\frac{1}{2}\iint_{\mathbb{R}^2} \omega r^2 \, dx \, dy, \tag{1.4.1}$$

where r is the distance from the origin to the point of integration. We choose the origin as the location of the centroid of the system. Furthermore, by choosing the centroid of each region of constant vorticity to coincide with its origin, we have for a system of N_v $(< \infty)$ vortices

$$H = -\frac{1}{2}\sum_{m=1}^{N_v} \omega_m (h_m^2 A_m + \iint_{V_m} r_m^2 \, dx \, dy), \tag{1.4.2}$$

where h_m is the distance of the vortex centroid from the absolute origin and r_m is the distance measured relative to the origin of the mth vortex V_m. We nondimensionalize the angular momentum as

$$J = -H/\left(\sum_{m=1}^{N_v} \Gamma_m A_m\right), \tag{1.4.3}$$

for configurations in which the denominator in this expression is nonzero. We evaluate the integral in (1.4.2) in terms of the shape expansion (1.2.1) as

$$\iint_{V_m} r_m^2 \, dx \, dy = \int_0^{2\pi} d\phi \int_0^{R_m(\phi)} r^2 r \, dr = \frac{1}{4}\int_0^{2\pi} R_m^4 \, d\phi = \frac{1}{4}\int_0^{2\pi} |z|^4 \, d\phi. \tag{1.4.4}$$

We thus reduce the area integral to an integral around a contour on which we have the required information: z describes the boundary of the mth vortex region; i.e.,

$$z = a_0\zeta(1 + a_1/\zeta + \cdots + a_n/\zeta^n + \cdots) \equiv R_m e^{i\phi}, \tag{1.4.5}$$

so that

$$dz = \frac{dz}{d\zeta}\, d\zeta = e^{i\phi}\, dR_m + iR_m e^{i\phi}\, d\phi. \tag{1.4.6}$$

Using a similar representation for dz^*, we obtain the expression

$$d\phi = \frac{1}{2i}\left(\frac{dz}{z} - \frac{dz^*}{z^*}\right). \tag{1.4.7}$$

On the vortex boundary, $\zeta = \exp i\theta$, so that $d\zeta = i\zeta\, d\theta$; thus, the differential $d\phi$ can be written

$$d\phi = \frac{1}{2}\,\zeta\left(\frac{1}{z}\frac{dz}{d\zeta} - \frac{1}{z^*}\frac{dz^*}{d\zeta}\right) d\theta. \tag{1.4.8}$$

Hence,

$$\iint\limits_{V_m} r_m^2\, dx\, dy = \frac{1}{8}\int_0^{2\pi} |z|^4\,\zeta\left(\frac{1}{z}\frac{dz}{d\zeta} - \frac{1}{z^*}\frac{dz^*}{d\zeta}\right) d\theta. \tag{1.4.9}$$

This integral is numerically evaluated using the steady-state solutions and Romberg integration.

The analysis of the energy of a system of vortices is more complicated. We consider the total kinetic energy of a system of vortices as

$$E = \frac{1}{2}\iint\limits_{\mathbb{R}^2} \nabla\psi \cdot \nabla\psi\; dx\, dy. \tag{1.4.10}$$

Using Green's Theorem, we write this as

$$E = \frac{1}{2}\left\{\lim_{R\to\infty} \oint\limits_{r=R} \psi\,\frac{\partial\psi}{\partial n}\, ds - \iint\limits_{\mathbb{R}^2} \psi\nabla^2\psi\; dx\, dy\right\}. \tag{1.4.11}$$

Thus,

$$E = \frac{1}{2}\lim_{R\to\infty} \oint\limits_{r=R} \psi\,\frac{\partial\psi}{\partial n}\, ds + \frac{1}{2}\iint\limits_{\mathbb{R}^2} \omega\psi\, dx\, dy. \tag{1.4.12}$$

For a system of finitely many vortices, we now require the far-field behavior (Saffman [1984]):

$$\psi \sim -\frac{\Gamma}{2\pi}\log R + \frac{\mathbf{I}\times\mathbf{x}\cdot\hat{\mathbf{z}}}{2\pi R^2} + O\left(\frac{1}{R^2}\right), \qquad \text{as } R\to\infty, \tag{1.4.13}$$

where $\mathbf{x}$ is the field point, Γ is the total circulation of the system, and $\mathbf{I}$ is the hydrodynamic impulse, defined for two-dimensional flows as

$$\mathbf{I} = \iint_{\mathbb{R}^2} \mathbf{x}\times\boldsymbol{\omega}\, dx\, dy. \tag{1.4.14}$$

In this frame of reference the vortices need not be stationary. We prescribe this far-field stream function behavior to compare different vortex configurations in equivalent settings. The first integral in (1.4.12) is the "infinite part" of the kinetic energy; its presence for two-dimensional flows is well known (Saffman [1984]). Thus, we define the excess kinetic energy as the second integral in (1.4.12), viz.,

$$T = \frac{1}{2}\iint_{\mathbb{R}^2} \omega\psi\, dx\, dy. \tag{1.4.15}$$

For systems with nonzero total circulation we nondimensionalize this quantity as

$$\tilde{T} = T/\Gamma^2. \tag{1.4.16}$$

By the choice (1.4.13) of the far-field stream function, this nondimensionalization of kinetic energy is not independent of the length scales of the problem. For example, the closed-form expression of this quantity for a circle of radius a centered at the origin is derived in Appendix C as

$$\tilde{T}_{circle} = \frac{1}{16\pi}(1-4\log a). \tag{1.4.17}$$

To eliminate this scale dependence, we define the reduced kinetic energy as the nondimensional excess kinetic energy of the system less the nondimensional excess

kinetic energy of an equivalent circular vortex, which is defined as a circular vortex, centered at the origin, with total area A and total circulation Γ equal to that of the system of vortices. From (1.4.17), we have that

$$\tilde{T}_{equivalent\ circle} = \frac{1}{16\pi}[1 - 2\log(A/\pi)]. \tag{1.4.18}$$

Thus, we write

$$\hat{T} = \tilde{T} - \tilde{T}_{equivalent\ circle}. \tag{1.4.19}$$

Several different nondimensionalizations of the kinetic energy are to be found in the literature; we choose this nondimensionalization (including the prescribed stream function behavior at infinity) as it provides a scale-invariant measure of the kinetic energy of the system for circular and elliptical vortices.

To evaluate the integral (1.4.15), we note that the vorticity is a nonzero constant in each of the vortex regions and zero elsewhere, so only the integral of the stream function over the vortices need be considered. In Appendix B the following expression for the integral of the stream function over a vortex V is derived:

$$\iint_V \psi\, dx\, dy = \frac{1}{2}\oint_{\partial V} \psi(x\, dy - y\, dx) - \frac{1}{4}\oint_{\partial V} (x^2+y^2)\left(\frac{\partial\psi}{\partial x}\, dy - \frac{\partial\psi}{\partial y}\, dx\right) + \frac{1}{4}\iint_V (x^2+y^2)\nabla^2\psi\, dx\, dy. \tag{1.4.20}$$

It is convenient to consider the contributions of the individual vortex regions to the stream function; thus, we write (1.4.20) for the contribution of the stream function induced by the lth vortex to the integral over the mth vortex as

$$\iint_{V_m} \psi^{(l)}\, dx\, dy = \frac{1}{2}\oint_{\partial V_m} \psi^{(l)}(x\, dy - y\, dx) - \frac{1}{4}\oint_{\partial V_m} r_m^2\left(\frac{\partial\psi^{(l)}}{\partial x}\, dy - \frac{\partial\psi^{(l)}}{\partial y}\, dx\right) - \frac{1}{4}\omega_l\,\delta_{l,m}\iint_{V_m} r_m^2\, dx\, dy, \tag{1.4.21}$$

where $\psi^{(l)}$ is the stream function at the mth vortex induced by the lth vortex, r_m is the radial coordinate relative to the local origin of the mth vortex, and $\delta_{l,m}$ is the Kronecker delta. Hence, the total excess kinetic energy for a system of N_v vortices may be represented as

$$T = \sum_{m=1}^{N_v} \frac{\omega_m}{2} \sum_{l=1}^{N_v} \iint_{V_m} \psi^{(l)}\, dx\, dy, \tag{1.4.22}$$

where the integral is given in (1.4.21).

To express these integrals in terms of the shape representations (1.2.1) and Schwarz velocity expansions (1.2.6), we first evaluate the stream function in terms of the Schwarz coefficients. The external velocity induced by the mth vortex at a point z_0 relative to the absolute origin is given by

$$(u - iv)_{m,\,induced} = -\frac{i\omega_m}{2} \sum_{n=0}^{\infty} \frac{g_n^{(m)}}{(z_0 - z_m)^{n+1}}, \tag{1.4.23}$$

where z_m is the position of the origin of the mth vortex relative to the absolute origin. The corresponding complex potential $w = \phi + i\psi$ is given by

$$w_{m,\,induced} = -\frac{i\omega_m}{2} \left[g_0^{(m)} \log(z_0 - z_m) - \sum_{n=1}^{\infty} \frac{g_n^{(m)}}{n(z_0 - z_m)^n} \right] + C_m, \tag{1.4.24}$$

where C_m is a constant. Thus, the total induced complex potential is

$$w_{induced} = \sum_{m=1}^{N_v} w_{m,\,induced}. \tag{1.4.25}$$

By the choice of asymptotic behavior of the stream function (1.4.13), we set

$$C_m = 0, \qquad m = 1, \ldots, N_v, \tag{1.4.26}$$

since with this choice, by (1.2.14),

$$\begin{aligned} w &\sim -\frac{i}{2} \sum_{m=1}^{N_v} \omega_m g_0^{(m)} \log(z_0 - z_m) + o(1) \\ \Longrightarrow \quad w &\sim -\frac{i\Gamma}{2\pi} \log z_0 + o(1), \qquad \text{as } |z_0| \to \infty, \end{aligned} \tag{1.4.27}$$

where Γ is the total circulation and z_0 is the coordinate relative to the absolute origin. At a point z on the boundary of the mth vortex, the value of the stream function induced by the lth vortex is given by

$$\psi_m^{(l)} = \Im\left\{-\frac{i\omega_l}{2}\left[g_0^{(l)}\log(z+z_m-z_l) - \sum_{n=1}^{\infty}\frac{g_n^{(l)}}{n(z+z_m-z_l)^n}\right]\right\}. \tag{1.4.28}$$

The value of the velocity on the boundary of the mth vortex induced by the lth vortex is

$$(u-iv)_{m,l} = -\frac{i\omega_l}{2}\sum_{n=0}^{\infty}\frac{g_n^{(l)}}{(z+z_m-z_l)^{n+1}}. \tag{1.4.29}$$

With these representations we now evaluate the integrals in (1.4.21). The integrand of the first integral is simplified by writing

$$x\,dy - y\,dx = -\Im\{z\,dz^*\} = -\Im\left\{z\frac{dz^*}{d\zeta}\,d\zeta\right\} = -\Im\left\{i\zeta z\frac{dz^*}{d\zeta}\,d\theta\right\}, \tag{1.4.30}$$

since $\zeta = \exp i\theta$ on the vortex boundary. Hence, using (1.4.28), we express the first integral in (1.4.21) as

$$\int_0^{2\pi}\Im\left\{\frac{i\omega_l}{2}\left[g_0^{(l)}\log(z+z_m-z_l) - \sum_{n=1}^{\infty}\frac{g_n^{(l)}}{n(z+z_m-z_l)^n}\right]\right\}\Im\left\{i\zeta z\frac{dz^*}{d\zeta}\,d\theta\right\}. \tag{1.4.31}$$

The integrand of the second integral in (1.4.21) is simplified by noting that

$$\frac{\partial\psi}{\partial x}\,dy - \frac{\partial\psi}{\partial y}\,dx = -(u\,dx + v\,dy) = -\Re\{(u-iv)dz\}. \tag{1.4.32}$$

On the vortex boundary we have that

$$dz = \frac{dz}{d\zeta}\,d\zeta = i\zeta\frac{dz}{d\zeta}\,d\theta. \tag{1.4.33}$$

Thus, with $x^2+y^2 = |z|^2$ on the boundary and the velocity given by (1.4.29), we write the second integral in (1.4.21) as

$$-\Re\left\{\frac{\omega_l}{2}\int_0^{2\pi}|z|^2\left(\sum_{n=0}^{\infty}\frac{g_n^{(l)}}{(z+z_m-z_l)^{n+1}}\right)\zeta\frac{dz}{d\zeta}\,d\theta\right\}. \tag{1.4.34}$$

Lastly, we note that the third integral in (1.4.21) is the same as the integral (1.4.9) obtained in the angular momentum calculations.

In the subsequent sections, we analyze the energetics of the vortex pair and the single vortex in a uniformly rotating field, which we consider next.

Chapter 2

The Single Vortex

2.1 Introduction

In this chapter we study a single simply connected region of uniform vorticity in a two-dimensional, inviscid, incompressible fluid. The theory is developed by using the method of Schwarz functions for the case of flow with external rotation γ and plane strain rate ϵ . Two special cases are analyzed:

1. externally rotating flow without strain; i.e., $\epsilon = 0$; and
2. straining flow without external rotation; i.e., $\gamma = 0$.

The general formulation presented also permits the analysis of the case of simple shearing flow, i.e., the case $\gamma = \pm\epsilon$.

The simplest of all finite area vortex flows is the circular region of constant vorticity in a uniformly rotating fluid. This solution, the Rankine vortex, admits complete analytic linear stability and energetics analyses (Lamb [1945]). Likewise, the Kirchhoff elliptical vortex (Kirchoff [1877]) has been entirely described (Love [1893], Lamb [1945], Kida [1981], Burbea & Landau [1982]). The steady states that bifurcate from the circular vortex were first found and studied by Deem & Zabusky [1978], using the boundary-integral method; they applied the techniques of contour dynamics in a limited study of the nonlinear stability of these configurations. Subsequently, Landau [1981], Burbea & Landau [1982], and Burbea [1982] contributed an exhaustive and rigorous study (including existence proofs) of the shape and stability of these symmetric singly connected steady states. These solutions are verified using the method of Schwarz functions, and further solutions

that bifurcate from these branches are found. We study the relationship of angular momentum and kinetic energy to the stability of these vortex states.

Introduction of plane strain into the flow approximates to first order the effect of a relatively distant second vortex. This complication presents a significantly different problem, which was first solved explicitly by Moore & Saffman [1971]. They obtained analytic solutions for a family of elliptical vortex solutions, which were later verified by Kida [1981], Burbea [1982], and Neu [1984]. Moore & Saffman analytically obtained the stability characteristics of the elliptical solution branch, also given by Burbea, and thereby predicted nonelliptical bifurcated solutions. We obtain these steady nonelliptical solutions numerically and study their stability properties.

2.2 Formulation

The formulation of the single vortex shape problem closely follows the presentation of Chapter 1, simplified by the consideration of only one vortex region and complicated by external rotation and straining fields. The boundary of the region with uniform vorticity ω_0 is determined by the conformal mapping of the unit circle in the ζ plane given by

$$z = a_0\zeta\,(1 + a_1/\zeta + \cdots + a_n/\zeta^n + \cdots)\,. \tag{2.2.1}$$

We take the origin of the physical plane to be the origin in this representation of the vortex boundary. The external velocity induced by this region is given by

$$(u - iv)_{induced} = -\frac{i\omega_0}{2}\left\{\frac{g_0}{z} + \frac{g_1}{z^2} + \cdots\right\}, \tag{2.2.2}$$

where

$$g_n = \text{ the coefficient of } \zeta^{-1} \text{ in } z^* z^n \frac{dz}{d\zeta}. \tag{2.2.3}$$

Following Moore & Saffman [1971], we write the velocity of the external flow field with uniform rotation γ and rate of strain ϵ with principal axes at $\pm\pi/4$ to the x-axis as

$$u_{external} = -(\gamma+\epsilon)\,y, \qquad v_{external} = (\gamma-\epsilon)\,x, \tag{2.2.4}$$

where γ and ϵ are real numbers. This is equivalent to

$$(u-iv)_{external} = i\epsilon z - i\gamma z^*. \tag{2.2.5}$$

The total velocity field is given by the sum of the induced and external velocities; the conjugate velocity field has a similar representation in terms of the conjugate coefficients, which are assumed to be independent. The governing equation for this problem is the boundary condition

$$R(\zeta) = (u-iv)\,\zeta\,dz/d\zeta - (u+iv)\,\zeta\,dz^*/d\zeta = 0. \tag{2.2.6}$$

Substituting the series expressions for the terms in this equality, we obtain the equation governing the shape of the vortex as

$$\sum_{k=-\infty}^{\infty} R(k)\,\zeta^k = 0. \tag{2.2.7}$$

To solve this equation, we choose a positive integer N and truncate all expansions to include terms up to and including order N. To satisfy the boundary conditions on the vortex, we equate each of the coefficients of ζ^k, $-N \le k \le N$, to zero, and thereby obtain $2N+1$ complex equations for the $2N+2$ complex shape coefficients.

We reduce by one the number of variables by requiring $a_0 = a_0^*$, which fixes the phase of ζ. The resultant system is underdetermined. Following the arguments of Appendix A, the coefficient of ζ^0 is necessarily zero, so setting $R(0)$ equal to

zero is a dependent equation. To remedy this situation, we include the equation specifying the area of the vortex. From (1.2.25), we write this relation as

$$A/\pi - a_0 a_0^*(1 - a_2 a_2^* - \cdots - (N-1)a_N a_N^*) = 0. \tag{2.2.8}$$

We thus obtain $2N+1$ complex equations, consisting of the above area equation and the $2N$ boundary condition equations,

$$R(k) = 0, \qquad k = -N, \ldots, -1, 1, \ldots, N, \tag{2.2.9}$$

for the $2N+1$ independent complex unknowns $a_0, a_1, \ldots, a_N, a_1^*, \ldots, a_N^*$. The system obtained is nonsingular, and, indeed, a_n^* is found to be the complex conjugate of a_n. The requirement that the centroid have zero displacement from the origin is found to be automatically satisfied by all solutions obtained; i.e., it is found that both g_1 and g_1^* are always zero. Since the system obtained is nonsingular, these equations are not explicitly imposed. Solutions of the resultant nonlinear system of equations,

$$\mathbf{F}(\mathbf{x}; \epsilon, \gamma) = \mathbf{0}, \tag{2.2.10}$$

are obtained using Newton's method, with LINPACK routines employed in the matrix manipulations.

The stability problem for single vortices describes the self-oscillations of the perturbed steady vortex solution. The formulation of the linear stability problem for the single vortex follows the procedure of §1.3. Linearization of the unsteady boundary condition that the vortex move with the fluid yields the equation

$$\begin{aligned}(U - iV)\frac{\partial z'}{\partial \theta} + (u' - iv')\frac{\partial Z}{\partial \theta} - (U + iV)\frac{\partial z^{*\prime}}{\partial \theta} - (u' + iv')\frac{\partial Z^*}{\partial \theta} \\ = \sigma \left\{ z^{*\prime}\frac{\partial Z}{\partial \theta} - z'\frac{\partial Z^*}{\partial \theta} \right\}.\end{aligned} \tag{2.2.11}$$

Here, we have assumed the expansions

$$z = Z + z'(\theta)e^{\sigma t}, \qquad u - iv = U - iV + [u'(\theta) - iv'(\theta)]e^{\sigma t}, \tag{2.2.12}$$

where capitalized quantities are the known steady solution and primed quantities denote perturbation values. We define the shape eigensolution by perturbing each of the coefficients of the shape expansion as in (1.3.11) and (1.3.12), where the perturbations to the coefficients a_n and a_n^*, viz., a_n' and $\tilde{a}_n'$, are taken as independent. To explicitly formulate the boundary condition (2.2.11) as an eigenvalue problem according to the procedure of §1.3, we now consider the effect of the perturbation to the shape coefficient a_j.

The right side of (2.2.11) can be evaluated directly according to the discussion of §1.3 : for the perturbation a_j' the corresponding shape disturbance is

$$z_j' = \begin{cases} a_0' \zeta (1 + a_1/\zeta + \cdots + a_n/\zeta^n + \cdots), & j = 0, \\ a_0 \, a_j' \, \zeta^{1-j}, & j = 1, 2, \ldots . \end{cases} \tag{2.2.13}$$

Recall that the shape perturbation of the conjugate coefficient a_j^*, given by $\tilde{a}_j'$, is independent of the conjugate of the shape perturbation a_j', given by c.c.$\{a_j'\}$. The θ-derivatives of the steady boundary in (2.2.11) are evaluated explicitly (e.g., as in (1.3.12)). The terms $\partial Z/\partial\theta$ and $\partial Z^*/\partial\theta$ are calculated as products of power series in ζ, so that the right side of (2.2.11) is evaluated as a power series in ζ.

An explicit perturbation expansion of the velocity field shows that we may consider the velocity perturbation as consisting of two contributions: (1) that induced by the boundary perturbation in the steady, i.e., unperturbed, velocity field, and (2) that caused by perturbing the velocity field while keeping the given vortex undisturbed. For the disturbance to a_j considered, the first contribution is given by the perturbation to the induced velocity field; i.e.,

$$(u' - iv')_{j,vortex} = \frac{d}{dz}(u - iv)_{induced}\bigg|_{z=Z} z_j' + \delta(u - iv)_{external} \tag{2.2.14}$$

$$= \frac{d}{dz}\left[-\frac{i\omega_1}{2}\sum_{n=0}^{\infty}\frac{g_n}{z^{n+1}}\right]\bigg|_{z=Z} z_j' + i(\epsilon z_j' - \gamma z_j^{*\prime}), \tag{2.2.15}$$

where Z is the steady shape and z_j' the shape perturbation due to a_j', given in

(2.2.13). The second contribution is given by

$$(u' - iv')_{j,velocity} = -\frac{i\omega_1}{2} \sum_{n=0}^{\infty} \frac{g'_n}{Z^{n+1}}, \tag{2.2.16}$$

where the primed Schwarz coefficients are the perturbations in these quantities due to a'_j. There are no external velocity contributions to this term, as the external field is steady.

We compute these numerically as follows. First, we approximate the first two terms in

$$(U - iV)\frac{\partial z'_j}{\partial \theta} + (u' - iv')_{j,vortex}\frac{\partial Z}{\partial \theta} - (U + iV)\frac{\partial z^{*\prime}_j}{\partial \theta} - (u' + iv')_{j,vortex}\frac{\partial Z^*}{\partial \theta} \tag{2.2.17}$$

as

$$\sum_{k=-N}^{N} \frac{1}{2\varepsilon} \left[R_1(k; a_j + \varepsilon) - R_1(k; a_j - \varepsilon) \right] \zeta^k, \tag{2.2.18}$$

where $\sum_{k=-N}^{N} R_1(k; a_j \pm \varepsilon)\, \zeta^k$ is the product of the truncated velocity expansion, into which the perturbed shape is substituted, and the θ-derivative of the perturbed boundary. This sum is given explicitly by

$$\left\{ -\frac{i\omega_1}{2} \sum_{n=0}^{N} \frac{g_n}{[z(a_j \pm \varepsilon)]^{n+1}} + i[\epsilon z(a_j \pm \varepsilon) - \gamma z^*(a_j \pm \varepsilon)] \right\} \frac{\partial}{\partial \theta} \left[z(a_j \pm \varepsilon) \right]. \tag{2.2.19}$$

In this formula $z(a_j \pm \varepsilon)$ represents the shape due to the perturbation to a_j :

$$z(a_j \pm \varepsilon) = \begin{cases} (a_0 \pm \varepsilon)\zeta(1 + a_1/\zeta + \cdots + a_n/\zeta^n + \cdots), & j = 0, \\ a_0\zeta(1 + a_1/\zeta + \cdots + (a_j \pm \varepsilon)/\zeta^j + \cdots + a_n/\zeta^n + \cdots), & j = 1, 2, \ldots . \end{cases} \tag{2.2.20}$$

The remaining terms in (2.2.17) are evaluated analogously. Central differencing of these expressions as in (2.2.18) yields (2.2.17) plus terms that are $O(\varepsilon^2)$.

The remaining contribution to the left side of governing Equation (2.2.11) is

$$(u' - iv')_{j,velocity}\frac{\partial Z}{\partial \theta} - (u' + iv')_{j,velocity}\frac{\partial Z^*}{\partial \theta}, \tag{2.2.21}$$

the first addend of which is computed as

$$\sum_{k=-N}^{N} \frac{1}{2\varepsilon} \left[R_2(k; a_j + \varepsilon) - R_2(k; a_j - \varepsilon) \right] \zeta^k. \tag{2.2.22}$$

Here, $\sum_{k=-N}^{N} R_2(k; a_j \pm \varepsilon)\, \zeta^k$ is the product of the truncated velocity perturbation and the boundary derivative of the steady shape; i.e.,

$$\sum_{k=-N}^{N} R_2(k; a_j \pm \varepsilon)\, \zeta^k = \left\{ -\frac{i\omega_1}{2} \sum_{n=0}^{N} \frac{g_n'(a_j \pm \varepsilon)}{[Z(a_j)]^{n+1}} \right\} \frac{\partial}{\partial \theta} \left[Z(a_j) \right]. \tag{2.2.23}$$

In this equation $Z(a_j)$ denotes the steady shape, and the first-order perturbation to the Schwarz coefficient is computed as the difference between the perturbed and steady values of the Schwarz coefficient; i.e.,

$$g_n'(a_j \pm \varepsilon) = g_n(a_j \pm \varepsilon) - g_n(a_j). \tag{2.2.24}$$

After adding a similar evaluation of the second term in this expression, we obtain a first-order correct approximation to (2.2.21).

The sum of these terms gives the left side of the boundary condition for the the disturbance to the jth shape coefficient. Repeating this calculation for each shape coefficient and equating the coefficients of the powers of ζ in this sum to those of the like powers of ζ in the right side of the boundary condition (2.2.11) gives $2N + 1$ equations in the $2N + 1$ unknown complex shape perturbations. We write this system as

$$\mathbf{M}\ \mathbf{v} = \sigma\, \mathbf{N}\ \mathbf{v}, \tag{2.2.25}$$

where the matrices $\mathbf{M}$ and $\mathbf{N}$ are functions of the steady shape and the parameters γ and ϵ, and the eigenvector $\mathbf{v}$ has components

$$v_1 = \tilde{a}_N', \ldots, v_{N+1} = \tilde{a}_0' = a'_0, \ldots, v_{2N+1} = a_N'. \tag{2.2.26}$$

This generalized eigenvalue system is left-multiplied by the inverse of the non-singular matrix $\mathbf{N}$, and the resulting system is solved with standard EISPACK routines.

A single zero eigenvalue is found for which the area variation of the corresponding eigenmode is nonzero; as the perturbed vortex in this case is a steady state, its conjugate is also, so $z^{*\prime} = \text{c.c.}\,\{z'\}$, implying that $\tilde{a}'_n = \text{c.c.}\,\{a'_n\}$. The remaining $2N$ eigenvalues occur in pairs, σ_1 and σ_2, for each of the 1st through Nth eigenmodes. If the mode is stable, i.e., $\Re\{\sigma\} = 0$, the eigenvalues occur in pairs with $\sigma_2 = \sigma_1^*$. Absorbing the magnitude of the disturbance into the perturbation z', for σ_1 we have the shapes

$$Z + e^{\sigma_1 t} z'_1 \qquad \text{and} \qquad Z^* + e^{\sigma_1 t} z_1^{*\prime}, \tag{2.2.27}$$

where z'_1 and $z_1^{*\prime}$ are determined by $\left\{a'_{1,n}\right\}_{n=0}^{N}$ and $\left\{\tilde{a}'_{1,n}\right\}_{n=0}^{N}$, respectively. Taking complex conjugates, we obtain

$$Z^* + e^{\sigma_1^* t}\,\text{c.c.}\{z'_1\} \qquad \text{and} \qquad Z + e^{\sigma_1^* t}\,\text{c.c.}\{z_1^{*\prime}\}. \tag{2.2.28}$$

Requiring these states to be eigenmodes, with $\sigma_2 = \sigma_1^*$ we have that

$$z'_2 = \text{c.c.}\{z_1^{*\prime}\} \qquad \text{and} \qquad z_2^{*\prime} = \text{c.c.}\{z'_1\}. \tag{2.2.29}$$

For suitably normalized eigenvectors, this condition implies that

$$a'_{2,n} = \text{c.c.}\{\tilde{a}'_{1,n}\} \qquad \text{and} \qquad \tilde{a}'_{2,n} = \text{c.c.}\{a'_{1,n}\}, \tag{2.2.30}$$

which are found in the numerical results. Physically realized perturbations for stable disturbances are obtained by taking combinations of both eigenvectors, i.e., $e^{\sigma_1 t} z'_1 + e^{\sigma_2 t} z'_2$, so that the conjugate of the perturbed state is a perturbation of the conjugate state. If the mode is unstable, we find that σ is purely real with

$\sigma_2 = -\sigma_1 = \sigma_1^*$. In this case we have the perturbations as given in (2.2.27) and their conjugates as in (2.2.28). Since these conjugates must be eigenmodes, we have that c.c. $\{z_j'\} = z_j^{*\prime}$ for $j = 1, 2$; normalizing the eigenvector such that $a_{j,0}'$ is real implies that

$$\text{c.c.}\left\{a_{j,n}'\right\} = \tilde{a}_{j,n}', \tag{2.2.31}$$

as indicated in the computed results. Physically realized unstable modes are obtained by taking the corresponding eigenvector only, so that the conjugate of the growing/decaying perturbation is a growing/decaying state.

The energy analysis proceeds along the lines of the development of §1.4. The nondimensional angular momentum of the single vortex is $J = -H/\Gamma A$, where

$$H = -\frac{1}{2}\iint_{\mathbb{R}^2} \omega r^2\, dx\, dy = -\frac{\omega}{16}\int_0^{2\pi} |z|^4\, \zeta \left(\frac{1}{z}\frac{dz}{d\zeta} - \frac{1}{z^*}\frac{dz^*}{d\zeta}\right) d\theta, \tag{2.2.32}$$

which is evaluated in terms of the shape coefficients by Romberg integration.

With the excess kinetic energy of the single vortex given by

$$T = \frac{1}{2}\iint_{\mathbb{R}^2} \omega\psi\, dx\, dy, \tag{2.2.33}$$

we consider the nondimensionalized energy $\tilde{T}$ and the reduced energy $\hat{T}$ defined by

$$\tilde{T} = T/\Gamma^2, \qquad \hat{T} = \tilde{T} - \tilde{T}_{equivalent\ circle}. \tag{2.2.34}$$

As mentioned in §1.4, we evaluate the energy in the frame in which there is no externally imposed rotation (see (1.4.13)). To evaluate the integral of the stream function in the energy expressions, we use the form derived in Appendix B; the integrands are evaluated in terms of the steady states as shown in §1.4, and the integrals are evaluated using Romberg integration.

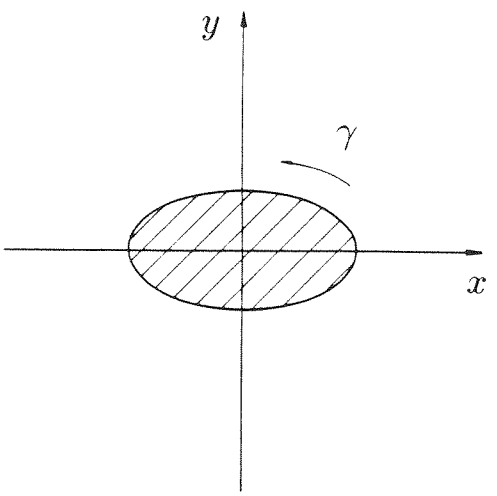

Figure 2.1 The single vortex in rotating, unstrained fluid.

2.3 The Single Vortex in Unstrained Fluid

In this section we consider a single vortex in an externally rotating fluid, as depicted in Figure 2.1. In the subsequent discussion, the area of all vortices is normalized to π, and the circulation of the vortex region is set to one. The external flow field is taken to have the following behavior:

$$(u - iv)_{external} = -i\gamma z^*, \tag{2.3.1}$$

so that the total circulation in the vortex is $\omega_0 - 2\gamma$ in the frame in which the vortex boundary is fixed. We denote the nondimensionalized rotation rate by

$$\gamma' \equiv \gamma/\omega_0. \tag{2.3.2}$$

For any γ', the simplest solution of this problem is given by the circular vortex, which was first studied by Thomson [1880]. This solution exists and is neutrally stable for any value of γ'. Analytic stability results (Lamb [1945]) yield the discrete eigenvalue spectrum

$$\sigma'_m \equiv \frac{\sigma_m}{\omega_0} = \frac{1}{2}(m-1)(1-2\gamma'). \tag{2.3.3}$$

The angular momentum and kinetic energy of the circular vortex region, computed with the far flow-field assumption (1.4.13), are derived in Appendix C. They are given in nondimensional form as, respectively,

$$J = \frac{1}{4\pi}, \qquad \tilde{T} = \frac{1}{16\pi}[1 - 2\log(A/\pi)]. \tag{2.3.4}$$

By definition (1.4.20), the reduced kinetic energy $\hat{T}$ is identically zero for a circular vortex.

Bifurcating from the circular solution are several families of symmetric vortex regions. Deem & Zabusky [1978] first found these solutions, which they named "V states," using a contour dynamics algorithm. Zabusky *et al.* [1979], Overman & Zabusky [1982a,b], and Zabusky & Overman [1983] study the time evolution of the Euler equations, using these steady shapes as initial configurations. Su [1979] obtains these solution shapes analytically by expanding the radial boundary coordinate as a perturbation series in a small parameter on the order of the distortion of the boundary from being circular. Burbea [1982] proves the existence of the "V states," which he obtained by using a numerical conformal mapping method. Burbea & Landau [1982] conduct a linear stability analysis by numerically solving the eigenvalue problem obtained from solution operators of the evolution equations of the system.

The solution space for this problem is shown in Figure 2.2, where ν_m, a nondimensional measure of the solution, is plotted against γ', the external rotation. For the mth solution branch, ν_m is defined as

$$\nu_m \equiv \frac{1 - a_m}{1 + a_m}. \tag{2.3.5}$$

Here, a_m is the mth coefficient of the conformal mapping (2.2.1) describing the vortex boundary. The index m denotes the dominant mode of the surface disturbance to the circular vortex along the mth branch: for the circular vortex $m = 1$, so that

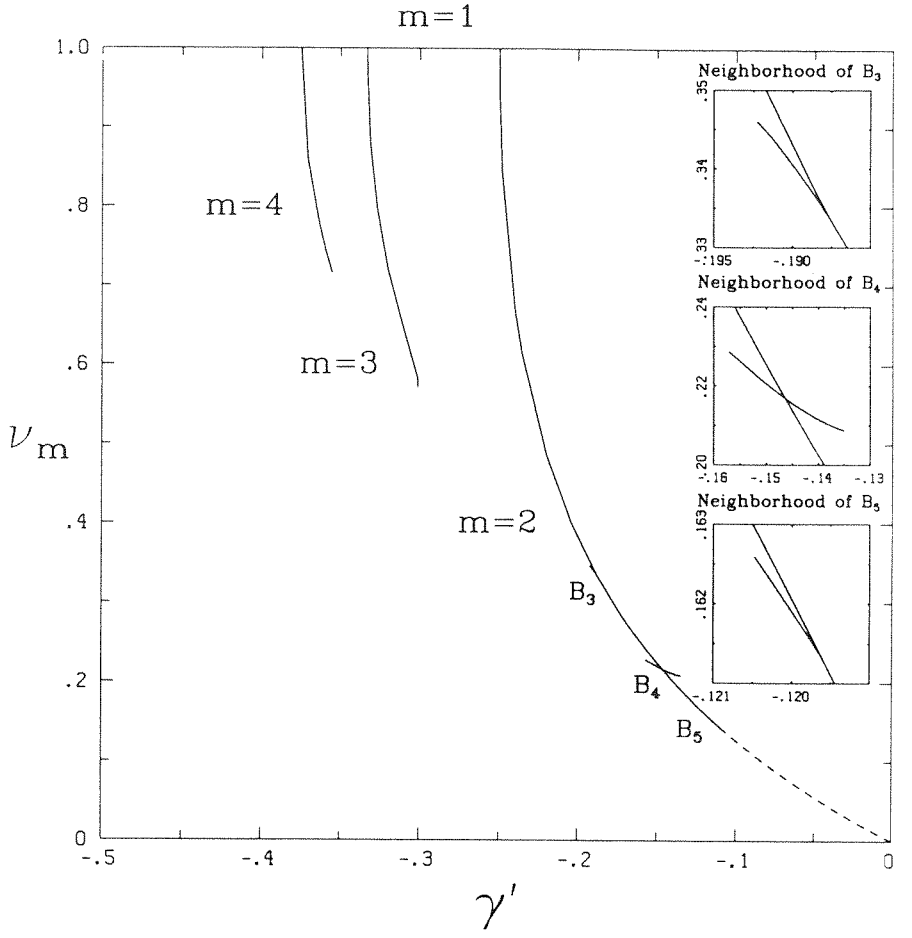

Figure 2.2 Solution paths for the single rotating vortex; ν_m is a family-dependent aspect ratio, and γ' is the nondimensionalized rotation rate. The insets show closeups of the bifurcation point regions. The dotted line indicates the analytical solution of Burbea & Landau [1982] where a converged numerical solution was not obtained.

$\nu_1 \equiv 1$, while for the elliptical vortices $m = 2$, whence $\nu_2 = (1-a_2)/(1+a_2)$, which equals the inverse axis ratio $(a/b)^{-1} \in (0,1]$ for the ellipses $(x/a)^2 + (y/b)^2 = 1$. The first three paths bifurcating from the path of circular vortices were followed until the convergence criteria could not be met.

Following the path of circular solutions from $\gamma' = 0$, the first bifurcation point is found at $\gamma' = -0.250$. The solutions that branch off here are the Kirchhoff elliptical vortices (Kirchhoff [1877], Lamb [1945]). Encountered along this solution branch are bifurcation points; the existence of these bifurcated solutions is implicit

in the work of Moore & Saffman [1971], in which the points of change of stability, i.e., the zeros of the eigenvalues, correspond to bifurcation points on the path of elliptical solutions. The first such point is at $(\gamma', \nu_2) \doteq (-0.1875, 0.3333)$, where the $k = 3$ mode goes unstable; this corresponds to an ellipse with axis ratio of 3:1, as first derived by Love [1893]. The numerically obtained locations of the first three bifurcation points, accurate to five figures, are catalogued in Table 2.1, and bifurcated solutions are shown in Figure 2.3. Along this branch the eigenvalue pair $\sigma = \pm i\gamma$ is associated with the $k = 1$ translational mode, the elliptical $k = 2$ modes have zero eigenvalues, and the higher modes have in general nonzero eigenvalues. The stability properties shown in Figure 2.3 near point B_k indicate the stability of the kth eigenmode, which remains unstable as the magnitude of the rotation rate is further decreased.

Single Rotating Elliptical Vortex Bifurcation Points				
	Origin	B_3	B_4	B_5
γ'	-0.25000	-0.18750	-0.14645	-0.11964
ν_2	1.0	0.33333	0.21685	0.16136

Table 2.1 Locations of the first three bifurcation points along the $m = 2$ branch.

The $m = 3$ branch of solutions forks off the circular solution at $\gamma' \doteq -0.3333$ (see Figure 2.2); similarly, the $m = 4$ solution path branches from the circular solution at $\gamma' \doteq -0.3750$. Along the mth branch, the eigenvalues $\sigma = \pm i\gamma$ are associated with the translational mode, and the m-fold $k = m$ modes have zero eigenvalue. The locations of the bifurcation points along this path, indicated by the stability data of Burbea & Landau, were obtained only qualitatively; convergence to the analytical bifurcation points values was not obtained and bifurcated branches were not sought. The general Schwarz method was found to require a prohibitively large number of modes along these branches. Whereas only a_0 and a_2 are nonzero along the elliptical branch of solutions, for the basic $m = 3$ branch,

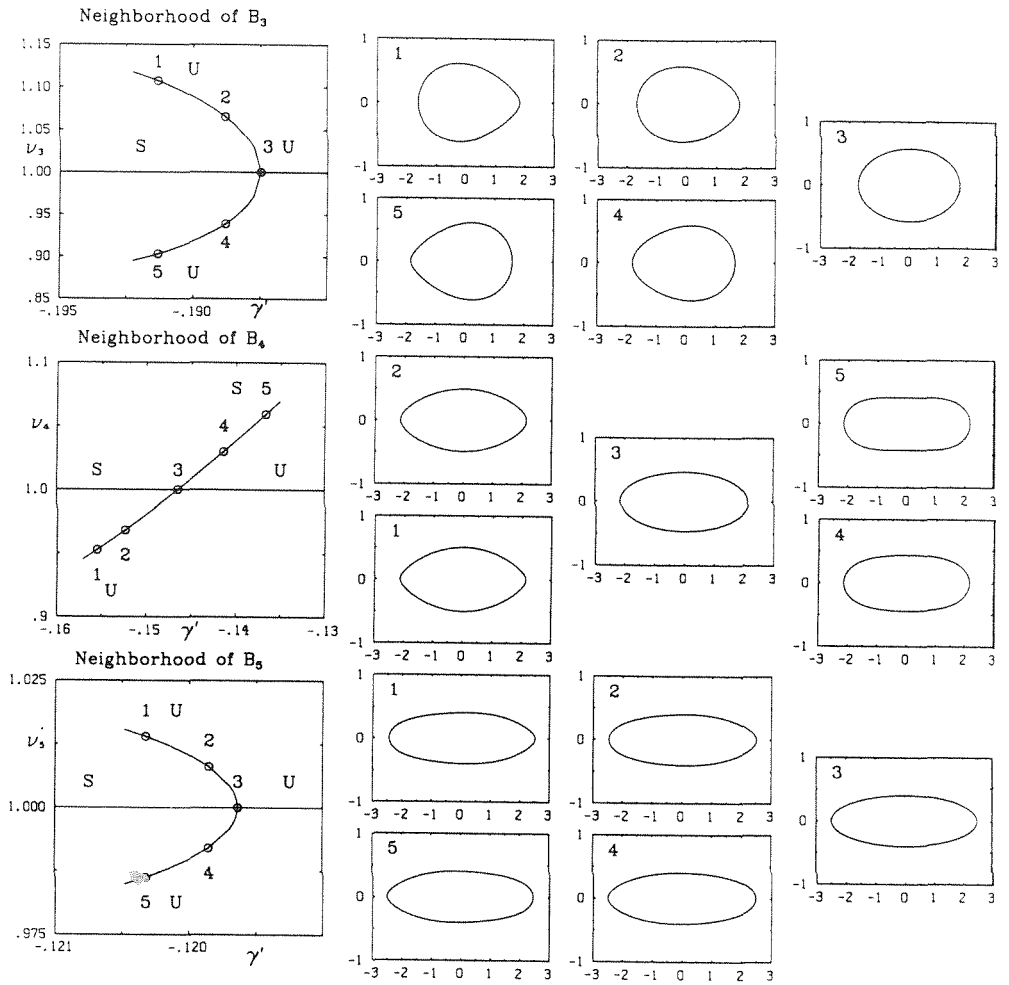

Figure 2.3 Bifurcations from the $m = 2$ (elliptical) branch of solutions: the diagrams to the right show the vortices at the correspondingly numbered circled points of the bifurcation diagrams. S implies stability and U instability to the kth eigenmode near point B_k.

for example, the shape coefficients a_0, a_3, a_6, ... are nonzero; this symmetry criterion is implicit in the work of Burbea & Landau. Wu *et al.* [1984] and Overman [1986] obtain limiting solutions along these branches of symmetric shapes.

Formulae for the angular momentum and kinetic energy of an elliptical vortex are derived in Appendix C for the far field assumption (1.4.13). For an elliptical vortex of axes ratio $\rho = a/b > 1$, where a and b are the lengths of the semimajor and semiminor axes, respectively, the nondimensional angular momentum and the

reduced kinetic energy are given, respectively, as

$$J = \frac{1}{8\pi}\frac{\rho^2+1}{\rho}, \qquad \hat{T} = \frac{1}{4\pi}\log\left(\frac{2\sqrt{\rho}}{1+\rho}\right). \tag{2.3.6}$$

The angular momentum and energy computed for the Schwarz elliptical solutions obtained match the analytic data to at least four significant figures for the solutions obtained, i.e., up to the third bifurcation point. The energy data computed for the $m = 2$ bifurcated solutions computed with $N = 16$ modes are compiled in Table 2.2; the energy data for all $m = 2$ solutions are plotted in Figure 2.4. As the vortices are further distorted, i.e., for decreasing $|\gamma'|$, the energy decreases while the angular momentum increases.

We now consider the stability of single vortex regions in terms of an energy extremum argument employed by Saffman & Szeto [1980] for the vortex pair and the infinite vortex array. Thomson [1887] states, Arnold [1978] proves, and Dritschel [1985] explains this principle, which can be stated as follows: For inviscid, incompressible uniform vorticity configurations, a steady state is a conditional extremum, i.e., a stationary point, of the kinetic energy functional with respect to all area-preserving isovortical solutions, i.e., all infinitesimal perturbations consistent with the Helmholz laws. Given certain regularity conditions, a sufficient condition for the nonlinear stability of such a solution is that it (locally) maximize or minimize the kinetic energy with respect to all isovortical variations. This criterion is analogous to the stability criterion proved by Putterman & Uhlenbeck [1969] for point vortices.

Surprisingly, we find that the angular momentum and energy for the vortices that bifurcate from the elliptical solution path fall along the energy curve of the elliptical solutions, to within four significant figures. Specifically, for a given bifurcated solution, the value of J is less than that of the elliptical solution at the same rotation rate, while the value of $\hat{T}$ is greater than that of the corresponding

m=2 First Bifurcated Branch					
γ'	$4\pi J$	$4\pi\hat{T}$	$4\pi J_{ell}$	$4\pi\hat{T}_{ell}$	γ'_{ell}
-0.1875	1.6667	-0.1438	1.6667	-0.1438	-0.1875
-0.1880	1.6570	-0.1420	1.6592	-0.1424	-0.1882
-0.1885	1.6485	-0.1404	1.6526	-0.1412	-0.1888
-0.1891	1.6374	-0.1383	1.6438	-0.1395	-0.1896
-0.1898	1.6265	-0.1363	1.6350	-0.1379	-0.1904
-0.1904	1.6159	-0.1343	1.6263	-0.1362	-0.1911
-0.1910	1.6059	-0.1323	1.6177	-0.1348	-0.1919
-0.1916	1.5956	-0.1304	1.6091	-0.1329	-0.1926
-0.1923	1.5858	-0.1285	1.6006	-0.1313	-0.1934

m=2 Second Bifurcated Branch					
γ'	$4\pi J$	$4\pi\hat{T}$	$4\pi J_{ell}$	$4\pi\hat{T}_{ell}$	γ'_{ell}
-0.1367	2.6496	-0.3007	2.6587	-0.3020	-0.1370
-0.1398	2.5728	-0.2901	2.5765	-0.2906	-0.1399
-0.1429	2.4970	-0.2794	2.4979	-0.2795	-0.1430
-0.1461	2.4227	-0.2686	2.4227	-0.2686	-0.1461
-0.1464	2.4142	-0.2674	2.4142	-0.2674	-0.1464
-0.1492	2.3502	-0.2579	2.3507	-0.2580	-0.1492
-0.1542	2.2798	-0.2473	2.2816	-0.2476	-0.1525
-0.1539	2.2454	-0.2421	2.2481	-0.2425	-0.1541

m=2 Third Bifurcated Branch					
γ'	$4\pi J$	$4\pi\hat{T}$	$4\pi J_{ell}$	$4\pi\hat{T}_{ell}$	γ'_{ell}
-0.1196	3.1794	-0.3685	3.1794	-0.3685	-0.1196
-0.1197	3.1772	-0.3682	3.1784	-0.3684	-0.1197
-0.1199	3.1716	-0.3674	3.1718	-0.3676	-0.1199
-0.1200	3.1660	-0.3669	3.1664	-0.3669	-0.1200

Table 2.2 Energy data for the $m = 2$ bifurcated branches. The J_{ell} and $\hat{T}_{ell}$ data are for the elliptical vortex of the same rotation rate. The value γ'_{ell} is the rotation rate of the ellipse with angular momentum and energy equal to that of the bifurcated solution.

ellipse; however, for a more negative rotation rate there exists an elliptical vortex solution whose angular momentum and energy equal those of the nonelliptical vortex. Hence, in the single vortex case it is apparently not possible to infer stability characteristics of the steady solutions by energy data alone. These concepts, however, will come into play in the analysis of the corotating vortex pair in the

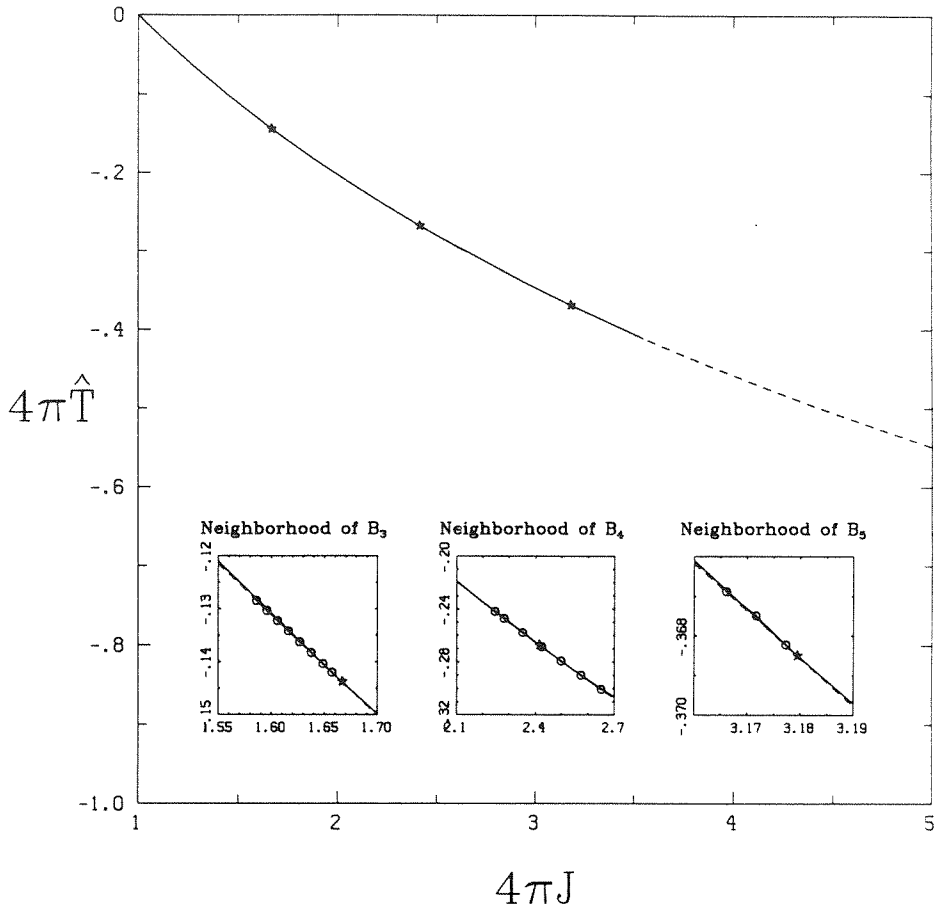

Figure 2.4 Energy versus angular momentum for the single rotating vortex solutions. Solid lines indicate numerically computed values; dashed lines are analytically computed values. Stars indicate bifurcation points; circled points in the insets are values for bifurcated solutions.

following chapter.

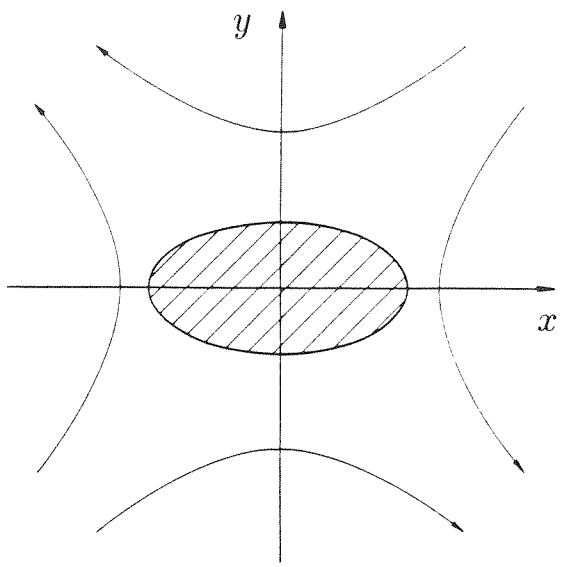

Figure 2.5 The single vortex in strained fluid.

2.4 The Single Vortex in Strained Fluid

We now consider a single vortex in an externally strained fluid, as shown in Figure 2.5. We again normalize the area of the vortex to π and set the circulation equal to one. The external flow field is taken as

$$(u - iv)_{external} = i\epsilon z, \tag{2.4.1}$$

where ϵ is the magnitude of the rate of strain with principal axes at $\pm 45°$ to the x-axis. This configuration is shown by Moore & Saffman [1971] to be a first approximation to the flow field induced by a relatively distant vortex.

This problem was first solved by Moore & Saffman, who obtained the family of elliptical vortices along the solution path given by

$$\epsilon' \equiv \frac{\epsilon}{\omega_0} = \frac{\rho(\rho - 1)}{(\rho^2 + 1)(\rho + 1)}, \tag{2.4.2}$$

where the ratio of semimajor to semiminor axes is given by $\rho = a/b > 1$. These results were obtained by direct solution of the Poisson equation in elliptical coordinates; an analytic linear stability analysis for the family of elliptic solutions was

also derived. Subsequently, elliptical solutions in a straining field were obtained analytically Kida [1981], who generalizes the Moore & Saffman result to the case of elliptical solutions whose orientation and axes lengths depend upon time. Neu [1984] expands upon Kida's findings by analytically solving the problem of a time-dependent elliptic cylinder subjected to a general irrotational three-dimensional strain. Burbea [1982] derives steady two-dimensional shape solutions for m-fold symmetric hypotrochoid regions of constant uniform vorticity in the presence of straining fields of order m, i.e., those whose stream functions are proportional to $\Re\{z^m\}$.

The method of Schwarz functions yields the branch of steady elliptical solutions, confirming the results of these authors. The solution space is depicted in Figure 2.6, where the inverse axis ratio $\nu = 1/\rho$ is plotted against the nondimensionalized strain ϵ'. There are two steady elliptical solutions for $0 < \epsilon' < \epsilon'_{max}$, where $(\epsilon'_{max}, \nu) \doteq (0.1501, 0.3460)$ is a fold point of the problem. The first three bifurcation points, denoted B_3, B_4, and B_5, are indicated, as well as the paths of nonelliptical solutions found. For the nonelliptical solutions we define the parameter ν as

$$\nu = \frac{1 - a_2}{1 + a_2}, \tag{2.4.3}$$

which reduces to the inverse axis ratio for elliptical vortices. Path-following techniques as suggested by Keller [1977] were employed in obtaining the solution paths, which were followed until the specified convergence criterion could not be fulfilled.

Moore & Saffman obtain the following expression for the mth eigenvalue of the linear stability problem for elliptical solutions:

$$\sigma'^{\,2}_m \equiv \left(\frac{\sigma_m}{\omega_0}\right)^2 = -\frac{1}{4}\left[\left(\frac{2m\rho}{\rho^2+1}\right)^2 - \left(\frac{\rho-1}{\rho+1}\right)^{2m}\right]. \tag{2.4.4}$$

Possible bifurcation points along the solution path are the points of change of stability, i.e., solutions for which σ'_m vanishes. Locations of the first three bifurcation

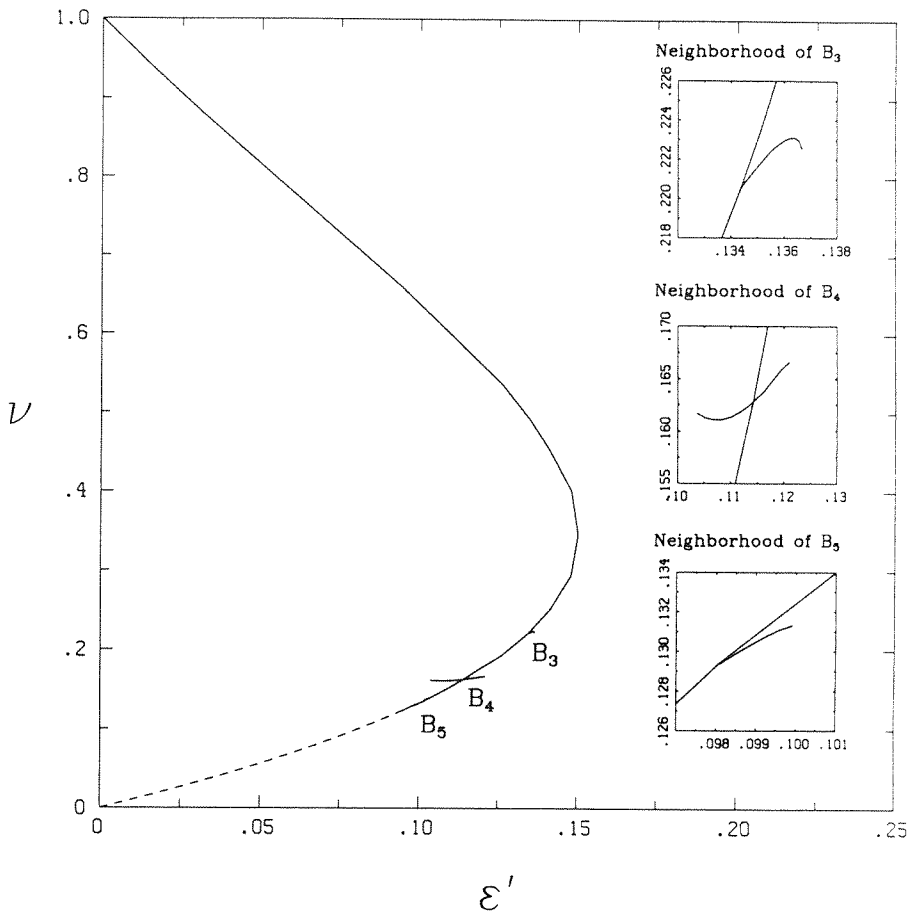

Figure 2.6 Solution paths for the single strained vortex; ν is the inverse aspect ratio, and ϵ' is the nondimensionalized strain rate. The insets show close-ups of the bifurcation point regions. The dotted line indicates the analytical solution (2.4.2), where a converged numerical solution was not obtained.

points are given in Table 2.3; these data match the analytically predicted values to five significant figures.

Single Strained Elliptical Vortex Bifurcation Points				
	Fold Point	B_3	B_4	B_5
ϵ'	0.15014	0.13425	0.11419	0.098083
ν	0.34601	0.22033	0.16280	0.12936

Table 2.3 Locations of the first three bifurcation points along the elliptical branch.

The index k of the path intersecting the elliptical solutions at point B_k corresponds to the eigenmode disturbance that changes stability at that point; this

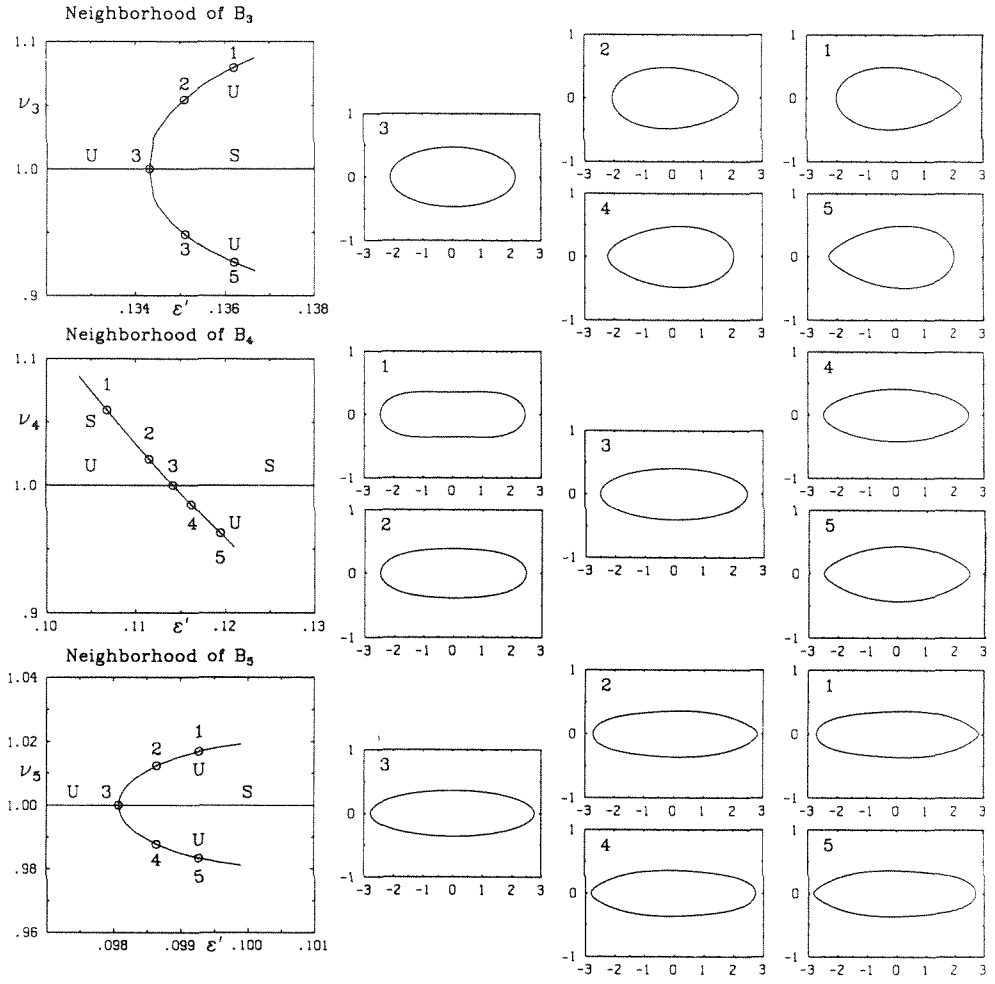

Figure 2.7 Solution paths and vortices for the first, second, and third bifurcated branches. The path-dependent shape parameter ν_m is defined in (2.3.5). The diagrams to the right show the vortices at the correspondingly numbered circled points of the bifurcation diagrams. S implies stability and U instability to the kth eigenmode near point B_k.

mode remains unstable as the strain rate is further decreased. Specific bifurcated vortex solutions are given in Figure 2.7 for $k = 3$, 4, and 5. The solution shapes along branch k are seen to have a k-fold disturbance imposed upon a basically elliptical shape. Whereas nearly circular vortices can be accurately described by relatively few Schwarz coefficients, the distorted nonelliptical shapes were calculated with $N = 16$ coefficients.

We find, in accordance with Moore & Saffman, that the less eccentric ellipti-

cal vortices, i.e., those on the upper solution branch in Figure 2.6, are neutrally stable, and the elliptical solutions of greater eccentricity along the lower branch are linearly unstable. The lower branch solutions and all bifurcated solutions are linearly unstable to the $k = 2$ disturbance mode; the stability properties shown in Figure 2.7 indicate the stability of the system to the subsequent modes; e.g., the stability of the $k = 3$ mode is indicated in the neighborhood of the third bifurcation point B_3, etc.

The possibility remains to associate these bifurcated solutions with those corresponding with the Kirchhoff elliptical vortex of the last section. Continuation in the parameters γ and ϵ together (i.e., vortices in externally strained and rotating fluid) should show a connection between these families of solutions and possibly indicate nonelliptical strained vortex solutions corresponding to the higher rotating V-states.

Chapter 3

The Vortex Pair

3.1 Introduction

A fundamental unit in many two-dimensional models of more complex flows is the vortex pair. Simple models for the behavior of the trailing vortices behind wings have been calculated using a vortex pair (Spreiter & Sacks [1951], Rossow [1977], Pierrehumbert [1980]). The vortex pair has also been studied as a model for the pairing interaction of coherent structures in shear layers (Saffman & Szeto [1980], Overman & Zabusky [1982a]).

In this chapter, we obtain solutions for the corotating vortex pair, i.e., $\omega_1 = \omega_2$, and discuss the formulation for the translating vortex pair, i.e., $\omega_1 = -\omega_2$. Unlike previous work, less restrictive symmetry requirements are imposed on the allowable vortex shapes. Analysis of the energetics of the corotating vortex pair is based upon a study of suitably nondimensionalized angular momentum and kinetic energy. The interdependence of these quantities is related to the directly computed linear stability results of the system using a general argument put forth by Kelvin [1887] and first interpreted for the vortex pair by Saffman & Szeto [1980]. Our results on the stability of the corotating pair disagree with the findings of Dritschel [1985].

3.2 Formulation

The vortex pair is the simplest multiple-vortex configuration which we consider, yet the proper formulation of this problem reveals characteristics significantly more subtle than those of the single vortex case. We consider two general vortex regions of fixed, prescribed areas A_1 and A_2, and circulations Γ_1 and Γ_2, where positive circulation is taken counterclockwise. Let the boundary of vortex 1 be given by

$$z = a_0\zeta\,(1 + a_1/\zeta + \cdots + a_n/\zeta^n + \cdots)\,, \tag{3.2.1}$$

and that of vortex 2 be described by the independent mapping

$$z = b_0\zeta\,(1 + b_1/\zeta + \cdots + b_n/\zeta^n + \cdots)\,, \tag{3.2.2}$$

for $|\zeta| = 1$, where z is the coordinate relative to the local origin of each vortex. With the distance between the centroids of these regions denoted by the positive real number l, the nondimensional area parameter is taken as

$$\alpha \equiv \frac{1}{2}(A_1 + A_2)/l^2. \tag{3.2.3}$$

We distinguish between the case of corotating vortices ($\Gamma_1 + \Gamma_2 \neq 0$) and that of translating vortices ($\Gamma_1 = -\Gamma_2$) in choosing the position of the vortex origins, which are chosen to coincide with their centroids. In the former case, depicted in Figure 3.1, requiring the system centroid to be at the origin implies

$$\Gamma_1 l_1 + \Gamma_2 l_2 = 0, \tag{3.2.4}$$

where l_1 and l_2 are the directed distances from the absolute origin to the origins of vortex 1 and vortex 2, respectively, so that

$$l_1 - l_2 = l. \tag{3.2.5}$$

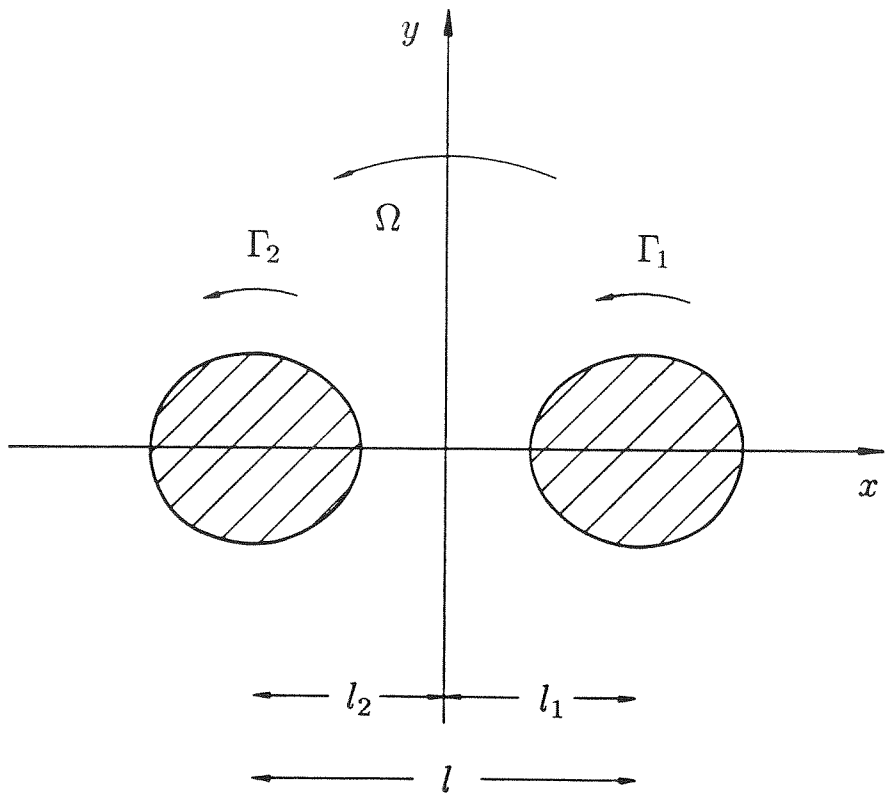

Figure 3.1 The corotating vortex pair.

Thus we have that

$$l_1 = \frac{\Gamma_2 l}{\Gamma_1 + \Gamma_2}, \qquad l_2 = -\frac{\Gamma_1 l}{\Gamma_1 + \Gamma_2}. \tag{3.2.6}$$

For the translating pair, shown in Figure 3.2, the system centroid is at infinity, so we fix the distance of the vortex origins from the system origin by weighting these distances by the vortex areas. We take

$$A_1 l_1 + A_2 l_2 = 0, \tag{3.2.7}$$

which, together with the definition (3.2.5), implies the center locations

$$l_1 = \frac{A_2 l}{A_1 + A_2}, \qquad l_2 = -\frac{A_1 l}{A_1 + A_2}. \tag{3.2.8}$$

Consider first the corotating vortex pair. The vortex-induced velocity at a point z external and relative to the first vortex consists of two contributions: that

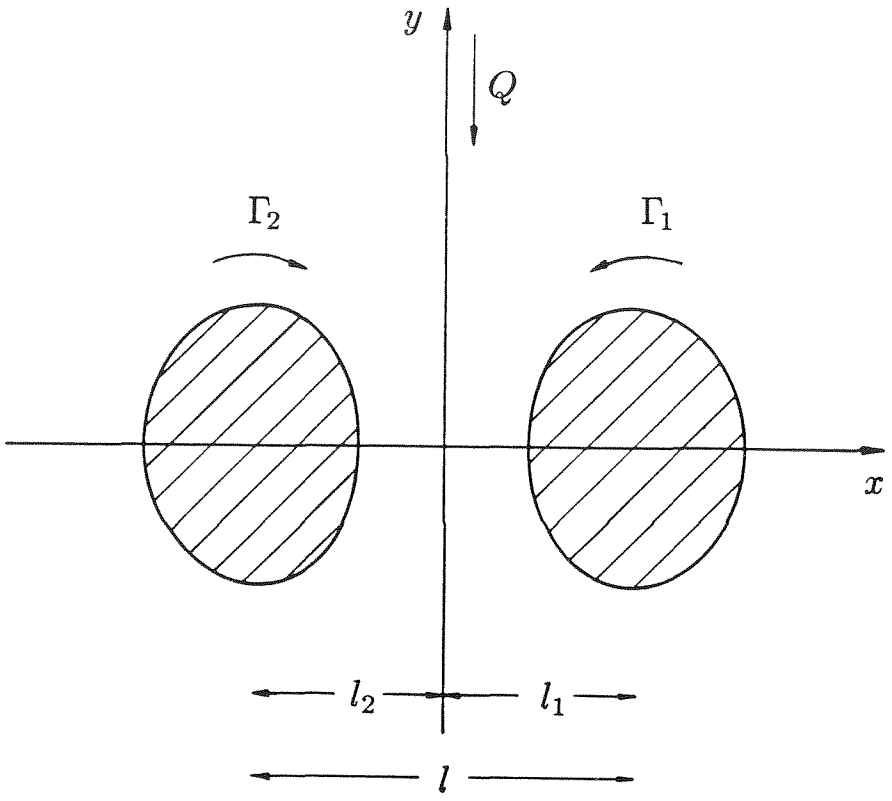

Figure 3.2 The counterrotating vortex pair.

from the vortex itself,

$$(u - iv)_{1,1} = -\frac{i\omega_1}{2} \sum_{n=0}^{\infty} \frac{g_n}{z^{n+1}}, \tag{3.2.9}$$

and that due to the second vortex,

$$(u - iv)_{1,2} = -\frac{i\omega_2}{2} \sum_{n=0}^{\infty} \frac{h_n}{(z + l)^{n+1}}. \tag{3.2.10}$$

Here, g_n and h_n are the nth Schwarz coefficients for the first and second vortices, respectively, and are related to the shape expansions for these regions by (1.2.10). To bring the vortex pair to rest, we impose an external rotation of unknown real angular velocity Ω relative to the absolute origin. The stream function for this rotation is

$$\psi_{ext} = -\frac{1}{2}\Omega(x^2 + y^2), \tag{3.2.11}$$

so that

$$(u - iv)_{ext} = -i\Omega z^*. \tag{3.2.12}$$

With respect to the first vortex this is represented as

$$(u - iv)_{1,\ ext} = -i\Omega(z + l_1)^*. \tag{3.2.13}$$

Thus, the total velocity external to the first vortex measured relative to that vortex is given by

$$(u - iv)_1 = -\frac{i\omega_1}{2}\sum_{n=0}^{\infty}\frac{g_n}{z^{n+1}} - \frac{i\omega_2}{2}\sum_{n=0}^{\infty}\frac{h_n}{(z+l)^{n+1}} - i\Omega(z + l_1)^*. \tag{3.2.14}$$

Similarly, for the second vortex we have

$$(u - iv)_2 = -\frac{i\omega_2}{2}\sum_{n=0}^{\infty}\frac{h_n}{z^{n+1}} - \frac{i\omega_1}{2}\sum_{n=0}^{\infty}\frac{g_n}{(z-l)^{n+1}} - i\Omega(z - l_2)^*, \tag{3.2.15}$$

where z is measured relative to the origin of the second vortex. We obtain like representations for the conjugate velocities in terms of the conjugate coefficients.

To determine the shapes, we substitute these expansions into the boundary condition Equation (1.2.22), to be satisfied on each vortex. To solve this equation, we expand the solution as a power series in $1/l$, the reciprocal of the intercentroid length; this is in effect an expansion in the nondimensionalized vortex area α since the vortex areas are fixed. We proceed as follows: The shape expansions are truncated to order N in ζ, and then expanded in $1/l$ as required. Consider the representation of the velocity with respect to the first vortex. As $0 < |z/l| < 1$, we expand the denominator in the second term as

$$\frac{1}{(z+l)^{n+1}} = \sum_{p=0}^{\infty}(-1)^p l^{-(n+p+1)}\frac{(n+p)!}{n!\,p!}z^p. \tag{3.2.16}$$

We truncate the series to retain terms of order l^{-L} and obtain

$$(u - iv)_1 = -\frac{i\omega_1}{2}\sum_{n=0}^{N}\frac{g_n}{z^{n+1}}$$

$$-\frac{i\omega_2}{2}\sum_{n=0}^{N}\sum_{p=0}^{L-n-1}h_n(-1)^p l^{-(n+p+1)}\frac{(n+p)!}{n!\,p!}z^p - i\Omega(z + l_1)^*. \tag{3.2.17}$$

Similar representations are obtained for the velocity with respect to the second vortex and for the conjugate velocities. Substituting these expansions into the boundary condition we obtain the truncated equations

$$\sum_{k=-N}^{N} R_1(k)\,\zeta^k = 0, \qquad \sum_{k=-N}^{N} R_2(k)\,\zeta^k = 0. \tag{3.2.18}$$

Equating the coefficients of ζ^k to zero provides $2\cdot(2N+1) = 4N+2$ equations. As unknowns there are the $2\cdot(2N+2) = 4N+4$ shape coefficients, the rotation rate Ω, and its conjugate Ω^*, for a total of $4N+6$ quantities. We require $\Omega = \Omega^*$ for a pure rotation, thereby eliminating one unknown. We fix the phase of ζ and reduce by two the number of unknowns by setting $a_0 = a_0^*$ and $b_0 = b_0^*$. As in the previous analysis, the equations for $R_1(0)$ and $R_2(0)$ are automatically satisfied, thereby reducing the number of equations to $4N$. We prescribe the areas of the vortices by adding the two equations:

$$A_1/\pi - a_0 a_0^*(1 - a_2 a_2^* - \cdots - (N-1)a_N a_N^*) = 0; \tag{3.2.19}$$

$$A_2/\pi - b_0 b_0^*(1 - b_2 b_2^* - \cdots - (N-1)b_N b_N^*) = 0. \tag{3.2.20}$$

In addition, we require the centroids of the vortices to coincide with the local vortex origins and add the four equations

$$g_1 = g_1^* = h_1 = h_1^* = 0. \tag{3.2.21}$$

We now have $4N+6$ equations for the $4N+3$ unknowns. We must examine other equations of motion to reveal the dependencies of these equations; a similar situation was found by MSS for the vortex street formulation. Since the centroid of the system is at rest, the following relation holds (Saffman [1984]):

$$\iint_{\mathbb{R}^2} \mathbf{u} \times \boldsymbol{\omega}\, dx\, dy = 0. \tag{3.2.22}$$

As shown in Appendix A, for the vortex pair this implies that the coefficients of ζ and ζ^{-1} are automatically zero for the second vortex if we explicitly set these coefficients to zero for the first vortex. Hence, the equations

$$R_2(1) = 0, \qquad R_2(-1) = 0 \tag{3.2.23}$$

are redundant and therefore not explicitly imposed. This implies $4N+4$ equations for the $4N + 3$ unknowns.

The final dependent equation can be found by considering the integral

$$\iint_{\mathbb{R}^2} \omega\,(\mathbf{x}\cdot\mathbf{u})\,dx\,dy. \tag{3.2.24}$$

As shown by Dritschel [1985], this integral vanishes under the assumption that $\psi \sim -(\Gamma/2\pi)\log R + o(1)$ as $R \to \infty$; in Appendix A the following relation is obtained:

$$\iint_V (\mathbf{x}\cdot\mathbf{u})\,dx\,dy = \frac{1}{2}\oint_{\partial V} r^2(\mathbf{u}\cdot\mathbf{n})\,ds. \tag{3.2.25}$$

With these results, it is shown that the relation

$$R_2(-2) + R_2(2) = 0 \tag{3.2.26}$$

is automatically satisfied for the second vortex, assuming it is symmetric about the x-axis. Since the pair of equations

$$R_2(-2) = 0, \qquad R_2(2) = 0 \tag{3.2.27}$$

is equivalent to the pair of equations

$$R_2(-2) + R_2(2) = 0, \qquad R_2(-2) - R_2(2) = 0, \tag{3.2.28}$$

we explicitly include the latter of the last two equations, and drop the former, as it is dependent. We thus obtain $4N + 3$ equations for the $4N + 3$ unknowns; the

nonsingularity of the Jacobian of this system verifies the independence of these equations.

Alternatively, we can consider the external rotation Ω and the conjugate quantity Ω^* as independent complex unknowns, and seek solutions for which Ω and Ω^* assume the same real values. In this case, we obtain a nonsingular system of $4N+4$ complex equations for $4N+4$ complex unknowns; the integral constraint of the preceding paragraph need not be imposed. We conjecture but cannot prove that this is related to the fact that the integral in (3.2.24) does not vanish for general velocity fields (e.g., those for which $u-iv$ and $u+iv$, and Ω and Ω^* are not complex conjugates). This formulation yields the same solutions as that for which Ω is assumed to equal Ω^*.

We now consider the translating vortex pair. The formulation of the shape problem for this configuration closely follows that of the corotating vortex pair, with one key difference: Since the pair is translating, we impose a constant external translational velocity to bring the system to rest; i.e.,

$$(u-iv)_{ext} = Q. \tag{3.2.29}$$

This complex quantity and its conjugate are treated as independent variables. Thus, in analogy to (3.2.14), the velocity relative to the first vortex is given by

$$(u-iv)_1 = -\frac{i\omega_1}{2}\sum_{n=0}^{\infty}\frac{g_n}{z^{n+1}} - \frac{i\omega_2}{2}\sum_{n=0}^{\infty}\frac{h_n}{(z+l)^{n+1}} + Q. \tag{3.2.30}$$

There are similar expansions for the velocity relative to the second vortex and for the conjugates of these quantities. We expand the terms in the reciprocal of the intercentroid length l, truncate the series, and substitute these expressions into the boundary condition (1.2.22). Equating the coefficients of ζ^k in the resultant series yields $4N+2$ equations for the $4N+4$ unknowns given by the 4N+2 shape coefficients, the external velocity Q, and the external conjugate velocity Q^*. We

eliminate the 2 equations corresponding to equating the coefficient of ζ^0 to zero, and add the 2 area equations, (3.2.19) and (3.2.20), and the 4 centroid equations (3.2.21) to obtain $4N + 6$ equations. By requiring the centroid of the steady system to be stationary, we have the condition (3.2.22), and thus do not impose equations (3.2.23). We thereby obtain $4N + 4$ equations in as many unknowns; our code indicates the nonsingularity of the Jacobian, which verifies their linear independence.

In analogy with the corotating pair formulation, we can eliminate one unknown by assuming, e.g., for the configuration depicted in Figure 3.2, that the external velocity Q is purely imaginary, so that $Q^* = -Q$. Substituting $-Q$ for each occurence of Q^* in the velocity representations, we obtain a nonsingular system of order $4N + 3$ by eliminating the first of the two equations in (3.2.28). We cannot justify this theoretically, yet we obtain identical solutions for both formulations.

Although our shape code performs correctly for the translating pair, we do not have confidence in the corresponding stability calculations and hence do not include our results for that configuration.

We study the linear stability of the vortex pair according to the framework of §1.3. The formulation of this problem is conceptually independent of whether the corotating or translating vortex pair is considered. The equation governing linear stability is given in (1.3.8); i.e.,

$$(U - iV)\frac{\partial z'}{\partial \theta} + (u' - iv')\frac{\partial Z}{\partial \theta} - (U + iV)\frac{\partial z^{*\prime}}{\partial \theta} - (u' + iv')\frac{\partial Z^*}{\partial \theta} = \sigma \left\{ z^{*\prime}\frac{\partial Z}{\partial \theta} - z'\frac{\partial Z^*}{\partial \theta} \right\}, \tag{3.2.31}$$

which is to be satisfied on the boundary of each vortex. Here, θ is the coordinate describing the unit circle in the ζ plane, and we have written

$$z = Z + z'(\theta)e^{\sigma t}\,, \qquad u - iv = U - iV + [u'(\theta) - iv'(\theta)]\,e^{\sigma t}. \tag{3.2.32}$$

We now describe the evaluation of this equation for a perturbation to the shape coefficient a_j of the first vortex. The evaluation procedure for perturbations to the other shape coefficients (i.e., a_j^*, b_j, and b_j^*) is similar.

The right side of (3.2.32) is evaluated as a power series in ζ according to the discussions of §§1.3 and 2.3 : the shape perturbation is given in (2.2.13), and the θ-derivatives of the steady boundary are evaluated explicitly.

The first contribution to the velocity perturbation, i.e., that induced by the perturbed vortex in the steady velocity field, is given by

$$(u'-iv')_{j,vortex} = \frac{d}{dz}(u-iv)_{ind}\bigg|_{z=Z} z_j' + \delta(u-iv)_{ext} \tag{3.2.33}$$

$$= \frac{d}{dz}\left[-\frac{i\omega_1}{2}\sum_{n=0}^{\infty}\frac{g_n}{z^{n+1}} - \frac{i\omega_2}{2}\sum_{n=0}^{\infty}\frac{h_n}{(z+l)^{n+1}}\right]\bigg|_{z=Z} z_j' + \delta(u-iv)_{ext}, \tag{3.2.34}$$

where the variation of the external velocity is given by

$$\delta(u-iv)_{ext} = \begin{cases} -i\Omega z_j^{*\prime}, & \text{for corotating vortices,} \\ 0, & \text{for translating vortices .} \end{cases} \tag{3.2.35}$$

Here, Z is the steady shape, and z_j' the shape perturbation due to a_j'. The second contribution to $u'-iv'$, that caused by perturbing the velocity field while keeping the given vortex undisturbed, is given by

$$(u'-iv')_{j,velocity} = -\frac{i\omega_1}{2}\sum_{n=0}^{\infty}\frac{g_n'}{Z^{n+1}} - \frac{i\omega_2}{2}\sum_{n=0}^{\infty}\frac{h_n'}{(Z+l)^{n+1}}, \tag{3.2.36}$$

where the primed Schwarz coefficients are the perturbations due to a_j'. There is no external velocity contribution to this term.

We compute these numerically as follows. First, we approximate the first two terms in

$$(U-iV)\frac{\partial z_j'}{\partial\theta} + (u'-iv')_{j,vortex}\frac{\partial Z}{\partial\theta} - (U+iV)\frac{\partial z_j^{*\prime}}{\partial\theta} - (u'+iv')_{j,vortex}\frac{\partial Z^*}{\partial\theta} \tag{3.2.37}$$

as the central difference, as in (2.2.18), of the sum that is the product of the truncated velocity expansion (e.g., (3.2.17)), into which the perturbed shape is substituted, and the θ-derivative of the perturbed boundary. For the case considered, this sum is given by

$$\sum_{k=-N}^{N} R_1(k; a_j \pm \varepsilon)\, \zeta^k = \frac{\partial}{\partial\theta}\left[z(a_j \pm \varepsilon)\right] \left\{ -\frac{i\omega_1}{2} \sum_{n=0}^{N} \frac{g_n}{[z(a_j \pm \varepsilon)]^{n+1}} \right.$$
$$\left. -\frac{i\omega_2}{2} \sum_{n=0}^{N} \sum_{n=N}^{L-n-1} h_n (-1)^p l^{-(n+p+1)} \frac{(n+p)!}{n!\, p!} [z(a_j \pm \varepsilon)]^p + (u - iv)_{ext}\Big|_{z=z(a_j \pm \varepsilon)} \right\}. \tag{3.2.38}$$

In this equation, $z(a_j \pm \varepsilon)$ represents the shape due to the perturbation to a_j as in (2.2.20). We evaluate the remaining terms in (3.2.37) analogously. Central differencing of these expressions yields the quantity (3.2.37) correct to $O(\varepsilon^2)$.

The second addend to the left side of governing Equation (3.2.31) is

$$(u' - iv')_{j,velocity} \frac{\partial Z}{\partial\theta} - (u' + iv')_{j,velocity} \frac{\partial Z^*}{\partial\theta}. \tag{3.2.39}$$

The first term is computed by central differencing the sum that is the product of the truncated velocity perturbation and the boundary derivative of the steady shape; i.e.,

$$\sum_{k=-N}^{N} R_2(k; a_j \pm \varepsilon)\, \zeta^k = \left\{ -\frac{i\omega_1}{2} \sum_{n=0}^{N} \frac{g_n'(a_j \pm \varepsilon)}{[Z(a_j)]^{n+1}} \right\} \frac{\partial}{\partial\theta}\left[Z(a_j)\right]. \tag{3.2.40}$$

The steady shape is denoted by $Z(a_j)$ in this equation, and the perturbation to the Schwarz coefficient is given by the difference between the perturbed and steady values as in (2.2.24). This yields a first-order correct approximation to the first term in (3.2.40); the second term is evaluated similarly. For the case we are considering, i.e., a perturbation to a coefficient of the first vortex, there is no change in the velocity induced by the independent second vortex; i.e., $h_n' = 0$; analogously, $g_n' = 0$ when shape perturbations to the second vortex are considered.

Repeating these calculations for each shape coefficient of each vortex and equating the coefficients of the powers of ζ in this sum to those of the like powers of ζ in the right side of the boundary condition (3.2.31) give $4N+2$ equations in the $4N+2$ unknown complex shape perturbations. We write this system as

$$\mathbf{M}\,\mathbf{v} = \sigma\,\mathbf{N}\,\mathbf{v}, \tag{3.2.41}$$

where $\mathbf{v}$ is the complex array of perturbation coefficients with elements

$$\begin{aligned} v_1 = \tilde{a}'_N, \ldots, v_{N+1} = \tilde{a}'_0 = a'_0, \ldots, v_{2N+1} = a'_N, \\ v_{2N+2} = \tilde{b}'_N, \ldots, v_{3N+2} = \tilde{b}'_0 = b'_0, \ldots, v_{4N+2} = b'_N. \end{aligned} \tag{3.2.42}$$

The matrices $\mathbf{M}$ and $\mathbf{N}$ depend on the steady shape expansion coefficients and the external velocity. The eigenvalue equation is left-multiplied by the inverse of the nonsingular matrix $\mathbf{N}$, and then solved with standard EISPACK routines.

One pair of zero eigenvalues is obtained whose eigenmodes correspond to vortices with nonzero linearized area variation relative to the steady state. The remaining $4N$ eigenvalues occur in quartets, σ_1, σ_2, σ_3, and σ_4, with pairs of eigenvalues related to the symmetric and antisymmetric modes of the 1st through Nth boundary harmonics. We consider only equal area vortices with circulations of equal magnitude in the following discussion. For the corotating pair there is one more pair of zero eigenvalues with a single linearly independent eigenvector; the magnitudes of these eigenvalues were found to be strongly dependent on the order of the truncation of the expansion and so were used to monitor the error of the numerical solution. The corresponding eigenmode is an antisymmetric shift of the vortices which, due to the degeneracy of the eigenvalue, grows linearly in time. A further neutral mode is obtained, which corresponds to a symmetric shift, i.e., a translation, of the vortices. This mode has purely imaginary eigenvalues with magnitude equal to the rotation rate and linearly lindependent eigenvectors.

If a given mode is stable, i.e., $\Re\{\sigma\} = 0$, the eigenvalues occur in pairs with, say, $\sigma_2 = \sigma_1^*$. An analysis similar to that presented in §2.2 shows that

$$a'_{2,n} = \text{c.c.}\{\tilde{a}'_{1,n}\} \qquad \text{and} \qquad \tilde{a}'_{2,n} = \text{c.c.}\{a'_{1,n}\}, \tag{3.2.43}$$

$$b'_{2,n} = \text{c.c.}\{\tilde{b}'_{1,n}\} \qquad \text{and} \qquad \tilde{b}'_{2,n} = \text{c.c.}\{b'_{1,n}\}. \tag{3.2.44}$$

Physically realized perturbations are obtained by taking combinations of both of these eigenstates, so that the conjugate of the perturbation is a perturbation of the conjugate state. If the mode is unstable, we find that σ is purely real so that $\sigma_2 = -\sigma_1$, with $\text{c.c.}\{z'_j\} = z_j^{*\prime}$, $j = 1, 2$, implying that

$$\text{c.c.}\left\{a'_{j,n}\right\} = \tilde{a}'_{j,n} \qquad \text{and} \qquad \text{c.c.}\left\{b'_{j,n}\right\} = \tilde{b}'_{j,n}. \tag{3.2.45}$$

Physically realized perturbations are obtained by taking the contribution of the unstable eigenvector only, since the conjugate of the growing/decaying mode is a growing/decaying state.

We now consider the energetics of the vortex pair and assume $\Gamma_1 + \Gamma_2 \neq 0$. With the centroid of each region at its origin, the angular momentum of the corotating vortex pair is written as

$$H = -\frac{1}{2}\sum_{m=1}^{2} \omega_m (h_m^2 A_m + \iint_{V_m} r_m^2 \, dx \, dy), \tag{3.2.46}$$

where h_m is the distance of the vortex centroid from the absolute origin, and r_m is the distance measured relative to the origin of the mth vortex. The nondimensionalized angular momentum is taken as

$$J = -\frac{H}{\Gamma_1 A_1 + \Gamma_2 A_2}. \tag{3.2.47}$$

Using Romberg integration we evaluate the integrals in (3.2.43) according to the form (1.4.9) derived in §1.4.

The excess kinetic energy of the vortex pair is given by

$$T = \frac{1}{2} \sum_{m=1}^{2} \omega_m \iint_{V_m} \psi \, dx \, dy, \tag{3.2.48}$$

and is nondimensionalized as

$$\tilde{T} = \frac{T}{(\Gamma_1 + \Gamma_2)^2}. \tag{3.2.49}$$

The reduced kinetic energy is this quantity less the nondimensionalized kinetic energy of a circular vortex of the same total area and circulation, so that

$$\hat{T} = \tilde{T} - \frac{1}{16\pi} \left\{ 1 - 2 \log \left[(A_1 + A_2)/\pi \right] \right\}. \tag{3.2.50}$$

We evaluate the integral in (3.2.45) according to the derivation of §1.4, in which the integral of the stream function is expressed in terms of integrals of the steady shape expansions.

In Appendix D, we describe an alternate method derived by Saffman [1985a] for the corotating vortex pair. In the next section, the results of the Schwarz function analysis of the corotating vortex pairs are discussed.

3.3 The Corotating Vortex Pair

The corotating vortex pair consists of two vortex regions of given areas A_1 and A_2, and circulations Γ_1 and Γ_2, such that $\Gamma_1 + \Gamma_2 \neq 0$. These vortices rotate about the centroid of the system with constant angular velocity Ω, in accordance with the elementary laws of vortex dynamics.

Several authors have considered this configuration. Saffman & Szeto [1980] were the first to solve for solution shapes and energies of the symmetric corotating uniform pair. They solve the shape problem numerically by using Newton's method on an integro-differential equation that defines the vortex boundary.

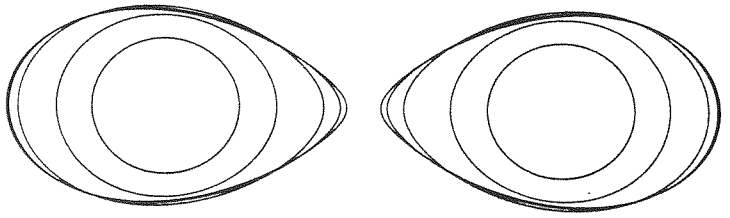

Figure 3.3 Corotating vortex pair solution shapes, scaled to the same inter-centroid distance. Solutions are shown for $\alpha = 0.10,\ 0.20,\ 0.30,\ 0.3120$ (lower branch), 0.3125 (upper branch).

Overman & Zabusky [1982a] obtain vortex pair shape solutions using a similar boundary integral method; they use perturbed and unperturbed steady states as initial conditions in a time-dependent contour dynamics code to study the merger of these regions. Dhanak [1985] and Dritschel [1985] consider polygonal arrays of symmetric uniform vortices, of which the pair is a special case. The former author derives perturbation series solutions, valid for small nondimensional areas, for both shapes and linear stability properties. The latter author obtains shape solutions by using a discretized boundary integral method to obtain a system of nonlinear equations, which he solves using an iterative technique of Pierrehumbert [1980]. Dritschel also studies numerically the energetics and linear stability characteristics of the pair and discusses the relationship of these properties.

Our shape results for the corotating vortex pair are summarized in Figures 3.3 and 3.4. Both areas are taken to be π, and the circulation of each region is set to one. For small nondimensional area α as defined in (3.2.3), the vortices are far apart and almost circular; in this case the rotation rate nearly equals that required to bring to rest point vortices of equivalent circulation, $\Omega_{pv} = -(\Gamma_1 + \Gamma_2)/(2\pi l^2)$. As α increases, the effects of finite area become pronounced as the regions deform and the relative rotation rate increases, as shown in Figure 3.4. Steady solutions are found for values of α up to the limiting value α_{max}, where $0.3125 < \alpha_{max} <$

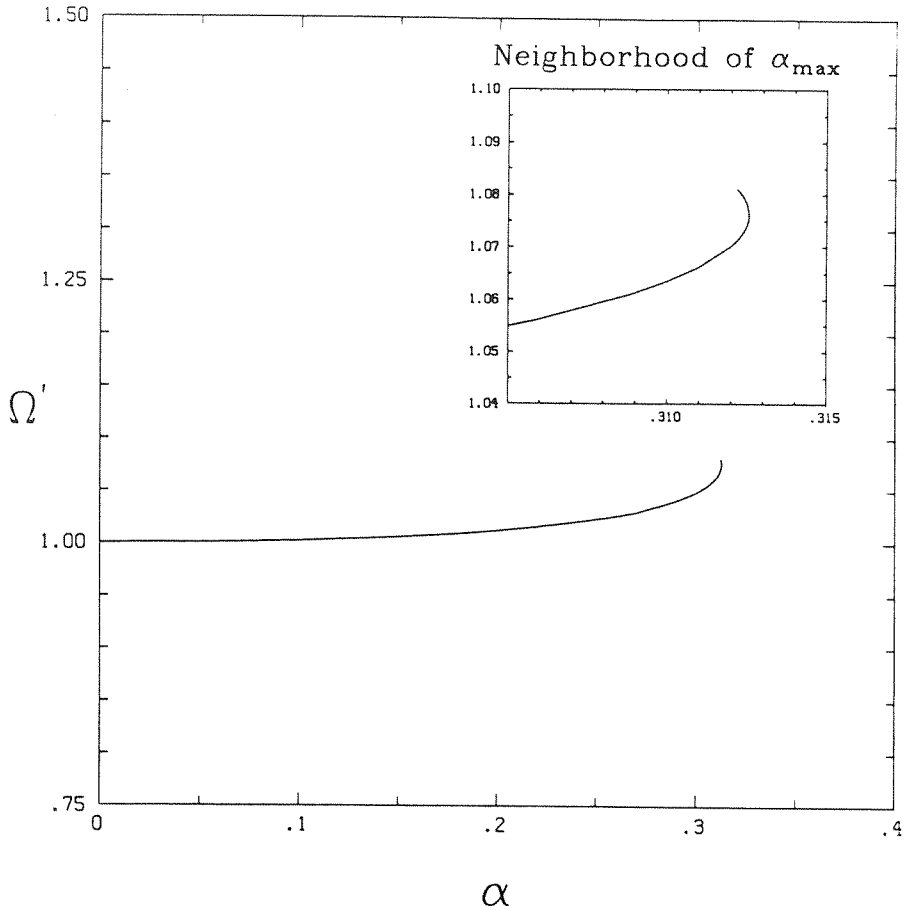

Figure 3.4 Corotating vortex pair rotation rate, nondimensionalized by that of point vortices with equivalent circulation located at the vortex centroids, versus nondimensional area, α.

0.3126; we obtain two possible steady solutions for $0.3122 < \alpha < \alpha_{max}$. The determinant of the Jacobian of the system remains one-signed and nonzero along the solution path on either side of the α-fold.

We did not seek to obtain solutions on the upper branch for $\alpha < 0.3122$; prior studies have documented upper branch solutions down to $\alpha \doteq 0.309$. The rotation rate of our solutions is found to agree with those of the previously mentioned authors to four significant figures. In the Schwarz function computations, $N = 8$ terms in the shape series are sufficient to obtain the small α solutions. For more deformed vortices, $N = 16$ terms were used, while $N = 32$ and $N = 48$ terms were taken to resolve solutions in the neighborhood of the maximum α. The

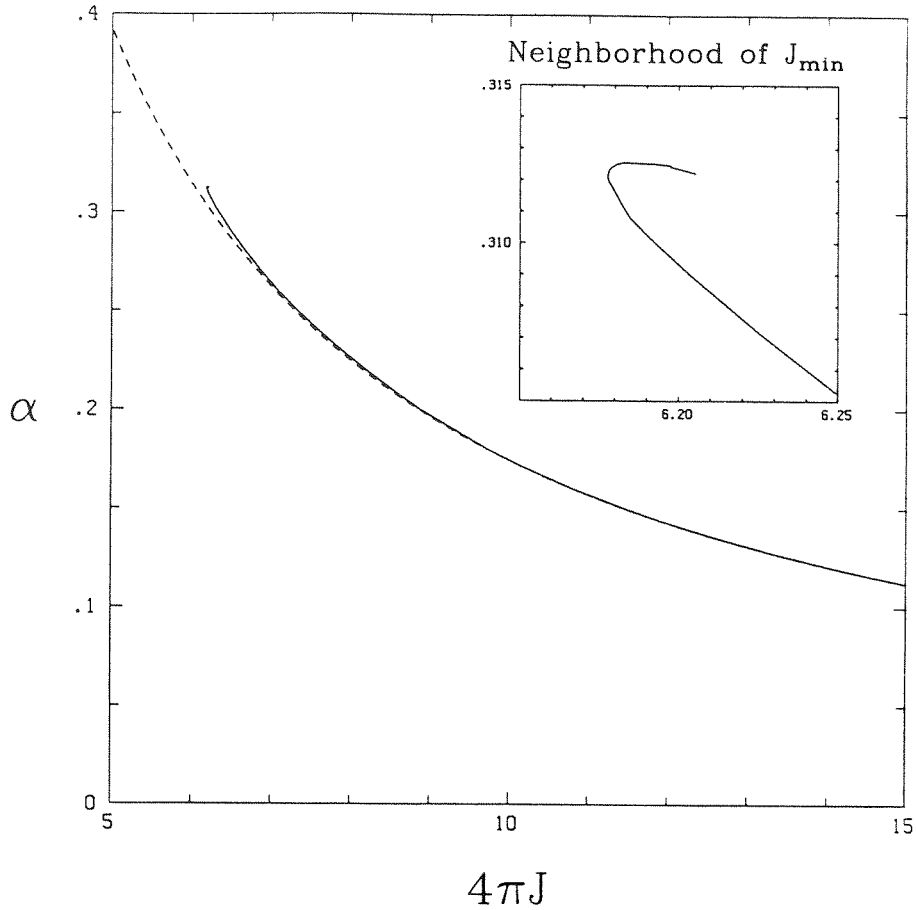

Figure 3.5 Area, α, versus angular momentum, J. The minimum of J occurs at a value of α less than α_{max}. The dashed line represents the values for the circular vortex approximation given in (3.3.1).

solutions obtained with the stream function formulation of Appendix D were found to agree to five figures with the Schwarz solutions up to $\alpha \doteq 0.250$, beyond which convergence required a very accurate initial guess and thus was not obtained due to finite computing resources.

The stability of this configuration has been a source of disagreement for some time. Saffman & Szeto discuss the stability of the corotating vortex pair in terms of the Kelvin energy argument mentioned in §2.3. This says that a steady state is a stationary point of the energy functional with respect to all area-preserving variations with the same circulation and angular momentum, i.e., all isovortical perturbations. This state is stable if it extremizes the kinetic energy functional

with respect to all other solutions with the same angular momentum. Considering $\hat{T}$ as a function of J, Saffman & Szeto obtain the energy data and infer the (neutral) stability of the lower branch of solutions (as depicted in Figure 3.4) up to the fold point in α, which, according to their calculations, corresponds to the minimum of angular momentum. Saffman & Szeto make this inference by claiming that these solutions are a local maxima (in our nondimensionalization) of the energy, as all other isovortical solutions have lower energy. The instability of the upper branch solutions is a consequence of this argument. Dritschel also obtains energy data for the vortex pair and in addition solves numerically for the linear stability characteristics of symmetric solution shapes. He finds an explicit change of stability at a value of $\alpha \doteq 0.3096$ on the lower solution branch, before the limiting values of either α or J (which, Dritschel finds, are not coincident); solutions for larger α, i.e., smaller J, and on the upper branch in α (or J) are found to be unstable. Moreover, the explicit change of stability Dritschel finds occurs before the fold in angular momentum, which Dritschel calculates to be at $\alpha \doteq 0.3120$. Dritschel reconciles the discrepancy between his findings and those of Saffman & Szeto by hypothesizing a bifurcation into a nonsymmetric solution (which his method of solution does not admit) at the point of stability change; to be consistent with the variational argument, the solutions along this hypothesized branch must be local maxima of the kinetic energy, so that the vortices on the lower branch for $0.3096 \lesssim \alpha \lesssim 0.3120$ do not extremize the energy functional and thus cannot be stable steady states. In a subsequent work, Dritschel [1986] argues the possibility of transition from a stable vortex pair solution to a stable single elliptical vortex solution near $\alpha \doteq 0.3096$.

We find, in agreement with Dritschel, that the symmetric elliptical mode is indeed the disturbance that undergoes a change of stability, while all other

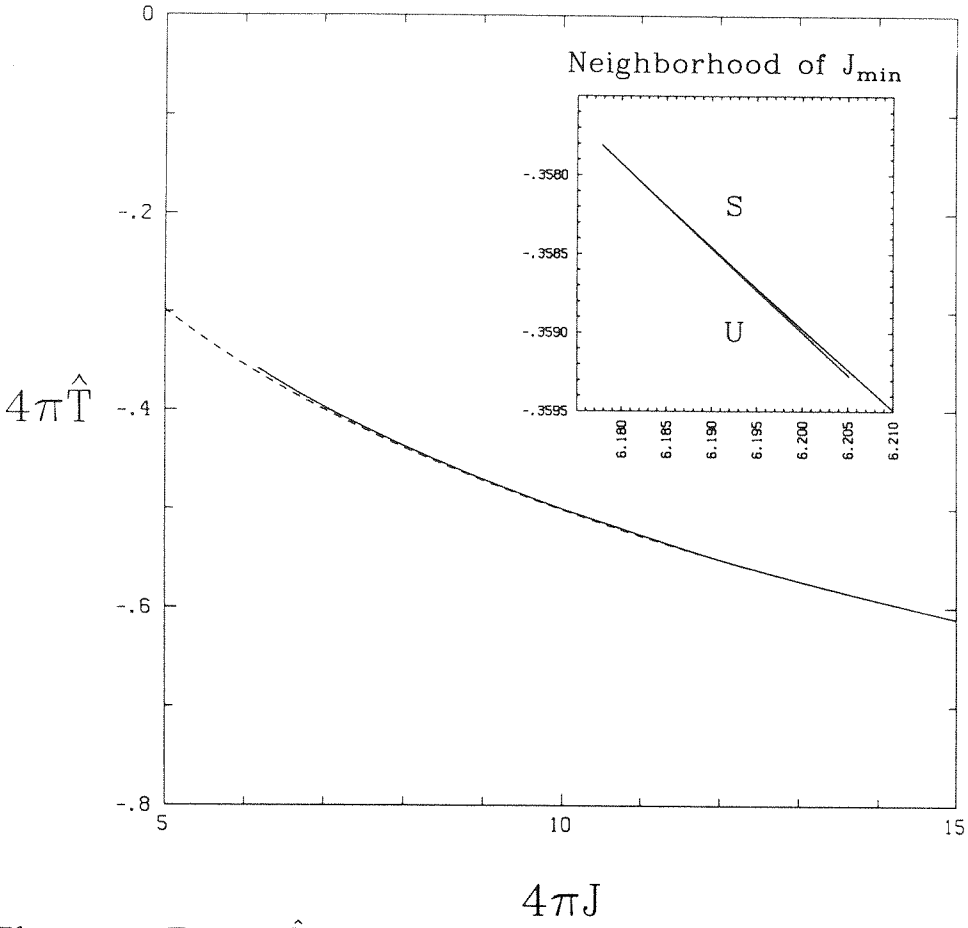

Figure 3.6 Energy, $\hat{T}$, versus angular momentum, J. The dashed line represents the values for the circular vortex approximation given in (3.3.1). The high energy branch corresponds to the stable solutions; the low energy branch consists of unstable solutions.

modes remain stable, as shown in Figure 3.7. Also, in near agreement with the numerical calculations of Dritschel but differing from those of Saffman & Szeto, we find that the angular momentum is minimized at $\alpha \doteq 0.3121$. However, differing from Dritschel both numerically and conceptually but agreeing with Saffman & Szeto theoretically, we compute the explicit change of stability to occur for the configuration that minimizes angular momentum and maximizes kinetic energy, as indicated in Figure 3.6.

As one check of the energy data for small α, we have the following analytic formulae, derived in Appendix C, for the kinetic energy and angular momentum of a pair of circular vortices, each of area A and circulation Γ, with centers separated

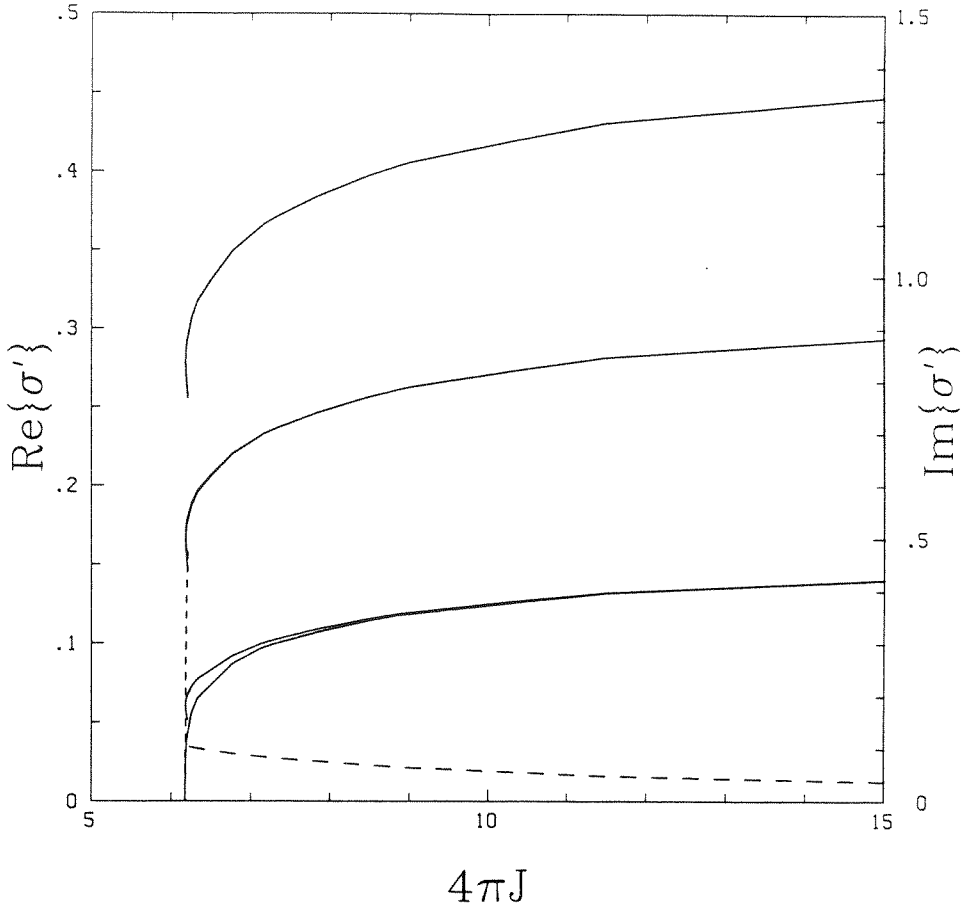

Figure 3.7 Eigenvalue, $\sigma' = \sigma/\omega_1$, versus angular momentum, J. The explicit change of stability occurs at the minimum of angular momentum. Purely imaginary quantities, denoted by solid lines, scale to the right vertical axis, as does the (imaginary) rotation rate eigenvalue, plotted as the coarsely dashed line. Real values, indicated by the finely dashed line, scale to the left vertical axis.

by a distance l, where $\alpha \equiv A/l^2$:

$$\hat{T} = -\frac{1}{32\pi}\left[1 - 2\log(4\alpha/\pi)\right], \qquad J = \frac{1}{8\pi}\left(2 + \pi/\alpha\right). \tag{3.3.1}$$

For large angular momentum (i.e., small α) these imply the following asymptotic relation:

$$\hat{T} \sim -\frac{1}{16\pi}\left[\log(2\pi J) + \frac{1}{2} - \frac{1}{4\pi J} + O\left(\frac{1}{(4\pi J)^2}\right)\right]. \tag{3.3.2}$$

These approximate results are depicted as dashed lines in Figures 3.5 and 3.6 and agree with the exact solution for a range of α values.

We find, as did previous investigators, that the calculations in the region of

Corotating Vortex Pair Energy Data			
α	$\Omega' = \Omega/\Omega_{pv}$	J	$\hat{T}$
0.0	1.000	∞	$-\infty$
0.001	1.000	125.08	-0.1426
0.005	1.000	25.08	-0.1105
0.010	1.000	12.58	-0.09676
0.050	1.001	2.580	-0.06473
0.100	1.002	1.330	-0.05093
0.150	1.006	0.9135	-0.04284
0.200	1.012	0.7059	-0.03709
0.250	1.024	0.5824	-0.03263
0.300	1.049	0.5034	-0.02908
0.310	1.063	0.4928	-0.02854
0.3120	1.070	0.4916	-0.02847
0.3121	1.071	0.4916	-0.02847
0.3122	1.071	0.4916	-0.02847
0.3123	1.072	0.4916	-0.02848
0.3124	1.073	0.4917	-0.02848
0.3125	1.074	0.4918	-0.02849
0.3125	1.078	0.4928	-0.02854
0.3124	1.079	0.4932	-0.02856
0.3123	1.080	0.4935	-0.02857
0.3122	1.081	0.4938	-0.02859

Table 3.1 Rotation rate and energy data for the corotating vortex pair.

interest are quite sensitive. The energy and angular momentum values change less than 0.1% between the solutions with $N = 16$ and $N = 32$ modes; these data match values interpolated from Dritschel's data to three significant figures. As stated in §3.2, the value of the neutral eigenvalue corresponding to the symmetric shift eigenmode was monitored for all solutions; for the $N = 48$ calculations, this quantity remained below 10^{-4} for the lower branch solutions with $0.3120 \leq \alpha \leq 0.3123$. Also, in his stability analysis Dritschel imposes the constancy of angular momentum for all perturbations; we do not require this constraint explicitly. Our computations indicate that the linearized angular momentum variation is indeed nonzero for the perturbed vortex states. The imposition of this constraint on

the Schwarz formulation and the subsequent effect on the perturbation remain unstudied problems.

The behavior of the numerically computed eigenvectors near the state with minimum angular momentum suggests the phenomenon described by Saffman [1985b] for finite amplitude water waves, namely, that the area-preserving zero eigenvalue has algebraic multiplicity four and geometric multiplicity one at the point of stability change. Consistent with this property is the lack of indication of a bifurcated solution branch. Also in keeping with this theory, there is no change of stability at $\alpha = \alpha_{max}$, where there should be two linearly independent eigenvectors corresponding to the area-preserving zero eigenvalue; we have not resolved the exact location of the fold point to verify this conjecture. We cannot offer analytic proof of these results, but believe the advances in the application of the Hamiltonian formulation of inviscid vortex dynamics (e.g., Hebert [1983], Jiménez [1986a], MacKay [1986]) may provide the necessary tools for such justification.

Chapter 4

The Single Infinite Row

4.1 Introduction

The configurations we have considered up to this point have consisted of finitely many vortices. We now apply the method of Schwarz functions to a straight row of infinitely many, regularly spaced, equivalent regions of uniform, constant vorticity. This configuration can be taken as a model of a developed shear layer (Christiansen & Zabusky [1973], Moore & Saffman [1975], Saffman [1981], Saffman & Szeto [1981], Pierrehumbert & Widnall [1981]), for which the stability properties are of considerable interest.

This geometry has been previously studied by using point vortices, analytically in the simplest case by Lamb [1945], and numerically with large-scale point vortex simulations by several authors, as reviewed by Aref [1983]. Moore & Saffman [1975] and Saffman & Szeto [1981] use elliptical regions of constant vorticity in their shear layer models. Saffman & Szeto [1981] and Pierrehumbert & Widnall [1981] numerically obtain solutions of the Euler equations for the infinite array of regions of constant vorticity. The former authors formulate the problem using a discretized boundary integral method and thereby obtain a system of nonlinear equations, which they solve by Newton's method. The latter authors formulate the problem in a similar fashion, but solve the resulting equations via an iterative technique developed by Pierrehumbert [1980].

In applying the method of Schwarz functions to this problem, we utilize the techniques developed by MSS in their model of the infinite Kármán vortex street.

They describe the considerations necessary to make tractable the analysis of the infinite number of vortices present, a situation which complicates the stability analysis of the problem.

To check the Schwarz function results, we develop an analytical model for the single array using elliptically desingularized vortices. Based on the theory developed by Melander, Styczek & Zabusky [1984] and Melander, Zabusky & Styczek [1986], this approximation is valid for elliptical vortices of small nondimensionalized area.

The shape solutions we calculate match those previously obtained, and the stability data we obtain numerically verify the results of the qualitative energy arguments of Saffman & Szeto. We find that the subharmonic disturbance of twice the period of the array spacing is indeed the linearly most unstable disturbance for this configuration.

4.2 Formulation

The Schwarz function formulations of the double infinite row vortex shape and stability problems were given by MSS; we modify that presentation for solution of the single infinite array.

We assume all vortices have the same shape, so that each vortex boundary is given by the same expansion

$$z = a_0\zeta\,(1 + a_1/\zeta + \cdots + a_n/\zeta^n + \cdots)\,, \tag{4.2.1}$$

where ζ is taken as the unit circle. The regions are assumed to have the same uniform vorticity $\omega_0 = \Gamma/A$, where Γ is the circulation of each region and A its area. The centroids of the vortices are separated by distance l, which may be complex: the phase of l specifies the angle between the x-axis and the direction parallel to the row. The configuration for real l is depicted in Figure 4.1. The

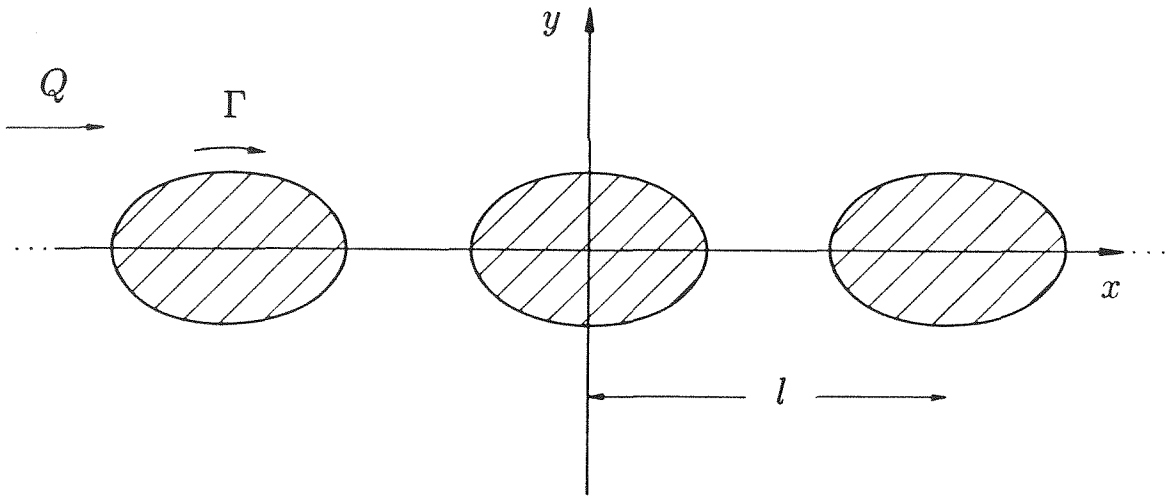

Figure 4.1 The single infinite vortex array.

origins of the vortices are taken to be at ml, $m \in \mathbb{Z}$. Thus, the total fluid velocity at a point z relative to one of the vortices is expressed as

$$u - iv = -\frac{i\omega_0}{2} \sum_{n=0}^{\infty} \sum_{m=-\infty}^{\infty} \frac{g_n}{(z - ml)^{n+1}} + Q, \tag{4.2.2}$$

where g_n is the nth Schwarz coefficient, given by (1.2.10), and constant external velocity $Q = U - iV$ is assumed. The velocity field for large values of $|z/l|$ is

$$u - iv \sim -\frac{i\Gamma}{2l} \cot\left(\frac{\pi z}{l}\right) + Q + o(1), \qquad |z/l| \to \infty. \tag{4.2.3}$$

The velocity far from the array is obtained by considering the limit $\left|\Im\{z/l\}\right| \to \infty$, which implies

$$U_\infty - iV_\infty \sim -\frac{i\Gamma}{2l} \operatorname{sgn}\left(\Im\{z/l\}\right) + Q + o(1). \tag{4.2.4}$$

For a steady vortex array, the first term in (4.2.4) corresponds to the induced far-field velocity; that the external velocity Q is found to be zero is one check of the numerical computations. The conjugate velocity has a representation similar to (4.2.2) with i replaced by $-i$, l by l^*, and the other coefficients by starred quantities, which are assumed independent of the actual complex conjugates.

To obtain steady shapes, we begin by substituting these expressions into the governing boundary condition (1.2.22). Since all vortex regions are assumed to

be equivalent, the boundary condition need only be satisfied on one vortex. As in the solution for the vortex pair, we effectively obtain an expansion of the solution as a power series in α by expanding the solution as a power series in $1/l$. The shape expansions are first truncated to order N in ζ, the velocity expansions are truncated at order $N+1$ in z, and the resulting series is expanded in $1/l$. In analogy with Equation (3.2.16) we obtain, for $m \neq 0$,

$$\frac{1}{(z-ml)^{n+1}} = \sum_{p=0}^{\infty} (-l)^{-(n+p+1)} \frac{(n+p)!}{n!\,p!} \frac{(-z)^p}{m^{(n+p+1)}} \,. \tag{4.2.5}$$

Substituting this expression into the velocity expansion (4.2.2), truncating the series to retain terms of order l^{-L}, and re-arranging terms we obtain

$$u - iv = -\frac{i\omega_0}{2} \left\{ \sum_{n=0}^{N} \frac{g_n}{z^{n+1}} + \sum_{n=0}^{N} \sum_{p=0}^{L-n-1} g_n (-l)^{-(n+p+1)} \frac{(n+p)!}{n!\,p!} (-z)^p \sum_{m=-\infty}^{\infty}{}' \frac{1}{m^{n+p+1}} \right\} + Q, \tag{4.2.6}$$

where the primed summation denotes exclusion of the $m = 0$ term. A similar expression is obtained for the conjugate velocity. As shown by MSS and derived in Appendix E, the m-sum term can be evaluated directly.

Substituting the truncated expansions into the boundary condition and equating the coefficients of ζ^k to zero, we obtain $2N+1$ equations for the $2N+4$ unknowns given by the shape coefficients and the velocities Q and Q^*. We eliminate one unknown by setting $a_0 = a_0^*$. By the arguments presented in Appendix A, the equation obtained by equating the coefficient of ζ^0 to zero is not independent, and is thus excluded. An equation specifying the vortex area, as in (2.2.8), and the two centroid equations $g_1 = g_1^* = 0$ are included to give a total of $2N+3$ equations. The system is found to be nonsingular, and solutions were obtained for a range of α values.

The stability problem for the infinite arrays is more complex than that of the configurations with finitely many vortices, as we seek to study the response

of the system to a perturbation of prescribed wavelength, in addition to the self-oscillations of the vortices. For the infinite array of vortices with periodic spacing l we denote by p the wavenumber of the infinitesimal disturbance to the steady solution. Without loss of generality, p is restricted to the range $0 \leq p \leq 1$, since incrementing p by an integer is equivalent to relabeling a perturbation eigenvector, as shown by MSS. Two cases are distinguished: (1) $p = 0$ (superharmonic disturbance) implies the perturbation has the same spatial period as the steady state, and (2) $p \neq 0$ (subharmonic disturbances) implies the perturbation has wavelength l/p or $(1-l)/p$, i.e., greater that l. The governing equation is the linearized time-dependent boundary condition given by (1.3.8):

$$(U - iV)\frac{\partial z'}{\partial \theta} + (u' - iv')\frac{\partial Z}{\partial \theta} - (U + iV)\frac{\partial z^{*\prime}}{\partial \theta} - (u' + iv')\frac{\partial Z^*}{\partial \theta} = \sigma \left\{ z^{*\prime}\frac{\partial Z}{\partial \theta} - z'\frac{\partial Z^*}{\partial \theta} \right\}. \tag{4.2.7}$$

In principle this must be satisfied on the boundary of each of the vortices, as the oscillations of each vortex may be different. The answer to this problem, which also occurs in the stability analysis of the double infinte rows, is given by MSS and is now reviewed and applied to the single array.

With $(u - iv)_m$ denoting the velocity induced by the vortex centered at ml, the linearized perturbation to this velocity caused by the perturbation to the jth shape coefficient of the mth vortex, $a'^{(m)}_j$, is given in (1.3.13); i.e.,

$$(u' - iv')_m = \frac{d(u - iv)}{da^{(m)}_j} a'^{(m)}_j. \tag{4.2.8}$$

Given the assumption that all of the vortices in the array have the same shape expansion, i.e., $a^{(m)}_j = a_j$ for all m, the derivative in (4.2.8) is the same function of the argument $z - ml$ for each vortex, i.e., for each value of the index m. We consider perturbations with wavelength l/p, so the shape perturbation of the mth

vortex is related to that of the zeroth vortex by

$$a'^{(m)}_j = a'_j e^{im\lambda}, \quad \tilde{a}'^{(m)}_j = \tilde{a}'_j e^{im\lambda}, \quad \text{where} \quad \lambda \equiv 2\pi p. \tag{4.2.9}$$

We are thus able to restrict the evaluation of the boundary condition governing stability to a single vortex.

We now address the evaluation of the governing equation for a perturbation to the jth shape coefficient. According to the procedures of §§1.3 and 3.2, each term in the right side of equation (4.2.7) is evaluated explicitly as a power series in ζ; thus, the entire right side is given as a power series in ζ. The two contributions to the velocity disturbance $u' - iv'$ on the left side of the stability equation are: (1) that induced by the perturbed vortex shape in the steady velocity field, and (2) that computed with the steady vortex boundary in the correspondingly perturbed velocity field. The first of these, $(u' - iv')_{j,vortex}$, is given by taking the variation of the velocity field given in (4.2.2):

$$(u' - iv')_{j,vortex} = \frac{d}{dz}(u - iv)\bigg|_{z=Z} z'_j \tag{4.2.10}$$

$$= \frac{d}{dz}\left[-\frac{i\omega_0}{2}\sum_{n=0}^{\infty}\sum_{m=-\infty}^{\infty}\frac{g_n}{(z-ml)^{n+1}}\right]\bigg|_{z=Z} z'_j, \tag{4.2.11}$$

where Z is the steady shape solution and z'_j is the perturbation to the shape due to a'_j. As the external velocity Q is constant, its contribution to this term is zero. The second contribution, $(u' - iv')_{j,velocity}$, is calculated using relation (4.2.9) as

$$(u' - iv')_{j,velocity} = -\frac{i\omega_0}{2}\sum_{n=0}^{\infty}\sum_{m=-\infty}^{\infty}\frac{g'_{n,j}e^{im\lambda}}{(Z-ml)^{n+1}}, \tag{4.2.12}$$

where $g'_{n,j}$ denotes the perturbation to the Schwarz coefficients due to the shape perturbation a'_j. The exponential attenuation to the perturbed Schwarz coefficient is a consequence of (4.2.9) and reflects the assumed periodicity (with wavenumber p) of the induced velocity variation at the mth vortex.

These contributions are incorporated into the left side of Equation (4.2.7), which is computed numerically in two parts. The first two terms of the addend

$$(U-iV)\frac{\partial z'_j}{\partial\theta}+(u'-iv')_{j,vortex}\frac{\partial Z}{\partial\theta}-(U+iV)\frac{\partial z^{*\prime}_j}{\partial\theta}-(u'+iv')_{j,vortex}\frac{\partial Z^*}{\partial\theta}, \quad (4.2.13)$$

are calculated as the central difference approximation given by

$$\sum_{k=-N}^{N}\frac{1}{2\varepsilon}\left[R_1(k;a_j+\varepsilon)-R_1(k;a_j-\varepsilon)\right]\zeta^k. \quad (4.2.14)$$

The term $\sum_{k=-N}^{N} R_1(k;a_j\pm\varepsilon)\,\zeta^k$ is given by the product of the truncated velocity expansion (4.2.6), into which the perturbed shape is substituted, and the boundary derivative of the perturbed shape, i.e.,

$$\sum_{k=-N}^{N} R_1(k;a_j\pm\varepsilon)\zeta^k=-\frac{i\omega_0}{2}\left\{\sum_{n=0}^{N}\frac{g_n}{[z(a_j\pm\varepsilon)]^{n+1}}\right.$$
$$\left.+\sum_{n=0}^{N}\sum_{p=0}^{L-n-1} g_n(-l)^{-(n+p+1)}\frac{(n+p)!}{n!\,p!}[-z(a_j\pm\varepsilon)]^p\sum_{m=-\infty}^{\infty}{}'\frac{1}{m^{n+p+1}}+Q\right\}\frac{\partial}{\partial\theta}[z(a_j\pm\varepsilon)]. \quad (4.2.15)$$

Direct expansion of the central difference of this expression, as in (4.2.14), yields the first two terms in (4.2.13) plus quantities that are $O(\varepsilon^2)$. The remaining terms in (4.2.13) are evaluated similarly.

The second addend to the left side of the governing equation is

$$(u'-iv')_{j,velocity}\frac{\partial Z}{\partial\theta}-(u'+iv')_{j,velocity}\frac{\partial Z^*}{\partial\theta}. \quad (4.2.16)$$

The first term here is approximated as

$$\sum_{k=-N}^{N}\frac{1}{2\varepsilon}\left[R_2(k;a_j+\varepsilon)-R_2(k;a_j-\varepsilon)\right]\zeta^k, \quad (4.2.17)$$

where $\sum_{k=-N}^{N} R_2(k; a_j \pm \varepsilon)\,\zeta^k$ is the product of the truncated array-induced perturbation velocity expansion and the θ-derivative of the steady shape. Thus,

$$\sum_{k=-N}^{N} R_2(k; a_j \pm \varepsilon)\zeta^k = -\frac{i\omega_0}{2}\left\{\sum_{n=0}^{N}\frac{g_n'(a_j \pm \varepsilon)}{[Z(a_j)]^{n+1}} + \sum_{n=0}^{N}\sum_{p=0}^{L-n-1} g_n'(a_j \pm \varepsilon)(-l)^{-(n+p+1)}\frac{(n+p)!}{n!\,p!}[-Z(a_j)]^p \sum_{m=-\infty}^{\infty}{}' \frac{e^{im\lambda}}{m^{n+p+1}}\right\}\frac{\partial}{\partial\theta}[Z(a_j)], \tag{4.2.18}$$

where $g_n'(a_j \pm \varepsilon)$ is the difference of the perturbed and steady Schwarz coefficients, as in (2.2.24). Using this expansion and a similar one for the conjugate term, we obtain a second-order valid approximation to (4.2.16). The explicit evaluation of the m-sum terms in these expressions is described in MSS and derived in Appendix E.

The left side of the boundary condition (4.2.7) for the perturbation to the jth shape coefficient is taken as the sum of these contributions. Repeating this calculation for each of the shape coefficients and equating the coefficients of like powers of ζ on each side of the governing equation yields $2N+1$ equations in $2N+1$ unknowns. We write the resulting matrix system as

$$\mathbf{M}\,\mathbf{v} = \sigma\,\mathbf{N}\,\mathbf{v}, \tag{4.2.19}$$

where $\mathbf{M}$ depends on the steady shapes and the wavenumber p, $\mathbf{N}$ depends on the steady shapes, and $\mathbf{v}$ is the complex array of perturbation coefficients with elements

$$v_1 = \tilde{a}_N', \ldots, v_{N+1} = \tilde{a}_0' = a_0', \ldots, v_{2N+1} = a_N'. \tag{4.2.20}$$

This system was solved using EISPACK routines.

For a given wavenumber p, a single zero eigenvalue is found whose eigenmode does not conserve area and corresponds to an array of vortices whose linearized

shape variations differ from those of the steady state by $O(1)$. The remaining $2N$ eigenvalues occur in pairs, σ_1 and σ_2, corresponding to the 1st through Nth eigenmodes. For superharmonic disturbances, the $k = 1$ cooperative eigenmode has a pair of zero eigenvalues with two linearly independent eigenvectors, which correspond to a uniform translation of the array without change of shape; the eigenvalues of the remaining modes are found to be nonzero. For subharmonic disturbances, we obtain the nonzero cooperative eigenvalue pair in addition to the eigenvalues of the 2nd through Nth shape modes. If a mode is stable, i.e., $\Re\{\sigma\} = 0$, then $\sigma_2 = \sigma_1^*$. In this case, analysis of the eigenmodes follows the discussion for the single vortex in §2.2 and indicates property (2.2.30) for the corresponding eigenvectors. The unstable modes have purely real eigenvalues, so that $\sigma_2 = -\sigma_1$. As for the single vortex, we find relation (2.2.31) is valid for the associated eigenvectors in this case. As indicated in MSS, to construct physically realized perturbations for single array vortices, one must combine eigenstates for disturbances of wavenumber p with those of wavenumber $1 - p$ to insure that the conjugate of the perturbation is the perturbation of a conjugate state.

4.3 Elliptically Desingularized Model

To check the results of the Schwarz function infinite array calculations described in the preceding section, we now consider a model of the infinite array using elliptically desingularized regions of uniform vorticity as suggested by Melander *et al.* [1984, 1986]. This approach provides Hamiltonian evolution equations for the position, orientation, and aspect ratio of uniform vortices of elliptical shape. These equations are obtained using a moment representation for each vortex and performing a perturbation expansion in the small parameter given by the ratio of the maximum vortex dimension to the minimum vortex intercentroid distance; truncating all moments of order greater than two yields the elliptical approxima-

tion. For details of this derivation, see Melander *et al.* [1986], wherein elliptically desingularized approximations of the corotating vortex pair and the translating vortex pair are studied. In this section, we apply this method to the single infinite array of vortices to obtain analytical expressions for the aspect ratio of the steady states as well as the growth rates of the linearized stability problem.

Assume the kth elliptical vortex has area A_k, circulation Γ_k, semimajor axis a_k, and semiminor axis b_k. Following Melander *et al.* [1986], we denote the position of the centroid of the kth vortex, equivalent to the center of the kth ellipse, by (x_k, y_k), the aspect ratio by $\lambda_k = a_k/b_k$, and the angle of orientation of the major axis with respect to the x-axis by ϕ_k. It proves convenient to introduce the independent variables δ_k, γ_k, and the quantity U_k, defined as

$$\delta_k \equiv \left(\frac{A_k}{8\pi\lambda_k}\right)^{1/2} (\lambda_k - 1)\cos 2\phi_k, \tag{4.3.1}$$

$$\gamma_k \equiv \left(\frac{A_k}{8\pi\lambda_k}\right)^{1/2} (\lambda_k - 1)\sin 2\phi_k, \tag{4.3.2}$$

$$U_k \equiv \left(\delta_k^2 + \gamma_k^2 + \frac{A_k}{2\pi}\right)^{1/2}. \tag{4.3.3}$$

The kinetic energy and equations of motion for each vortex are obtained by summing the effects of each of the other vortices. For a collection of finitely many elliptically desingularized vortices, it can be shown that the Hamiltonian, equal to the excess energy, is given by the expression

$$H = -\frac{1}{2}\iint_{\mathbb{R}^2} \omega\psi \, dx\, dy = \frac{1}{8\pi}\sum_{k=1}^{N}\left\{\Gamma_k^2 \log\left[1 + \frac{2\pi}{A_k}\left(\delta_k^2 + \gamma_k^2\right)\right] - \frac{\Gamma_k^2}{2} + \sum_{j=1}^{N}{}' \Gamma_k\Gamma_j \log R_{kj}^2 \right.$$
$$\left. - 2\sum_{j=1}^{N}{}' \frac{\Gamma_k\Gamma_j}{R_{kj}^2}\left[\frac{\cos 2\theta_{kj}}{R_{kj}^2}(\delta_k U_k + \delta_j U_j) + \frac{\sin 2\theta_{kj}}{R_{kj}^2}(\gamma_k U_k + \gamma_j U_j)\right]\right\}, \tag{4.3.4}$$

where the primed summation denotes exclusion of the $j = k$ terms, and R_{kj} denotes the intercentroid distance given by

$$R_{kj}^2 \equiv (x_k - x_j)^2 + (y_k - y_j)^2. \tag{4.3.5}$$

The equations of motion can be shown to assume the Hamiltonian form:

$$\Gamma_k \dot{x}_k = -\frac{\partial H}{\partial y_k}, \qquad \Gamma_k \dot{\delta}_k = -\frac{\partial H}{\partial \gamma_k}, \tag{4.3.6}$$

$$\Gamma_k \dot{y}_k = \frac{\partial H}{\partial x_k}, \qquad \Gamma_k \dot{\gamma}_k = \frac{\partial H}{\partial \delta_k}. \tag{4.3.7}$$

For the single infinite array of uniform elliptically desingularized vortices, the equations describing the interaction of each pair of vortices are equivalent to those in the case of finitely many vortices. Hence, the kinetic energy for an array of vortices with equal area A and equal circulation Γ is given by

$$H = \frac{\Gamma^2}{8\pi} \sum_{k=-\infty}^{\infty} \left\{ \log\left[1 + \frac{2\pi}{A}\left(\delta_k^2 + \gamma_k^2\right)\right] - \frac{1}{2} + \sum_{j=-\infty}^{\infty}{}' \log R_{kj}^2 \right.$$
$$\left. - 2 \sum_{j=-\infty}^{\infty}{}' \left[\frac{\cos 2\theta_{kj}}{R_{kj}^2}(\delta_k U_k + \delta_j U_j) + \frac{\sin 2\theta_{kj}}{R_{kj}^2}(\gamma_k U_k + \gamma_j U_j) \right] \right\}. \tag{4.3.8}$$

As for infinitely many point vortices, the excess energy is infinite; however, it is not the energy per se that governs the motion, but its derivatives that determine configurations and their stability.

We consider the configuration of equivalent vortices uniformly spaced a distance l apart along the x-axis, and thus restrict our analysis to the zeroth vortex, which we assume is centered at the origin. By taking the derivatives of the Hamiltonian in accordance with (4.3.6)–(4.3.7), we obtain the equations of motion for the position and orientation of the zeroth vortex. Since we seek solutions in which all vortices are equivalent, we write

$$\delta \equiv \delta_0 = \delta_k, \quad \gamma \equiv \gamma_0 = \gamma_k, \quad U \equiv U_0 = U_k. \tag{4.3.9}$$

Furthermore, introducing the notation

$$\Delta x_{kj} \equiv x_k - x_j, \quad \Delta y_{kj} \equiv y_k - y_j, \tag{4.3.10}$$

we express the trigonometric functions in these expressions in terms of the coordinates of the vortex centers via the relationships

$$\cos 2\theta_{kj} = \frac{(\Delta x_{kj})^2 - (\Delta y_{kj})^2}{(\Delta x_{kj})^2 + (\Delta y_{kj})^2}, \qquad \sin 2\theta_{kj} = \frac{2\Delta x_{kj}\Delta y_{kj}}{(\Delta x_{kj})^2 + (\Delta y_{kj})^2}. \tag{4.3.11}$$

The equations of motion of the zeroth vortex are obtained as

$$\frac{dx_0}{dt} = -\frac{\Gamma}{2\pi}\left\{ \sum_{j=-\infty}^{\infty}{}' \frac{\Delta y_{0j}}{R_{0j}^2} + 2 \sum_{j=-\infty}^{\infty}{}' \left[\delta U \frac{3(\Delta x_{0j})^2 \Delta y_{0j} - (\Delta y_{0j})^3}{R_{0j}^6} \right.\right.$$
$$\left.\left. + \gamma U \frac{3\Delta x_{0j}(\Delta y_{0j})^2 - (\Delta x_{0j})^3}{R_{0j}^6} \right] \right\}, \tag{4.3.12}$$

$$\frac{dy_0}{dt} = \frac{\Gamma}{2\pi}\left\{ \sum_{j=-\infty}^{\infty}{}' \frac{\Delta x_{0j}}{R_{0j}^2} - 2 \sum_{j=-\infty}^{\infty}{}' \left[\delta U \frac{3\Delta x_{0j}(\Delta y_{0j})^2 - (\Delta x_{0j})^3}{R_{0j}^6} \right.\right.$$
$$\left.\left. - \gamma U \frac{3(\Delta x_{0j})^2 \Delta y_{0j} - (\Delta y_{0j})^3}{R_{0j}^6} \right] \right\}, \tag{4.3.13}$$

$$\frac{d\delta}{dt} = -\frac{\Gamma}{4\pi}\frac{\gamma}{U^2}\left(1 - \frac{2\pi^2}{3L^2}\delta U\right), \tag{4.3.14}$$

$$\frac{d\gamma}{dt} = \frac{\Gamma}{4\pi}\left(\frac{\delta}{U^2} - \frac{2\pi^2}{3L^2}\frac{\delta^2 + U^2}{U}\right). \tag{4.3.15}$$

We equate the above time derivatives to zero to obtain the steady states of this system. Clearly, the center coordinates $(x_k, y_k) = (kl, 0)$ imply that the time derivatives of x_0 and y_0 vanish. Substituting these positions into the evolution equations for δ and γ, simplifying, and expressing δ and γ in terms of the aspect ratio λ and angle of orientation ϕ, we obtain the coupled system of equations

$$\frac{\lambda - 1}{\lambda + 1}\sin 2\phi \left[1 - \frac{\pi\alpha}{12}\frac{\lambda^2 - 1}{\lambda}\cos 2\phi\right] = 0, \tag{4.3.16}$$

$$\frac{\lambda - 1}{\lambda + 1}\cos 2\phi - \frac{\pi\alpha}{12}\frac{(\lambda + 1)^2}{\lambda}\left[1 + \left(\frac{\lambda - 1}{\lambda + 1}\right)^2 \cos^2 2\phi\right] = 0. \tag{4.3.17}$$

The correct solution to these equations is found by requiring $\sin 2\phi = 0$; i.e., $\phi = 0$ or $\phi = \pi/2$. This satisfies (4.3.16) and, from (4.3.17), yields the following cubic equation for the aspect ratio:

$$\lambda^3 + \left(1 \pm \frac{6}{\pi\alpha}\right)\lambda^2 + \left(1 \mp \frac{6}{\pi\alpha}\right)\lambda + 1 = 0, \tag{4.3.18}$$

where the $\{-,+\}$ combination corresponds to $\phi = 0$, and $\{+,-\}$ to $\phi = \pi/2$. Clearly, if λ is a solution for one choice of angle (i.e., $\phi = 0$ or $\phi = \pi/2$), then $1/\lambda$ is a solution of the the equation corresponding to the other angle (i.e., $\phi = \pi/2$ or $\phi = 0$). We expect λ to be near 1 for small α and to increase as α does; a root of Equation (4.3.18) for $\phi = 0$ is found that satisfies this behavior:

$$\lambda \sim 1 + \frac{2\pi}{3}\alpha + \frac{2\pi^2}{9}\alpha^2 + O(\alpha^3) \quad \text{as} \quad \alpha \to 0. \tag{4.3.19}$$

The steady states of this system provide the basis upon which we make a linear stability analysis; the Hamiltonian formulation is particularly well suited to this undertaking. We perturb each of the canonical variables in the Hamiltonian and linearize to obtain the perturbed Hamiltonian. Likewise, linearization of the Hamiltonian equations of motion provides the stability equations for the perturbed quantities. After some algebra, we find the first-order Hamiltonian given by

$$\begin{aligned}
H' = \frac{\Gamma^2}{4\pi} \sum_{k=-\infty}^{\infty} \Bigg\{ & \frac{\delta_k'\delta_k + \gamma_k'\gamma_k}{U_k^2} + \sum_{j=-\infty}^{\infty}{}' \frac{\Delta x_{kj}'\Delta x_{kj} + \Delta y_{kj}'\Delta y_{kj}}{R_{kj}^2} \\
& - 2 \sum_{j=-\infty}^{\infty}{}' \frac{\Delta x_{kj}\left[3(\Delta y_{kj})^2 - (\Delta x_{kj})^2\right]}{R_{kj}^6}\left[\Delta x_{kj}'(\delta_k U_k + \delta_j U_j) - \Delta y_{kj}'(\gamma_k U_k + \gamma_j U_j)\right] \\
& - 2 \sum_{j=-\infty}^{\infty}{}' \frac{\Delta y_{kj}\left[(\Delta y_{kj})^2 - 3(\Delta x_{kj})^2\right]}{R_{kj}^6}\left[\Delta y_{kj}'(\delta_k U_k + \delta_j U_j) - \Delta x_{kj}'(\gamma_k U_k + \gamma_j U_j)\right] \\
& - \sum_{j=-\infty}^{\infty}{}' \frac{\cos 2\theta_{kj}}{R_{kj}^2}\left[\frac{\delta_k(\delta_k'\delta_k + \gamma_k'\gamma_k)}{U_k} + \frac{\delta_j(\delta_j'\delta_j + \gamma_j'\gamma_j)}{U_j} + \delta_k' U_k + \delta_j' U_j\right] \\
& - \sum_{j=-\infty}^{\infty}{}' \frac{\sin 2\theta_{kj}}{R_{kj}^2}\left[\frac{\gamma_k(\delta_k'\delta_k + \gamma_k'\gamma_k)}{U_k} + \frac{\gamma_j(\delta_j'\delta_j + \gamma_j'\gamma_j)}{U_j} + \gamma_k' U_k + \gamma_j' U_j\right]\Bigg\}.
\end{aligned} \tag{4.3.20}$$

Linearization of the governing Equations (4.3.6)–(4.3.7) yields the Hamiltonian system governing first-order stability:

$$\Gamma_k \dot{x}_k' = -\frac{\partial H'}{\partial y_k}, \qquad \Gamma_k \dot{\delta}_k' = -\frac{\partial H'}{\partial \gamma_k}, \tag{4.3.21}$$

$$\Gamma_k \dot{y}_k' = \frac{\partial H'}{\partial x_k}, \qquad \Gamma_k \dot{\gamma}_k' = \frac{\partial H'}{\partial \delta_k}. \tag{4.3.22}$$

The linear stability of the steady states to subharmonic disturbances is studied by substituting the steady-state values into the derivatives of the perturbed Hamiltonian and assuming normal mode perturbations for all primed variables of the form $x'_k = e^{i2k\pi p}x'_0$. The above equations for the perturbations yield the matrix equation

$$\frac{d\mathbf{v}}{dt} = -\frac{\pi\Gamma}{l^2}\begin{pmatrix} 0 & a & 0 & b \\ a & 0 & c & 0 \\ 0 & -b & 0 & d \\ -c & 0 & e & 0 \end{pmatrix}\mathbf{v}, \tag{4.3.23}$$

where

$$\mathbf{v} = [x'_0, y'_0, \delta'_0, \gamma'_0]^T, \tag{4.3.24}$$

$$a = p(1-p) + 4\pi^2\frac{\delta U}{l^2}p^2(1-p)^2, \tag{4.3.25}$$

$$b = i\,\frac{2\pi}{3}\frac{U}{l}\,p(1-p)(1-2p), \tag{4.3.26}$$

$$c = i\,\frac{2\pi}{3}\frac{\delta^2+U^2}{Ul}\,p(1-p)(1-2p), \tag{4.3.27}$$

$$d = \frac{1}{4\pi^2}\frac{l^2}{U^2} - \frac{1}{6}\frac{\delta}{U}, \tag{4.3.28}$$

$$e = -\frac{1}{4\pi^2}\frac{l^2}{U^2}\left(1 - 2\,\frac{\delta^2}{U^2}\right) + \frac{1}{6}\frac{\delta}{U}\left(3 - \frac{\delta^2}{U^2}\right). \tag{4.3.29}$$

The squares of the eigenvalues of this matrix can be expressed explicitly as

$$\mu_\pm^2 = \frac{a^2 - 2bc + de}{2}\left(1 \pm \sqrt{1 - 4\,\frac{a^2de + ab^2e + ac^2d + b^2c^2}{(a^2 - 2bc + de)^2}}\right). \tag{4.3.30}$$

Substituting into this result the quantities a, b, c, d, and e written in terms of p, λ, and α and expanding yields the distinct eigenvalue families μ_+ and μ_-; further simplifying these using the relationship (4.3.19) between λ and α, we obtain the asymptotic growth rates of the perturbation for small α:

$$\sigma_+ = \pm\frac{\pi\Gamma}{l^2}\,p(1-p)\left\{1 + \frac{2\pi^2}{3}p(1-p)\,\alpha^2 + \cdots\right\}, \tag{4.3.31}$$

$$\sigma_- = \pm\frac{i\Gamma}{2l^2\alpha}\left\{1 - \frac{(2\pi\alpha)^2}{9} - \frac{(2\pi\alpha)^3}{9}p^2\,(1-p)^2\,(1-2p)^2 + \cdots\right\}. \tag{4.3.32}$$

The latter eigenvalues correspond to single vortex, high-frequency boundary oscillations, which grow without bound as the vortex area diminishes; the former eigenvalues are the growth rates of the cooperative disturbances, which exhibit the dominant point vortex array behavior as vortex area vanishes (Lamb [1945]). In the superharmonic limit, the zero eigenvalue pair σ_+ has two linearly independent eigenvectors corresponding to translational modes, while the eigenmodes of the nonzero pair σ_- are boundary oscillations. In the next section we compare the behavior of this elliptical model with the results of the Schwarz function analysis.

4.4 Results

The Schwarz function analysis was applied to vortex arrays in which each vortex has area equal to π and circulation equal to one. The solution path is shown in Figure 4.2., where the ratio of maximum length to maximum width of the vortex is plotted against nondimensionalized area. Solutions are obtained up to the fold point at $\alpha \doteq 0.2377$, and an upper branch of solutions is computed for $0.2330 < \alpha < 0.2377$. The accuracy was tested by checking that the obtained value of the external stream velocity Q was indeed zero, and by verifying an increase in significant figures of the solution with an increase in the order N of the truncation. For small α, $N = 8$ and $N = 16$ modes were used, while for larger α data were collected with $N = 16$ and $N = 32$ modes, with less than .5% discrepancy in aspect ratio for the more distorted solutions. Our results are found to agree with those of Saffman & Szeto [1981] and Pierrehumbert & Widnall [1981] to three significant figures. The use of Newton's method in the solution allowed monitoring of the determinant as a test for possible solutions bifurcating from the main symmetric solution path; no such solutions were indicated. The finely dashed line in Figure 4.2 denotes the aspect ratio of elliptically desingularized vortex arrays, as given by the numerical solution of (4.3.18), which satisfies the asymptotic behavior indicated in

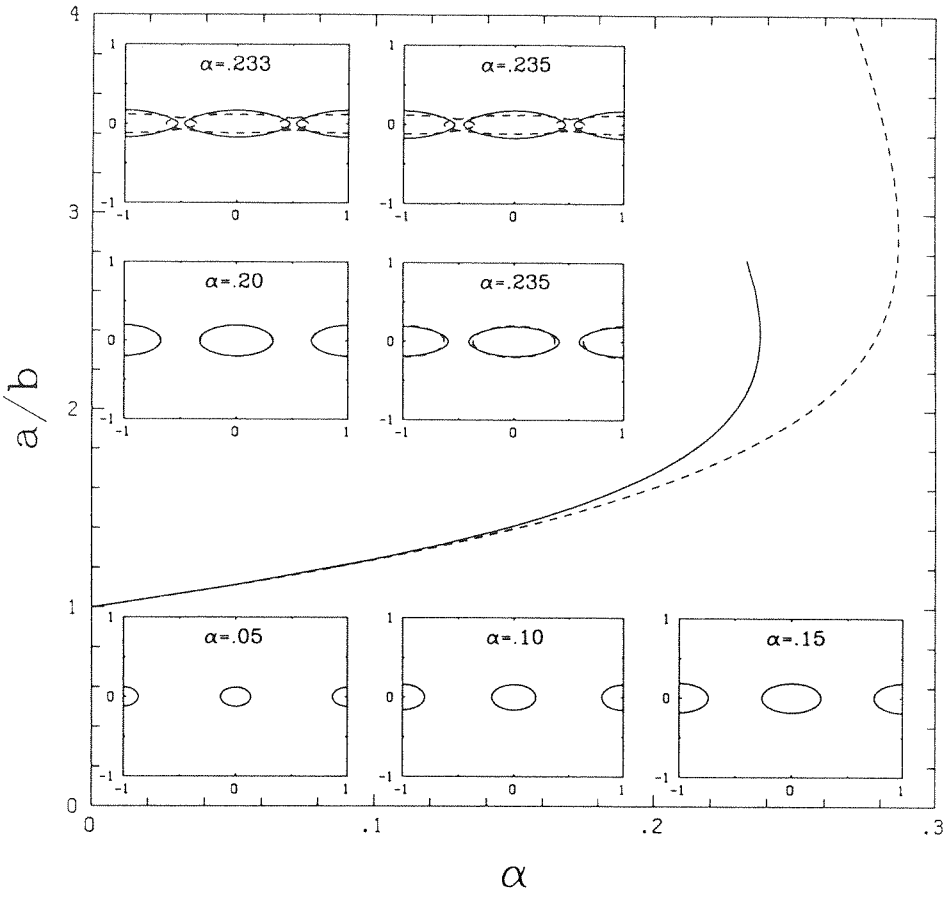

Figure 4.2 The single vortex array solution path: aspect ratio a/b versus nondimensionalized area α. The solid line indicates numerical solutions; the dashed line denotes the elliptically desingularized solutions. Solution vortices are shown for various values of α, with intercentroid distance l normalized to one.

(4.3.19). The elliptical model is seen to approximate accurately the actual solution away from the fold point, as well as provide qualitatively the correct fold point behavior for larger α.

The main objective of this investigation is to quantify the stability properties of this configuration. Saffman & Szeto consider the stability of the array of symmetric vortices to two-dimensional disturbances in terms of the energy argument based on Kelvin's variational principle, described in §§2.3 and 3.4. They argue that the lower branch of solutions (in Figure 4.2) must be stable to superharmonic

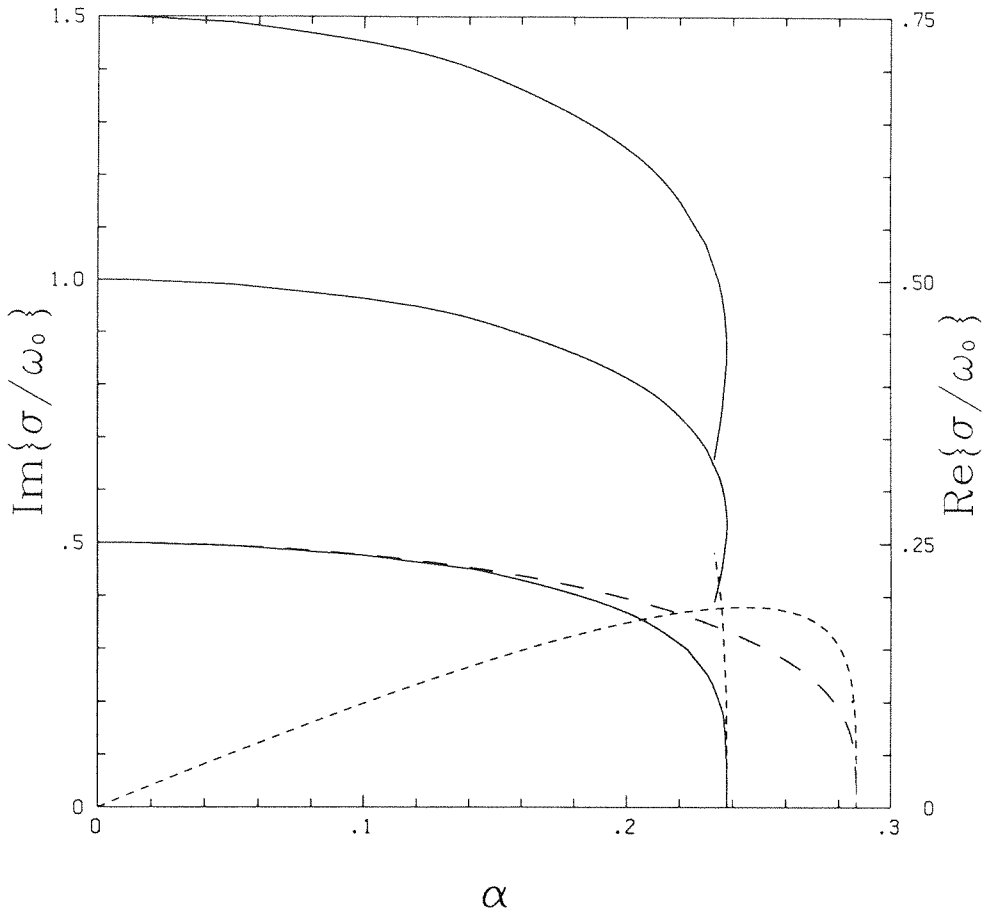

Figure 4.3 Superharmonic eigenvalues of the single vortex array, normalized by the vorticity. Imaginary quantities are denoted by solid lines (Schwarz solutions) and the coarsely dashed line (elliptical solutions) and are scaled on the left vertical axis. Real quantities are indicated by finely dashed lines and are scaled to the right vertical axis.

disturbances, while the upper branch is unstable. This is indeed the result we find numerically. The behavior of the three leading superharmonic eigenvalues, normalized by the vorticity, is shown in Figure 4.3 as a function of α. Solid lines, scaled to the left vertical axis, denote imaginary values of the Schwarz eigenvalues; the coarsely dashed line indicates the imaginary superharmonic frequency of the oscillations of elliptically desingularized vortices; finely dashed lines, scaled to the right vertical axis, indicate real values. These results show that the less deformed solutions on the lower branch are linearly (neutrally) stable to shape deformations.

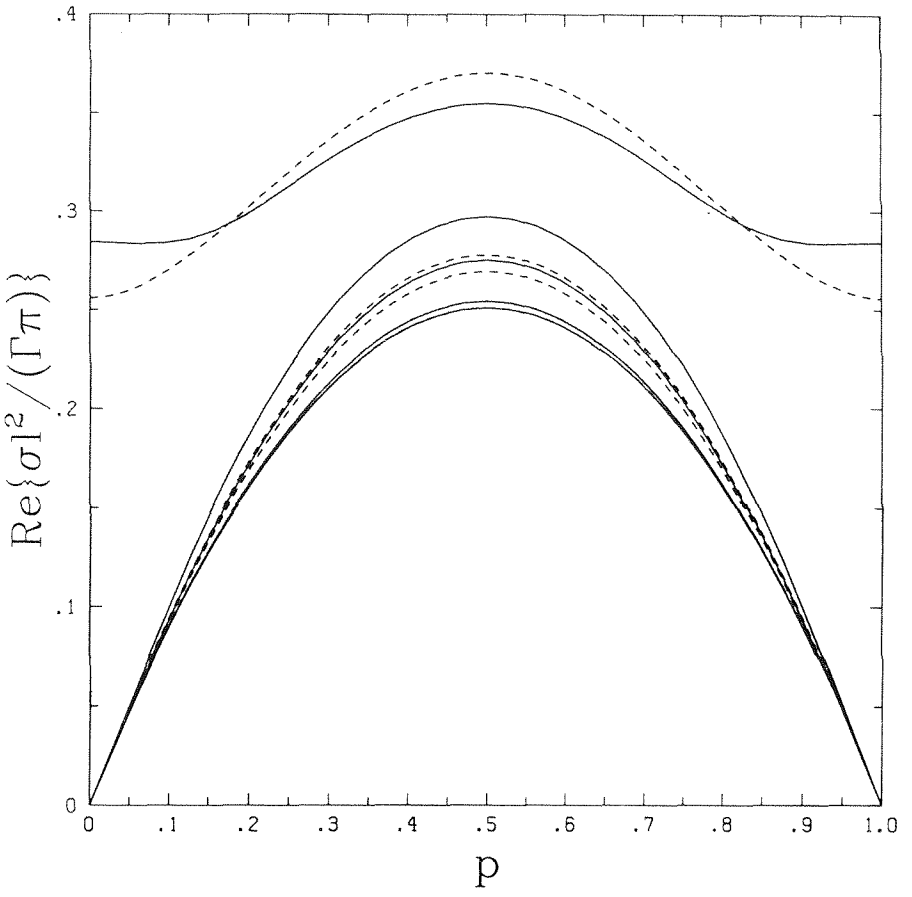

Figure 4.4 Leading subharmonic growth rates of the single vortex array, normalized by $\Gamma\pi/l^2$. Curves are plotted for $\alpha = 0.05$, 0.10, 0.20, 0.23, 0.235 (top branch), bottom to top. Solid lines denote results of the Schwarz function analysis; dashed lines indicate values for elliptically desingularized vortices.

It is also seen that the elliptical desingularization exhibits qualitatively the fold point behavior, with change of stability, of the actual solution.

The infinite array is found to be linearly unstable to all subharmonic disturbances. This result is also in agreement with the variational arguments of Saffman & Szeto. Cooperative mode growth rates, normalized by the quantity $\Gamma\pi/l^2$, are depicted for various α values in Figure 4.4, in which solid lines denote the Schwarz results and dashed lines the elliptically desingularized data given by the +-subscripted growth rate determined by (4.3.30). It is seen that the leading

subharmonic eigenvalue is symmetric about $p = \frac{1}{2}$, being strictly increasing for $0 < p < \frac{1}{2}$ and strictly decreasing for $\frac{1}{2} < p < 1$. The pairing instability ($p = \frac{1}{2}$) is the most unstable disturbance, in analogy with the numerical results for single infinite arrays of point vortices (Lamb [1945]), hollow vortices (Baker, Saffman & Sheffield [1976]), and Stuart vortices (Pierrehumbert & Widnall [1982]), as well as experimental results for mixing layers (Winant & Browand [1974]).

Although these results clearly indicate the relative destabilizing effect of finite regions of vorticity, it must be noted that the corresponding point vortex configuration is also linearly unstable to subharmonic disturbances. Perhaps the most significant result is that the area-enhanced pairing instability is dominant, and there is no unusual (e.g., nonmonotonic) behavior in the growth rate for other wavelengths, e.g., near $p = \frac{1}{3}$, which might correspond to experimentally observed vortex-tripling events (Ho & Huang [1982]).

Chapter 5

The Double Infinite Row

5.1 Introduction

In this chapter we consider an extension of the work of Meiron, Saffman & Schatzman [1984] on the Kármán vortex street. MSS used the method of Schwarz functions to obtain solutions of the Euler equations for arbitrary regions of constant vorticity in an unbounded domain. Although the actual Kármán vortex street is readily obtained experimentally, the theoretical explanation of the stability properties of its idealized counterpart poses formidable difficulties. Kármán [1912] modeled the vortex structure occurring behind a cylinder for Reynolds number between approximately 90 and 160 by a regular pattern of point vortices in inviscid flow. Linear stability analysis (Lamb [1945]) shows this configuration to be unstable to two-dimensional disturbances except for a vortex spacing aspect ratio of $\kappa_c = (\sinh^{-1} 1)/\pi$. Kochin [1939] and Domm [1956] later showed the point vortex configuration to be unstable at higher order.

The question of whether constant vorticity structures of finite extent stabilized the street was first addressed in a mathematically consistent manner by Saffman & Schatzman [1981], who concluded that two staggered infinite rows of finite regions of uniform vorticity were indeed stable for a range of aspect ratios. Kida [1982] qualitatively confirmed this assertion and corrected the erroneous assumption of Saffman & Schatzman that subharmonic disturbances are symmetric about $p = \frac{1}{2}$. The results presented in MSS confirm that subharmonic disturbances are not symmetric, but dispute the contention that finite area stabilizes

the street for vortices of equal areas. Jiménez [1986a] and MacKay [1986] show that the singular stability properties of the ideal vortex street are a consequence of its Hamiltonian structure; in a subsequent work, Jiménez [1986b] considers a perturbation expansion for rows of vortices of unequal areas and obtains the same qualitative behavior.

Our interest in considering this geometry is the effect of unequal areas on the stability properties of the street. The main result of the investigations of MSS was that the modeling of the street by regions of constant vorticity did not fundamentally alter the stability results of the Kármán point vortex model. We find that the modification to unequal areas also does not change the basic stability properties of this configuration, providing numerical confirmation of the work of Jiménez.

5.2 Formulation

In this section we review the development of the shape and stability problem for double infinite row as studied by MSS. All vortices in a given row are assumed to have the same shape with equal areas and vorticities; the boundary of each vortex in the first row is given by

$$z = a_0\zeta\,(1 + a_1/\zeta + \cdots + a_n/\zeta^n + \cdots)\,, \tag{5.2.1}$$

and each vortex in the second row is described by

$$z = b_0\zeta\,(1 + b_1/\zeta + \cdots + b_n/\zeta^n + \cdots)\,, \tag{5.2.2}$$

where ζ traverses the unit circle. The centroids of the vortices in the first row are taken to be at ml, and those of the vortices in the second row are located at $ml - l(d + i\kappa)$, where $l \in \mathbb{C}$ is the intercentroid distance, $d \in \mathbb{R}$ is the relative stagger of the vortices, $\kappa \in \mathbb{R}$ is the aspect ratio, and $m \in \mathbb{Z}$ is an index. The

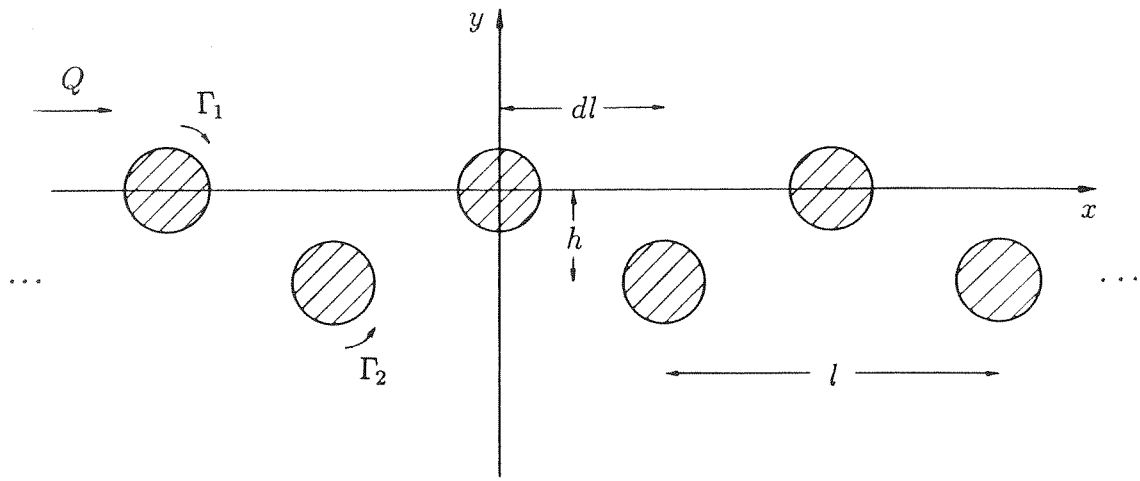

Figure 5.1 The double infinite vortex array.

configuration for real l is depicted in Figure 5.1. To model the wake it is assumed that the circulations of the vortices in the rows are given by $\Gamma_1 = -\Gamma_2 = \Gamma$, with the vorticities and areas of the regions related by $\omega_1 = \Gamma/A_1$ and $\omega_2 = -\Gamma/A_2$. Also, we set the relative stagger between the rows to one-half. We define the average area A, the nondimensional area α, and the area difference Δ as

$$A \equiv \frac{1}{2}(A_1 + A_2), \qquad \alpha \equiv A/l^2, \qquad \Delta \equiv \frac{1}{2}(A_1 - A_2)/A, \tag{5.2.3}$$

so that

$$A_1 = (1 + \Delta)A \qquad \text{and} \qquad A_2 = (1 - \Delta)A. \tag{5.2.4}$$

In analogy with the development of the previous sections, the total velocity at a point z relative to a vortex in the first row is expressed as

$$\begin{aligned} u - iv = &-\frac{i\omega_1}{2}\sum_{n=0}^{\infty}\sum_{m=-\infty}^{\infty}\frac{g_n}{(z - ml)^{n+1}} \\ &-\frac{i\omega_2}{2}\sum_{n=0}^{\infty}\sum_{m=-\infty}^{\infty}\frac{h_n}{[z - ml + l(d + i\kappa)]^{n+1}} + Q, \end{aligned} \tag{5.2.5}$$

where g_n and h_n are the nth Schwarz coefficients, given by (1.2.9), of the first and second row vorticies, and $Q = U - iV$ is the constant external velocity, required

to negate the self-induced translation of the array. The conjugate velocity has a representation similar to (5.2.5) with i replaced by $-i$, l by l^*, and the other coefficients by starred quantities.

We substitute these expressions into the governing boundary condition Equation (1.2.22) to obtain the steady shapes. The boundary condition is to be satisfied on one vortex in each row by the assumption of equivalent vortex shapes within each row. The solution is found as a power series in α by expanding the solution as a power series in $1/l$, as in the single infinite row problem. The shape expansions are truncated at order N in ζ, the velocity expansions are truncated at order $N+1$ in z, and the resulting series is expanded in $1/l$. Substitution of these expansions into the velocity expression (5.2.5) and rearrangement of the terms of the truncated series yield the following expression for the velocity relative to a vortex in the first row:

$$u - iv = -\frac{i\omega_1}{2}\left\{\sum_{n=0}^{N}\frac{g_n}{z^{n+1}} + \sum_{n=0}^{N}\sum_{p=0}^{L-n-1} g_n(-l)^{-(n+p+1)}\frac{(n+p)!}{n!\,p!}(-z)^p \sum_{m=-\infty}^{\infty}{}' \frac{1}{m^{p+n+1}}\right\}$$
$$- \frac{i\omega_2}{2}\left\{\sum_{n=0}^{N}\sum_{p=0}^{L-n-1} h_n(-l)^{-(n+p+1)}\frac{(n+p)!}{n!\,p!}(-z)^p \sum_{m=-\infty}^{\infty}\frac{1}{(m-d-i\kappa)^{p+n+1}}\right\} + Q. \tag{5.2.6}$$

Similar expressions are obtained for the velocity relative to the second row and for the conjugate velocities. The sums involving m can be evaluated explicitly, as shown by MSS and derived in Appendix E.

Substituting the truncated expansions into the boundary condition on each vortex and equating the coefficients of ζ^k to zero for $-N \le k \le N$ imply $4N+2$ equations for the $4N+6$ unknowns given by the shape coefficients and the velocities Q and Q^*. Without loss of generality, we set $a_0 = a_0^*$ and $b_0 = b_0^*$, thereby eliminating two of the unknowns. The equations implied by equating the coefficient of ζ^0 to zero are dependent and thus excluded, yielding $4N$ equations. We specify

the area of the vortices by adding the two Equations (3.2.19) and (3.2.20); also, the centroids are chosen to coincide with the vortex origins according to the four equations given in (3.2.21). For the configuration considered, the vorticity centroid is at rest, so the following relation holds:

$$\iint_{\mathbb{R}^2} \mathbf{u} \times \boldsymbol{\omega}\, dx\, dy = 0. \tag{5.2.7}$$

As shown in Appendix A, this implies that the coefficients of ζ and ζ^{-1} are perforce zero for the second row vortex if we explicitly include these equations for the first row vortex. This eliminates two equations, thereby providing $4N + 4$ equations for as many unknowns; the resulting system is found to be nonsingular.

We now consider the stability problem for the double row. As in §4.2, let p denote the wavenumber of the infinitesimal disturbance to the steady solution, where p is restricted to the range $0 \leq p \leq 1$ without loss of generality. Superharmonic disturbances are those for $p = 0$ or $p = 1$, and subharmonic disturbances are given for $0 < p < 1$. The equation governing stability is the linearized time-dependent boundary condition

$$\begin{aligned}(U - iV)\frac{\partial z'}{\partial \theta} + (u' - iv')\frac{\partial Z}{\partial \theta} - (U + iV)\frac{\partial z^{*\prime}}{\partial \theta} - (u' + iv')\frac{\partial Z^*}{\partial \theta} \\ = \sigma \left\{ z^{*\prime}\frac{\partial Z}{\partial \theta} - z'\frac{\partial Z^*}{\partial \theta} \right\}.\end{aligned} \tag{5.2.8}$$

Symmetry considerations presented by MSS and analogous to those explained in §4.2 imply that this equation need be satisfied on only one vortex in each row, provided we relate the shape perturbations of the mth vortex to those of the base vortex in each row by

$$a'^{(m)}_n = a'_n e^{im\lambda}, \qquad \tilde{a}'^{(m)}_n = \tilde{a}'_n e^{im\lambda}, \tag{5.2.9}$$

$$b'^{(m)}_n = b'_n e^{im\lambda}, \qquad \tilde{b}'^{(m)}_n = \tilde{b}'_n e^{im\lambda}, \tag{5.2.10}$$

where the wavelength λ is 2π times the subharmonic wavenumber p.

The procedures of §§2.2 and 3.2 describe the method of evaluation of the right side of the stability equation, while the numerical evaluation of the left side is complicated by the presence of the second row of vortices. Consider a perturbation of the jth shape coefficient of the first row vortex and follow the notation of §4.2. The evaluation of the left side of the stability equation is separated into two components. The first two terms of (4.2.13) are approximated as (4.2.14), where $\sum_{k=-N}^{N} R_1(k; a_j \pm \varepsilon)\, \zeta^k$ is evaluated as

$$\frac{\partial}{\partial\theta}[z(a_j \pm \varepsilon)] \left\{ -\frac{i\omega_1}{2} \left[\sum_{n=0}^{N} \frac{g_n}{[z(a_j \pm \varepsilon)]^{n+1}} \right.\right.$$
$$\left. + \sum_{n=0}^{N} \sum_{p=0}^{L-n-1} g_n (-l)^{-(n+p+1)} \frac{(n+p)!}{n!\,p!} [-z(a_j \pm \varepsilon)]^p \sum_{m=-\infty}^{\infty}{}' \frac{1}{m^p} \right]$$
$$\left. -\frac{i\omega_2}{2} \left[\sum_{n=0}^{N} \sum_{p=0}^{L-n-1} h_n (-l)^{-(n+p+1)} \frac{(n+p)!}{n!\,p!} [-z(a_j \pm \varepsilon)]^p \sum_{m=-\infty}^{\infty} \frac{1}{(m-d-i\kappa)^p} \right] + Q \right\}. \tag{5.2.11}$$

This yields an approximation accurate to $O(\varepsilon^2)$. The first term in the second addend, (4.2.16), is computed as (4.2.17), correct to $O(\varepsilon^2)$, where the sum $\sum_{k=-N}^{N} R_2(k; a_j \pm \varepsilon)\, \zeta^k$ is given by

$$\frac{\partial}{\partial\theta}[Z(a_j)] \left\{ -\frac{i\omega_1}{2} \left[\sum_{n=0}^{N} \frac{g_n'(a_j \pm \varepsilon)}{[Z(a_j)]^{n+1}} \right.\right.$$
$$\left. + \sum_{n=0}^{N} \sum_{p=0}^{L-n-1} g_n'(a_j \pm \varepsilon)(-l)^{-(n+p+1)} \frac{(n+p)!}{n!\,p!} [-Z(a_j)]^p \sum_{m=-\infty}^{\infty}{}' \frac{e^{im\lambda}}{m^p} \right]$$
$$\left. -\frac{i\omega_2}{2} \left[\sum_{n=0}^{N} \sum_{p=0}^{L-n-1} h_n'(a_j \pm \varepsilon)(-l)^{-(n+p+1)} \frac{(n+p)!}{n!\,p!} [-Z(a_j)]^p \sum_{m=-\infty}^{\infty} \frac{e^{im\lambda}}{(m-d-i\kappa)^p} \right] \right\}. \tag{5.2.12}$$

These evaluations are repeated for each shape coefficient of each vortex. Coefficients of like powers of ζ are equated to obtain $4N+2$ equations for $4N+2$

unknowns, written as

$$\mathbf{M}\ \mathbf{v} = \sigma\, \mathbf{N}\ \mathbf{v}, \tag{5.2.13}$$

where $\mathbf{M}$ is a function of the steady shape and perturbation wavenumber, $\mathbf{N}$ depends only on the steady solution, and $\mathbf{v}$ is the vector of shape perturbations given by

$$\begin{aligned} v_1 = \tilde{a}'_N, \ldots, v_{N+1} = \tilde{a}'_0 = a'_0, \ldots, v_{2N+1} = a'_N, \\ v_{2N+2} = \tilde{b}'_N, \ldots, v_{3N+2} = \tilde{b}'_0 = b'_0, \ldots, v_{4N+2} = b'_N. \end{aligned} \tag{5.2.14}$$

This equation is left-multiplied by the inverse of the nonsingular matrix $\mathbf{N}$ and solved with standard EISPACK routines.

We consider only subharmonic disturbances and obtain one pair of zero eigenvalues corresponding to eigenmodes for which area is not conserved. The remaining $4N$ eigenvalues occur in quartets corresponding to the cooperative mode, upon which we shall focus our analysis, and $N-1$ (stable) oscillatory shape modes. According to the symmetry conditions discussed in MSS, the quartet of cooperative eigenvalues for fixed area and aspect ratio occurs in pairs such that, say, $\Im\{\sigma_1\} < 0$, $\Im\{\sigma_2\} < 0$ and $\Im\{\sigma_3\} > 0$, $\Im\{\sigma_4\} > 0$. At wavenumbers for which this mode is stable, $\Re\{\sigma_1\} = \Re\{\sigma_2\} = \Re\{\sigma_3\} = \Re\{\sigma_4\} = 0$, whereas at wavenumbers for which the mode is unstable, $\Re\{\sigma_1\} = -\Re\{\sigma_2\} \neq 0$ or $\Re\{\sigma_3\} = -\Re\{\sigma_4\} \neq 0$. For a given pair, say $\{\sigma_1, \sigma_2\}$, we compute the point of change of stability by finding the zeros of

$$H(p; \alpha, \kappa) \equiv (\sigma_1 - \sigma_2)^2, \tag{5.2.15}$$

which is considered as a function of wavenumber for fixed area and aspect ratio. This function is real-valued such that when the mode is stable H is negative, whereas when the mode is unstable H is positive. We find the wavenumbers at which there is a change of stability by computing the zeros of this function.

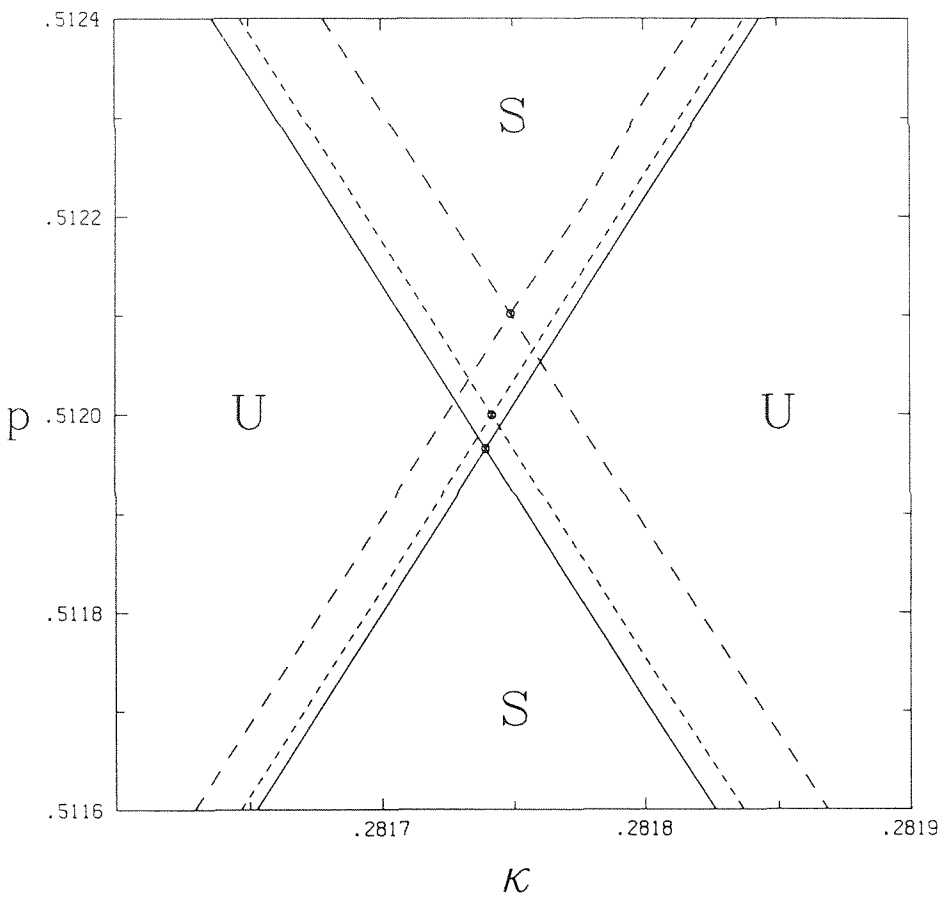

Figure 5.2 Neighborhood of the stability boundary for the $\alpha = 0.05$ vortex street with area differences $\Delta = 0.0$ (solid line), 0.05 (finely dashed line), and 0.10 (coarsely dashed line). S and U denote (neutrally) stable and unstable regimes, respectively.

5.3 Results

The method of Schwarz functions was applied to study vortex arrays in which the circulations of the vortices were $\Gamma_1 = -\Gamma_2 = 1$. The goal of this investigation was to assess the effect of unequal area on the stability properties of the street. The average of the areas of the first and second row vortices was set equal to π, with the areas of the vortices in each row set according to (5.2.4)

Solutions were obtained for the cases $\alpha = 0.005$, 0.05, and 0.10 with relative area differences $\Delta = 0.0$, 0.025, 0.05, and 0.10, representing area differences be-

tween the vortices of 0.0%, 5.13%, 10.5%, and 22.2%, respectively. Calculations for $\alpha = 0.005$ were done with $N = 8$, $L = 9$ and with $N = 16$, $L = 17$; the resulting difference in location of the stability boundary were negligible. For the larger area calculations $N = 16$, $L = 17$ were used. The stability boundary for the $\alpha = 0.05$ case is shown in Figure 5.2, where the aspect ratio $\kappa = h/l$ of the street is plotted along the horizontal axis and the subharmonic wave number p is graphed along the vertical axis. As the stability diagram is symmetric about the line $p = \frac{1}{2}$, only the region near the stability point with $p > \frac{1}{2}$ is depicted. The locations of the points of neutral stability are compiled in Table 5.1 and shown in Figure 5.3. The characteristic cross of the point vortex and MSS results is retained with the variations of area between the rows. The neutrally stable aspect ratio and wavenumber are both increasing functions of area and area difference.

These findings imply that unequal area does not qualitatively affect the stability properties of the inviscid street of finite vortices. This conclusion is consistent with the theoretical results of Jiménez [1986a] and MacKay [1986], wherein the stability of the inviscid, fore-to-aft symmetric street of finite, uniform vortices is studied as a special case of more general Hamiltonian systems with specific symmetries. These works show the existence of an isolated linearly stable state corresponding to the neutral stability point, which MSS and we have numerically computed.

Our numerical results confirm qualitatively the perturbation analysis of Jiménez [1986b], whose results are shown as the dashed lines in Figure 5.3. From these diagrams it is apparent that our values do not match those of Jiménez for even the equal area ($\Delta = 0$) case. However, the differences between the results decrease with decreasing α for all Δ. This discrepancy can be attributed to the fact that we are numerically solving the linear stabilty problem, whereas Jiménez

$\alpha = 0.005$ Stability Cross Location				
	$\Delta = 0.0$	$\Delta = 0.025$	$\Delta = 0.050$	$\Delta = 0.10$
$\kappa'_\times$	$1.373\,(-5)$	$1.374\,(-5)$	$1.377\,(-5)$	$1.387\,(-5)$
$p'_\times$	$1.162\,(-4)$	$1.163\,(-4)$	$1.165\,(-4)$	$1.174\,(-4)$

$\alpha = 0.05$ Stability Cross Location				
	$\Delta = 0.0$	$\Delta = 0.025$	$\Delta = 0.050$	$\Delta = 0.10$
$\kappa'_\times$	$1.190\,(-3)$	$1.190\,(-3)$	$1.192\,(-3)$	$1.199\,(-3)$
$p'_\times$	$1.196\,(-2)$	$1.197\,(-2)$	$1.120\,(-2)$	$1.210\,(-2)$

$\alpha = 0.10$ Stability Cross Location				
	$\Delta = 0.0$	$\Delta = 0.0250$	$\Delta = 0.050$	$\Delta = 0.10$
$\kappa'_\times$	$3.716\,(-3)$	$3.717\,(-3)$	$3.722\,(-3)$	$3.740\,(-3)$
$p'_\times$	$4.825\,(-2)$	$4.829\,(-2)$	$4.842\,(-2)$	$4.894\,(-2)$

Table 5.1 Locations of the point of neutral stability for vortex streets of various areas and area differences. Here, $\kappa'_\times \equiv \kappa_\times - \kappa_c$ and $p'_\times \equiv p_\times - p_c$ where the point vortex values are given by $(\kappa_c, p_c) \doteq (0.28055, 0.5)$.

obtains only the leading behavior from an asymptotic expansion for small areas. Kida [1982] predicts a stabilizing effect of finite area, but according to Jiménez there are errors in Kida's work which, when corrected, yield the stability cross; however, its location does not exactly agree with that predicted by Jiménez. In Appendix F we discuss a model of the street based on elliptically desingularized vortices as suggested by Melander *et al.* [1984, 1986]. However, we were unable to complete that analysis, which should reproduce the Jiménez results to leading order.

To quantify the relationship between Jiménez's results and ours, we note that from the MSS analysis, $\kappa'_\times \equiv \kappa_\times - \kappa_c$ and $p'_\times \equiv p_\times - p_c$ are proportional to α^2; Jiménez shows that the variation of these quantities with respect to Δ occurs to leading order as $\Delta^2\alpha^2$. Assuming the quadratic expansion

$$\kappa'_\times = \beta(1 + \gamma\Delta^2)\alpha^2 \qquad \text{and} \qquad p'_\times = \lambda(1 + \mu\Delta^2)\alpha^2, \tag{5.3.1}$$

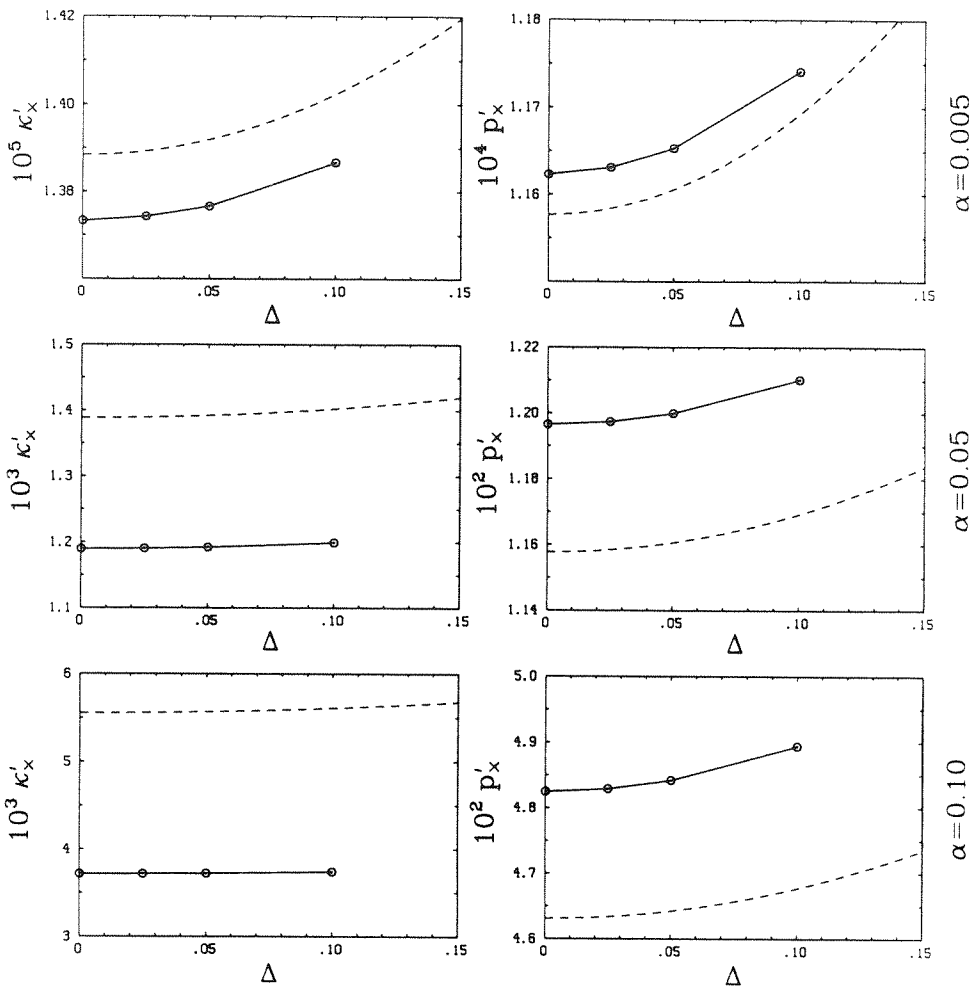

Figure 5.3 Locations of neutral stability point as functions of area difference for the $\alpha = 0.005$, 0.05, and 0.10 vortex streets. Circled points are computed values and dashed lines are results of Jiménez [1986b].

we have from the results for $\alpha = 0.005$, $\Delta = 0.0$, and $\Delta = 0.025$ that

$$\beta = 0.0549, \quad \gamma = 1.14, \quad \lambda = 4.65, \quad \mu = 0.956. \tag{5.3.2}$$

These compare favorably with Jiménez's analytically obtained values of

$$\beta = 0.0555, \quad \gamma = 1.00, \quad \lambda = 4.63, \quad \mu = 1.00. \tag{5.3.3}$$

As expected, this close correspondence between asymptotic theory and numerical experiment deteriorates for larger α and larger Δ.

There are still several unanswered questions about the vortex street. The nonlinear stability of the inviscid street of uniform vortices of finite area remains an unresolved problem, although we are inclined to draw analogies with the point vortex case and hypothesize that it is unstable. The mechanism for the observed stability of the street is still unknown; viscosity (i.e., dissipation) is a prime candidate, but to our knowledge no consistent mathematical stability analyses that include this term have been completed. The effects of a sinusoidal upstream disturbance (Eckelmann [1986]) or an oscillating body (Williamson [1987]) on the form and stability of the street are striking, yet they remain largely unexplained phenomena.

Appendix A

Kinematic Constraints for Vortices

In this appendix we discuss the constraints used in the formulation of the equations used to determine vortex shapes. We derive conditions for the single vortex, the vortex pair, and the infinite vortex rows.

Consider first the constraint that the velocity field must satisfy the continuity equation. Integrating this equation and applying Green's Theorem we obtain

$$\iint_V \nabla \cdot \mathbf{u}\, dx\, dy = \oint_{\partial V} u\, dy - v\, dx = \oint_{\partial V} u_n\, ds = 0. \tag{A1}$$

This condition holds for each vortex region V in the flow. The boundary condition used in the formulation of these problems is the vanishing of the normal velocity, which is expanded at the boundary of each vortex as

$$u_n = i\,\frac{d\theta}{ds} \sum_{k=-\infty}^{\infty} R(k)\zeta^k. \tag{A2}$$

Using this expression, we rewrite the boundary integral (A1) as

$$\int_0^{2\pi} u_n \frac{ds}{d\theta}\, d\theta = \sum_{k=-\infty}^{\infty} R(k) \oint_{|\zeta|=1} \zeta^{k-1}\, d\zeta. \tag{A3}$$

Thus, we find for each vortex

$$\oint_{\partial V} u_n\, ds = 0 \Rightarrow 2\pi R(0) = 0, \tag{A4}$$

where we have used the fact that

$$\oint_{|\zeta|=1} \zeta^{k-1}\, d\zeta = 2\pi i\, \delta_{k,0}. \tag{A5}$$

Hence, for a valid solution shape, the velocity field automatically satisfies the equation $R(0) = 0$ for each vortex; to impose this condition explicitly would be adding a dependent equation.

Consider now the vortex pair and the infinite double arrays. In either case an external flow is imposed to bring the vortices to rest. In this frame the vorticity centroid of the system has zero velocity. Thus, for two-dimensional uniform vorticity regions

$$\iint_{\mathbb{R}^2} \mathbf{u} \times \boldsymbol{\omega}\, dx\, dy = -\hat{\mathbf{z}} \times \iint_{\mathbb{R}^2} \omega \mathbf{u}\, dx\, dy = 0. \tag{A6}$$

By Green's Theorem,

$$\iint_V \mathbf{u}\, dx\, dy = \oint_{\partial V} \mathbf{x} u_n\, ds, \tag{A7}$$

so that (A6) implies

$$\omega_1 \oint_{\partial V_1} \mathbf{x} u_n\, ds + \omega_2 \oint_{\partial V_2} \mathbf{x} u_n\, ds = 0, \tag{A8}$$

where for the vortex pair V_1 and V_2 are the first and second vortices, while for the double rows V_1 and V_2 are vortices in the first and second rows, respectively. From this expression, we obtain the following equivalent equation

$$\omega_1 \oint_{\partial V_1} (z \pm z^*) u_n\, ds + \omega_2 \oint_{\partial V_2} (z \pm z^*) u_n\, ds = 0. \tag{A9}$$

The governing boundary condition is the vanishing of the normal velocity u_n on each vortex; assume this equation to be satisfied on the vortex 1. With this premise, (A9) is equivalent to the condition that

$$\oint_{\partial V_2} (z \pm z^*) u_n\, ds = 0. \tag{A10}$$

The boundary of this vortex is given by

$$z = b_0\zeta(1 + b_1/\zeta + b_2/\zeta^2 + \cdots). \tag{A11}$$

From this expansion we express the sum of z and its conjugate as

$$z \pm z^* = b_0 \sum_{k=-\infty}^{\infty} B_{\pm}(k)\zeta^k, \tag{A12}$$

where

$$B_{\pm}(k) = \begin{cases} b_{-(k-1)}, & k \leq -2; \\ b_2 \pm 1, & k = -1; \\ b_1 \pm b_1^*, & k = 0; \\ 1 \pm b_2^*, & k = 1; \\ \pm b_{k+1}^*, & k \geq 2. \end{cases} \tag{A13}$$

Substituting this expression into the integral and using (A2), we find (A10) equivalent to the following condition:

$$R_2(-1) \pm R_2(1) + \sum_{k=2}^{\infty} [b_k R_2(k-1) \pm b_k^* R_2(1-k)] = 0. \tag{A14}$$

To leading order we have that

$$R_2(-1) + R_2(1) = 0 \quad \text{and} \quad R_2(-1) - R_2(1) = 0, \tag{A15}$$

which is equivalent to

$$R_2(-1) = 0 \quad \text{and} \quad R_2(1) = 0. \tag{A16}$$

Thus, given condition (A6) and a valid solution for the first vortex, the velocity field satisfies the equations given in (A16); explicitly requiring these constraints does not add independent equations.

We obtain the equivalent condition used in the stream function implementation discussed in Appendix D as follows. The normal velocity equals the tangential derivative of the stream function on the vortex boundary. We assume that the

stream function assumes a constant value on the first vortex, so that the vanishing of the integral on the second vortex in condition (A8) is not an independent condition. We write this condition, equivalent to (A10), as

$$\oint_{\partial V_2} z \, d\psi = 0. \tag{A17}$$

Integrating this expression by parts and evaluating the integral over the unit circle in the ζ-plane, we obtain

$$\int_0^{2\pi} \psi \, \frac{dz}{d\zeta} \, \frac{d\zeta}{d\theta} \, d\theta = 0. \tag{A18}$$

We substitute in series representations of the derivatives and obtain

$$\int_0^{2\pi} \psi \, e^{i\theta} \left[1 - \sum_{k=1}^{\infty} (k-1) b_k e^{-ik\theta} \right] d\theta = 0. \tag{A19}$$

To leading order this expression yields the dependent conditions for the second vortex

$$\int_0^{2\pi} \psi \, \cos\theta \, d\theta = 0, \qquad \int_0^{2\pi} \psi \, \sin\theta \, d\theta = 0. \tag{A20}$$

For the vortex pair, we further consider the quantity

$$\iint_{\mathbb{R}^2} \omega \, (\mathbf{x} \cdot \mathbf{u}) \, dx \, dy. \tag{A21}$$

As shown in Dritschel (1985), this quantity vanishes for general two-dimensional incompressible flows. Thus, we have

$$\omega_1 \iint_{V_1} \mathbf{x} \cdot \mathbf{u} \, dx \, dy + \omega_2 \iint_{V_2} \mathbf{x} \cdot \mathbf{u} \, dx \, dy = 0. \tag{A22}$$

Using the continuity equation and Green's Theorem, we write the integrals in this expression as

$$\iint_{V_m} \mathbf{x} \cdot \mathbf{u} \, dx \, dy = \frac{1}{2} \oint_{\partial V_m} r^2 u_n \, ds. \tag{A23}$$

The condition on the vortex pair then becomes

$$\omega_1 \oint_{\partial V_1} r^2 u_n \, ds + \omega_2 \oint_{\partial V_2} r^2 u_n \, ds = 0. \tag{A24}$$

We again assume that the governing zero normal boundary velocity condition is satisfied on the first vortex; hence, the vanishing of the integral on the second vortex is not an independent condition. With $r^2 = zz^*$ and z given by expansion (A11) on the boundary, we expand r^2 as

$$r^2 = b_0^2 \sum_{k=-\infty}^{\infty} C(k)\zeta^k, \tag{A25}$$

where $C(k)$ is defined as

$$C(k) = \begin{cases} b_k^* + \sum_{j=1}^{\infty} b_{k+j}^* b_j, & \text{if } k > 0; \\ 1 + \sum_{j=1}^{\infty} b_j b_j^*, & \text{if } k = 0; \\ b_k + \sum_{j=1}^{\infty} b_{k+j} b_j^*, & \text{if } k < 0. \end{cases} \tag{A26}$$

We use the expansion of the normal velocity on the boundary given by (A2) and substitute into the integral over the second vortex in (A24) to obtain a power series in ζ. Using relationship (A5), we find, after some algebra, that to satisfy the vanishing of the integral in (A24) over the second vortex, the following is required:

$$\sum_{k=2}^{\infty} [R_2(k)C(-k) + R_2(-k)C(k)] = 0, \tag{A27}$$

where we have assumed $R_2(0)$, $R_2(1)$, and $R_2(-1)$ are all zero, in accordance with the previous derivations. To leading order in shape coefficients, this implies

$$R_2(2)b_2 + R_2(-2)b_2^* = 0. \tag{A28}$$

Thus, solutions for which $b_k = b_k^*$, i.e., shapes symmetric about the x-axis, automatically satisfy the following equation:

$$R_2(2) + R_2(-2) = 0. \tag{A29}$$

We also consider (A24) for the stream function formulation of Appendix D. The vanishing of the integral on the second vortex is not an independent condition, as the stream function is explicitly required to be constant on the first vortex. Integrating this integral by parts yields the (dependent) condition

$$\int_0^{2\pi} \psi \, \frac{d(r^2)}{d\zeta} \, \frac{d\zeta}{d\theta} \, d\theta = 0. \tag{A30}$$

Upon substituting in the expression (A25) for r^2, this equation becomes

$$b_0^2 \sum_{k=2}^{\infty} k \left[C(k) \int_0^{2\pi} \psi \, \zeta^k \, d\theta \; - \; C(-k) \int_0^{2\pi} \psi \, \zeta^{-k} \, d\theta \right] = 0, \tag{A31}$$

where the coefficients $C(k)$ are given in (A26), and we have assumed the results given in (A20). To leading order in the shape coefficients we obtain the following dependent condition:

$$(b_2 - b_2^*) \int_0^{2\pi} \psi \, \cos 2\theta \, d\theta \; - \; i(b_2 + b_2^*) \int_0^{2\pi} \psi \, \sin 2\theta \, d\theta = 0. \tag{A32}$$

For solutions in which $b_k = b_k^*$, the real part of this equation vanishes identically, so only the second integral is not independent. Thus, the imaginary part of this equation yields the dependent condition

$$\int_0^{2\pi} \psi \, \sin 2\theta \, d\theta = 0. \tag{A33}$$

Appendix B

An Energy Integral for Vortices

In this appendix we derive an expression for the integral of the stream function over a vortex V. From the two-dimensional Green's Theorem

$$\iint_V \psi \, dx \, dy = \oint_{\partial V} x\psi \, dy - \iint_V x \frac{\partial \psi}{\partial x} \, dx \, dy \tag{B1}$$

and

$$\iint_V \psi \, dx \, dy = -\oint_{\partial V} y\psi \, dx - \iint_V y \frac{\partial \psi}{\partial y} \, dx \, dy. \tag{B2}$$

Repeating the application of Green's Theorem to the second integrals in these expressions, we find

$$\iint_V x \frac{\partial \psi}{\partial x} \, dx \, dy = \frac{1}{2} \oint_{\partial V} x^2 \frac{\partial \psi}{\partial x} \, dy - \frac{1}{2} \iint_V x \frac{\partial^2 \psi}{\partial x^2} \, dx \, dy \tag{B3}$$

and

$$\iint_V y \frac{\partial \psi}{\partial y} \, dx \, dy = -\frac{1}{2} \oint_{\partial V} y^2 \frac{\partial \psi}{\partial y} \, dx - \frac{1}{2} \iint_V y \frac{\partial^2 \psi}{\partial y^2} \, dx \, dy. \tag{B4}$$

Also by Green's Theorem we have that

$$\oint_{\partial V} y^2 \frac{\partial \psi}{\partial x} \, dx - \iint_V y^2 \frac{\partial^2 \psi}{\partial x^2} \, dx \, dy = 0 \quad \text{and} \quad \oint_{\partial V} x^2 \frac{\partial \psi}{\partial y} \, dy - \iint_V x^2 \frac{\partial^2 \psi}{\partial y^2} \, dx \, dy = 0. \tag{B5}$$

Combining these results and simplifying, we obtain

$$\iint_V \psi \, dx \, dy = \frac{1}{2} \oint_{\partial V} \psi(x \, dy - y \, dx) - \frac{1}{4} \oint_{\partial V} (x^2 + y^2) \left(\frac{\partial \psi}{\partial x} \, dy - \frac{\partial \psi}{\partial y} \, dx \right) + \frac{1}{4} \iint_V (x^2 + y^2) \nabla^2 \psi \, dx \, dy. \tag{B6}$$

Appendix C

Analytic Formulae for Vortex Configurations.

In this appendix we derive formulae for the stream function, angular momentum, and kinetic energy of the single circular and elliptical regions of uniform vorticity. Also, explicit angular momentum and energy formulae are derived for a pair of circular uniform vorticity regions. We assume two-dimensional inviscid, incompressible flow, with density normalized to unity. We require the stream function to have the asymptotic behavior

$$\psi \sim -\frac{\Gamma}{2\pi} \log R + o(1), \qquad \text{as } R \to \infty. \tag{C1}$$

The angular momentum is defined as

$$H = -\frac{1}{2} \iint_{\mathbb{R}^2} \omega r^2 \, dx \, dy, \tag{C2}$$

and nondimensionalized as

$$J = -H / \left(\sum_m \Gamma_m A_m \right). \tag{C3}$$

The excess kinetic energy is defined as

$$T = \frac{1}{2} \iint_{\mathbb{R}^2} \omega \psi \, dx \, dy, \tag{C4}$$

which is nondimensionalized for flows with nonzero total circulation Γ as

$$\tilde{T} = T/\Gamma^2, \tag{C5}$$

and further reduced as the scale-invariant quantity

$$\hat{T} = \tilde{T} - \tilde{T}_{equivalent\ circle}, \tag{C6}$$

where $\tilde{T}_{equivalent\ circle}$ is the nondimensional excess kinetic energy of a circular vortex of the same total area and circulation as the configuration under consideration.

Consider first the circular region of constant vorticity ω_0 with radius $r = a$ centered at the origin, such that $\Gamma = \omega_0 \pi a^2$. For this geometry the Poisson equation is independent of θ and has the solution

$$\psi = A_0 r^2 + A_1 \log r + A_2. \tag{C7}$$

We solve for the solution stream function by imposing the asymptotic condition (C1) and requiring the continuity of ψ and $\partial\psi/\partial r$ at the boundary of the vortex. We find that

$$\psi = \begin{cases} -\frac{\Gamma}{4\pi}(r/a)^2 + \frac{\Gamma}{4\pi}(1 - 2\log a), & 0 \le r \le a; \\ -\frac{\Gamma}{2\pi}\log r, & r \ge a. \end{cases} \tag{C8}$$

The angular momentum expression can be integrated immediately:

$$H = -\frac{1}{2}\iint_{\mathbf{R}^2} \omega r^2 \, dx\, dy = -\omega_0 \pi \int_0^a r^3 \, dr = -\frac{1}{4}\omega_0 \pi a^4 \implies J = \frac{1}{4\pi}. \tag{C9}$$

For the kinetic energy, the integral of the stream function is obtained as

$$\iint_V \psi \, dx\, dy = 2\pi \left[-\frac{\Gamma}{4\pi a^2} \int_0^a r^3 \, dr + \frac{\Gamma}{4\pi}(1 - 2\log a) \int_0^a r \, dr \right] = \frac{\Gamma a^2}{8}(1 - 4\log a). \tag{C10}$$

Hence, the excess kinetic energy is given by

$$T = \frac{\Gamma^2}{16\pi}(1 - 4\log a) = \frac{\Gamma^2}{16\pi}[1 - 2\log(A/\pi)]. \tag{C11}$$

Note that, by definition, $\hat{T} = 0$ for a circular vortex.

For the region of uniform vorticity ω_0 bounded by the ellipse with semimajor axis a and semiminor axis b, we use the Schwarz function representation of the

velocity field to obtain the stream function. The exterior conformal mapping of the unit circle in the ζ-plane to the ellipse is given by

$$z = \alpha\zeta + \beta/\zeta, \qquad \text{where} \qquad \alpha = \frac{1}{2}(a+b), \quad \beta = \frac{1}{2}(a-b) \in \mathbb{R}. \tag{C12}$$

The area of this region is given by

$$A = \pi ab = \pi(\alpha^2 - \beta^2). \tag{C13}$$

On the boundary of the vortex, we have the Schwarz expansion (1.2.3); from (C12) we have the expansion

$$z^* = \alpha/\zeta + \beta\zeta = \frac{\alpha^2 - \beta^2}{\alpha}\frac{1}{\zeta} + \frac{\beta}{\alpha}z. \tag{C14}$$

Outside the vortex, the induced velocity is expanded in inverse powers of z, so we infer that

$$u - iv = -\frac{i\Gamma}{2\pi}\frac{1}{\alpha\zeta}. \tag{C15}$$

We solve for the complex potential by integrating this expression with respect to z and choosing the constant of integration such that $w \sim -(i\Gamma/2\pi)\log z + o(1)$ as $|z| \to \infty$; we find that

$$w = -\frac{i\Gamma}{2\pi}\left(\log\alpha\zeta + \frac{\beta}{2\alpha}\frac{1}{\zeta^2}\right). \tag{C16}$$

The integral in expression (C2) for the angular momentum can be integrated immediately, using the definition of the elliptical boundary, to obtain

$$\iint_V r^2\,dx\,dy = \frac{\pi ab}{4}(a^2 + b^2). \tag{C17}$$

Thus, the angular momentum is given by

$$H = -\frac{1}{8}\omega_0\pi ab(a^2+b^2) \implies J = \frac{1}{8\pi}\frac{\rho^2+1}{\rho}, \tag{C18}$$

where $\rho \equiv a/b$ is the axis ratio. To obtain the excess kinetic energy for the elliptical vortex, we consider the integral of the stream function; recall from Equation (1.4.21) we may write this as

$$\iint_V \psi \, dx \, dy = \frac{1}{2} \oint_{\partial V} \psi(x \, dy - y \, dx) - \frac{1}{4} \oint_{\partial V} r^2 \left(\frac{\partial \psi}{\partial x} \, dy - \frac{\partial \psi}{\partial y} \, dx \right) - \frac{\omega_0}{4} \iint_V r^2 \, dx \, dy. \tag{C19}$$

Explicit evaluation of these integrals yields

$$\oint_{\partial V} \psi(x \, dy - y \, dx) = -\frac{\Gamma^2}{\pi \omega_0} \log \left(\frac{a+b}{2} \right), \tag{C20}$$

$$\oint_{\partial V} r^2 \left(\frac{\partial \psi}{\partial x} \, dy - \frac{\partial \psi}{\partial y} \, dx \right) = -\Re \left\{ \oint_{\partial V} |z|^2 (u - iv) \, dz \right\} = -\frac{\Gamma}{4}(a^2 + b^2). \tag{C21}$$

The third integral in (C19) is just the angular momentum integral evaluated in (C17). Combining these results, we find the excess kinetic energy of the ellipse as

$$T = \frac{\Gamma^2}{16\pi} \left[1 - 4 \log \left(\frac{a+b}{2} \right) \right]. \tag{C22}$$

Using the result (C11) for the energy of the circle of area A, we obtain the reduced energy of the ellipse as

$$\hat{T} = \tilde{T} - \frac{1}{16\pi} \left[1 - 2 \log ab \right] = \frac{1}{4\pi} \log \left(\frac{2\sqrt{\rho}}{1+\rho} \right). \tag{C23}$$

We obtain a relation between $\hat{T}$ and J valid for large J (i.e., large aspect ratio ellipses) by expanding $1/\rho$ as an asymptotic series in J valid for large J,

$$1/\rho \sim \frac{1}{8\pi J} \left[1 + \frac{1}{(8\pi J)^2} + O\left(\frac{1}{(8\pi J)^3} \right) \right], \tag{C24}$$

substituting into expression (C23), and simplifying to yield

$$\hat{T} \sim -\frac{1}{8\pi} \log (2\pi J) - \frac{1}{16\pi} \frac{1}{2\pi J} + O\left(\frac{1}{(2\pi J)^2} \right). \tag{C25}$$

We now consider two circular regions of uniform vorticity separated by a distance l along the x-axis; this configuration is *not* a steady solution of the Euler equations. Let the circulations be Γ_1 and Γ_2 and the centers of the circles, with radii r_1 and r_2, be at $x = l_1 > 0$ and $x = l_2 < 0$, such that $l = l_1 - l_2 > 0$. From the definition of angular momentum (C2), we have that

$$H = -\frac{1}{2}\sum_{k=1}^{2}\omega_k\left[l_k^2 A_k + \int_0^{2\pi} d\theta \int_0^{r_k} r^2 r\, dr\right]. \tag{C26}$$

Evaluation of this expression yields the result that

$$H = -\frac{1}{2}\left[\Gamma_1\left(l_1^2 + \frac{r_1^2}{2}\right) + \Gamma_2\left(l_2^2 + \frac{r_2^2}{2}\right)\right]. \tag{C27}$$

This relation is nondimensionalized according to (3.2.47) to obtain

$$J = \frac{1}{2}\left(\frac{1}{2\pi} + \frac{\Gamma_1 l_1^2 + \Gamma_2 l_2^2}{\Gamma_1 A_1 + \Gamma_2 A_2}\right). \tag{C28}$$

For the case of equal corotating vortices, i.e., $A_1 = A_2 = A$, $\Gamma_1 = \Gamma_2 = \Gamma$, $l_1 = -l_2 = l/2$, etc., we have that

$$H = -\frac{\Gamma}{4}\left(l^2 + 2r^2\right), \qquad J = \frac{1}{8\pi}\left[2 + \frac{\pi}{\alpha}\right]. \tag{C29}$$

To evaluate the kinetic energy of this configuration, we use expression (1.4.21) for the integral of the stream function. To obtain an explicit expression for the stream function, we consider the velocity external to the vortices written as

$$(u - iv)_{external} = -\frac{i\Gamma_1}{2\pi}\frac{1}{z_1} - \frac{i\Gamma_2}{2\pi}\frac{1}{z_2}, \tag{C30}$$

where z_k is the coordinate measured from the center of the kth vortex. The corresponding stream function is given by

$$\psi = \Im\left\{-\frac{i\Gamma_1}{2\pi}\log z_1 - \frac{i\Gamma_2}{2\pi}\log z_2\right\}. \tag{C31}$$

With coordinate z relative to the center of the first vortex we write

$$\psi^{(1)} = \psi^{(11)} + \psi^{(12)} = \Im\left\{-\frac{i\Gamma_1}{2\pi}\log z\right\} + \Im\left\{-\frac{i\Gamma_2}{2\pi}\log(z+l)\right\}, \tag{C32}$$

with a similar expression for the stream function relative to the second vortex. The evaluation of the integrals in (1.4.21) is straightforward, using the methods derived in that §1.4, and we find that

$$\iint_{V_1} \psi^{(1)}\, dx\, dy = \frac{\Gamma_1 A_1}{8\pi}\left[1 - 2\log\frac{A_1}{\pi} - 4\frac{\Gamma_2}{\Gamma_1}\log l\right], \tag{C33}$$

with a similar result for the second vortex. Combining these values and simplifying, we obtain

$$T = \frac{\Gamma_1^2}{16\pi}\left[1 - 2\log\frac{A_1}{\pi} - 4\frac{\Gamma_2}{\Gamma_1}\log l\right] + \frac{\Gamma_2^2}{16\pi}\left[1 - 2\log\frac{A_2}{\pi} - 4\frac{\Gamma_1}{\Gamma_2}\log l\right]. \tag{C34}$$

The reduced kinetic energy for the pair of corotating circular vortices is given by

$$\hat{T} = \frac{1}{(\Gamma_1+\Gamma_2)^2}\left\{\frac{\Gamma_1^2}{16\pi}\left[1 - 2\log\frac{A_1}{\pi} - 4\frac{\Gamma_2}{\Gamma_1}\log l\right] + \frac{\Gamma_2^2}{16\pi}\left[1 - 2\log\frac{A_2}{\pi} - 4\frac{\Gamma_1}{\Gamma_2}\log l\right]\right\}$$
$$- \frac{1}{16\pi}\left[1 - 2\log\left(\frac{A_1+A_2}{\pi}\right)\right]. \tag{C35}$$

In the corotating equal vortex case used in computations, i.e., $A_1 = A_2 = A = \pi$, $\Gamma_1 = \Gamma_2 = \Gamma = 1$, etc., we find

$$\hat{T} = -\frac{1}{32\pi}\left[1 + 4\log(l/2)\right] = -\frac{1}{32\pi}\left[1 - 2\log(4\alpha/\pi)\right], \tag{C36}$$

where $\alpha = A/l^2$. From Equations (C29) and (C34) we obtain the asymptotic relationship for equal corotating vortices between the energy and angular momentum valid for large J as

$$T \sim \frac{\Gamma^2}{4\pi}\left[-\log\left(\frac{8J}{\pi}\right) + \frac{1}{2} - 2\log A + \frac{1}{4\pi J} + O\left(\frac{1}{(4\pi J)^2}\right)\right]. \tag{C37}$$

This result agrees with the analytic result of Saffman & Szeto [1980], who used a different angular momentum normalization. Similarly, from (C29) and (C36) we obtain the asymptotic result for the reduced energy as

$$\hat{T} \sim -\frac{1}{16\pi}\left[\log(2\pi J) + \frac{1}{2} - \frac{1}{4\pi J} + O\left(\frac{1}{(4\pi J)^2}\right)\right]. \tag{C38}$$

Appendix D

Stream Function Formulation for Corotating Vortices

In this appendix we consider a formulation, proposed and implemented by Saffman [1985a], of the corotating vortex pair problem that is based on the constancy of the stream function on the boundary of the vortex regions. We again assume the general expansions of the vortex regions as given in (3.2.1) and (3.2.2) for arbitrary areas and circulations.

From (3.2.14), we have the velocity with respect to the first vortex expanded as a series in z, the coordinate relative to that vortex, using the Schwarz coefficients of each of the vortex regions. In analogy with the development of §1.4, we integrate this expression to obtain the stream function relative to the first vortex as

$$\psi_1 = \Im\left\{-\frac{i\omega_1}{2}\left[g_0 \log z - \sum_{n=1}^{\infty}\frac{g_n}{nz^n}\right]\right\}$$
$$+\Im\left\{-\frac{i\omega_2}{2}\left[h_0 \log(z+l) - \sum_{n=1}^{\infty}\frac{h_n}{n(z+l)^n}\right]\right\} + \Im\left\{-i\Omega|z+l_1|^2\right\}. \qquad \text{(D1)}$$

Using the relationship (1.2.14) between the vortex area and the zeroth Schwarz coefficient, the stream function at a point z_k relative to the first vortex is written

$$\psi_{1,k} = -\frac{\omega_1 A_1}{2\pi}\log|z_k| + \frac{\omega_1}{2}\Re\left\{\sum_{n=1}^{\infty}\frac{g_n}{nz_k^n}\right\} - \frac{\omega_2 A_2}{2\pi}\log|z_k+l|$$
$$+\frac{\omega_2}{2}\Re\left\{\sum_{n=1}^{\infty}\frac{h_n}{n(z_k+l)^n}\right\} - \frac{\Omega}{2}|z_k+l_1|^2; \qquad \text{(D2)}$$

we find a similar representation for the stream function relative to the second vortex.

Instead of the boundary condition (1.2.22), we take as the governing equation the equivalent requirement that the stream function on the steady vortex bound-

aries be constant. The unknowns in this formulation are the coefficients of the vortex shape expansions, the real rotation rate Ω, and the value of the stream function on the boundary of one of the vortices. Unlike the Schwarz formulation, we do *not* treat complex conjugate quantities as independent. Truncating the shape expansions at the Nth coefficient yields $4N+2$ real unknowns given by the real and imaginary parts of the shape coefficients, where, without loss of generality, we choose the expansion coefficients a_0 and b_0 to be real. The rotation rate and the stream function on the boundary of the first vortex provide a total of $4N+4$ real unknowns. The above series for the stream function are truncated to include up to the Nth Schwarz coefficient.

We obtain equations for the stream function by evaluating it at collocation points on the boundary of the first vortex. We choose the $2N+1$ z-plane locations that are images under the shape mapping of points equally spaced on the unit circle in the ζ-plane, i.e., the values

$$z_k = z\left(\zeta = e^{i\theta_k}\right), \quad k = 0, \ldots, 2N, \qquad \text{where} \quad \theta_k = \frac{2\pi k}{2N+1}. \tag{D3}$$

Requiring the stream function on the first vortex (as given by (D2) truncated to include N terms) to have the constant value ψ_1^0 at these $2N+1$ points provides $2N+1$ real equations.

As in §3.2, we add equations prescribing the geometry of the configuration. We fix the vortex areas according to (1.2.14) by the two real equations

$$\frac{A_1}{\pi} - \Re\{g_0\} = 0, \qquad \frac{A_2}{\pi} - \Re\{h_0\} = 0. \tag{D4}$$

Also, from (1.2.15), we require the centroids to be at the vortex origins by adding the four real equations

$$\Re\{g_1\} = \Im\{g_1\} = \Re\{h_1\} = \Im\{h_1\} = 0. \tag{D5}$$

From the dependencies found in the Schwarz formulation of this problem, we infer that the value of the stream function at $2N+1$ points on the second vortex is not independent. Assuming the independence of the stream function on the boundary of the first vortex, the stream function on the second vortex boundary satisfies the following three relations:

$$\int_0^{2\pi} \psi \, \sin\theta \, d\theta = 0, \tag{D6}$$

$$\int_0^{2\pi} \psi \, \cos\theta \, d\theta = 0, \tag{D7}$$

$$\int_0^{2\pi} \psi \, \sin 2\theta \, d\theta = 0. \tag{D8}$$

These relations are derived in Appendix A. The first two relationships follow from the vanishing of the integral of the cross product of the velocity with the vorticity, i.e., (3.2.22), while the last condition is implied by the vanishing of the integral given in (3.2.24). These orthogonality relationships suggest Fourier decomposition of the stream function; the dependent conditions (D6)–(D8) can then be easily eliminated. We apply the following condition to the stream function on the second vortex: a (sufficiently smooth) function is constant if and only if all but the zeroth coefficient of its Fourier decomposition vanish. We define the Fourier expansion pair

$$\psi_{2,k} = \sum_{n=-N}^{N} \Psi_{2,n} \, e^{in\theta_k}, \tag{D9}$$

$$\Psi_{2,n} = \frac{1}{2N+1} \sum_{k=0}^{2N} \psi_{2,k} \, e^{-in\theta_k}. \tag{D10}$$

The truncated approximations to the trigonometric integrals are given by

$$\int_0^{2\pi} \psi \, \cos n\theta \, d\theta \;\propto\; \Re\left\{\Psi_{2,n} + \Psi_{2,-n}\right\}, \tag{D11}$$

$$\int_0^{2\pi} \psi \, \sin n\theta \, d\theta \;\propto\; \Im\left\{\Psi_{2,n} - \Psi_{2,-n}\right\}. \tag{D12}$$

We require the stream function to be constant on the second vortex by imposing the following $2N-3$ equations:

$$\Re\{\Psi_{2,n}+\Psi_{2,-n}\}=0, \qquad n=2,\ldots,N, \tag{D13}$$

$$\Im\{\Psi_{2,n}-\Psi_{2,-n}\}=0, \qquad n=3,\ldots,N. \tag{D14}$$

The equations eliminated for $n=1,2$ correspond to the dependent conditions (D6)-(D8). Furthermore, the value of the stream function on the second vortex is proportional to (D11) evaluated for $n=0$; this value is not an independent quantity if the value of the stream function on the first vortex is fixed.

We thereby obtain a system of $4N+4$ real equations for the $4N+4$ unknowns that describe the corotating vortex pair. This system is found to be nonsingular and is solved using Newton iteration.

For the stability problem, we begin with the unsteady boundary condition (1.3.1) that the vortex boundary move with the fluid. The condition that the normal velocity of the vortex, which equals the tangential derivative of the stream function, equal the normal velocity of the fluid at the vortex boundary is given by

$$\frac{\partial\psi}{\partial s}=\frac{\partial x}{\partial t}\frac{\partial y}{\partial s}-\frac{\partial y}{\partial t}\frac{\partial x}{\partial s}. \tag{D15}$$

With $\partial/\partial s=(\partial\theta/\partial s)\ \partial/\partial\theta$, this condition becomes the governing equation

$$\frac{\partial\psi}{\partial\theta}=\frac{\partial x}{\partial t}\frac{\partial y}{\partial\theta}-\frac{\partial y}{\partial t}\frac{\partial x}{\partial\theta}. \tag{D16}$$

For the unsteady configuration we write

$$x=X+x', \quad y=Y+y', \quad \psi=\Psi+\psi', \tag{D17}$$

where primed quantities are perturbation values. Substituting these relations into the exact boundary condition yields, to leading order,

$$\frac{\partial\Psi}{\partial\theta}=0; \tag{D18}$$

i.e., the stream function is constant on the steady vortex boundaries, which is the governing equation for the steady shape problem. To first order in the primed quantities we obtain

$$\frac{\partial \psi'}{\partial \theta} = \frac{\partial x'}{\partial t}\frac{\partial Y}{\partial \theta} - \frac{\partial y'}{\partial t}\frac{\partial X}{\partial \theta}. \tag{D19}$$

We assume exponential time dependence for all primed quantities,

$$\psi' = \psi'(\theta)e^{\sigma t}, \quad x' = x'(\theta)e^{\sigma t}, \quad y' = y'(\theta)e^{\sigma t}, \tag{D20}$$

and substitute these into (3.2.19) to obtain the linear stability equation to be satisfied on each vortex:

$$\frac{\partial \psi'}{\partial \theta} = \sigma \left\{ x' \frac{\partial Y}{\partial \theta} - y' \frac{\partial X}{\partial \theta} \right\}. \tag{D21}$$

From this equality, we see that if σ is an eigenvalue, then σ^* is an eigenvalue (since this is a real equation), $-\sigma$ is an eigenvalue (since the equation is invariant under the transformation $(t, \theta) \rightarrow (-t, -\theta)$), and $-\sigma^*$ is an eigenvalue (since the transformed equation is also real).

For a perturbation to each of the N shape coefficients of each vortex, we evaluate this equation at the $2N + 1$ collocation points on each boundary. Thus, at each point we obtain a relationship between the following $4N + 2$ unknown real shape perturbations:

$$\begin{aligned} &a'_0, \Re\{a'_1\}, \Im\{a'_1\}, \ldots, \Re\{a'_N\}, \Im\{a'_N\}, \\ &b'_0, \Re\{b'_1\}, \Im\{b'_1\}, \ldots, \Re\{b'_N\}, \Im\{b'_N\}. \end{aligned} \tag{D22}$$

We now describe the evaluation procedure for the perturbation to the lth shape coefficient on the first vortex; the method is similar for the second vortex. The perturbed stream function on the left side of (D21) is approximated by

$$\psi_1'^{(l)} = \frac{1}{2\varepsilon}\left[\psi_1(a_l + \varepsilon) - \psi_1(a_l - \varepsilon)\right] = \frac{\partial \psi_1}{\partial a_l} + O(\varepsilon^2), \tag{D23}$$

where the evaluation of ψ_1 is given by (D1). The θ-derivative of this quantity is evaluated via Fourier methods. In analogy with (D9), we have the Fourier expansion

$$\psi_{1,k}^{\prime(l)} = \sum_{n=-N}^{N} \Psi_{1,n}^{\prime(l)} \, e^{in\theta_k}, \tag{D24}$$

where the Fourier coefficients are evaluated as

$$\Psi_{1,n}^{\prime(l)} = \frac{1}{2N+1} \sum_{k=0}^{2N} \psi_{1,k}^{\prime(l)} \, e^{-in\theta_k}. \tag{D25}$$

From (D24) we differentiate ψ_1' with respect to θ and evaluate this at the kth collocation point as

$$\frac{\partial}{\partial\theta} \psi_{1,k}^{\prime(l)} = \sum_{n=-N}^{N} in \, \Psi_{1,n}^{\prime(l)} \, e^{in\theta_k}. \tag{D26}$$

The evaluation of the right side of equation (D21) is a bit more involved. The derivative of the boundary position is given by (1.3.12) as

$$\frac{\partial Z}{\partial\theta} = ia_0 \left(\zeta - (1-1)a_1 - (2-1)\frac{a_2}{\zeta} - \cdots - (N-1)\frac{a_N}{\zeta^{N-1}} \right). \tag{D27}$$

From this relation we obtain the tangent to the vortex boundary at the kth collocation point as

$$\left(\frac{\partial X}{\partial\theta}\right)\Big|_k = \Re\left\{ \frac{dZ}{d\theta}\Big|_{\theta=\theta_k} \right\}, \qquad \left(\frac{\partial Y}{\partial\theta}\right)\Big|_k = \Im\left\{ \frac{dZ}{d\theta}\Big|_{\theta=\theta_k} \right\}. \tag{D28}$$

Also, from the expansion for the perturbed shape given by (1.3.10), the real and imaginary parts of the induced perturbation to the vortex boundary at the kth collocation point are given by

$$x_{1,k}^{\prime(l)} = \begin{cases} a_0' \, (X_k/a_0), & l = 0, \\ a_0 \left[\Re\{a_l'\} \, \Re\{e^{i(1-n)\theta_k}\} - \Im\{a_l'\} \, \Im\{e^{i(1-n)\theta_k}\} \right], & l = 1, \ldots, N, \end{cases} \tag{D29}$$

$$y_{1,k}^{\prime(l)} = \begin{cases} a_0' \, (Y_k/a_0), & l = 0, \\ a_0 \left[\Re\{a_l'\} \, \Im\{e^{i(1-n)\theta_k}\} - \Im\{a_l'\} \, \Re\{e^{i(1-n)\theta_k}\} \right], & l = 1, \ldots, N. \end{cases} \tag{D30}$$

Using these expressions, the right side of the stability equation is evaluated at each of the collocation points for perturbations to each of the shape coefficients given in (D22).

Collecting the coefficients of each of these eigenmode elements, we obtain $4N + 2$ equations corresponding to each of the $2N + 1$ collocation points on each vortex. Thus, equation (D21) is solved as the system

$$\mathbf{A}\,\mathbf{w} = \sigma\,\mathbf{B}\,\mathbf{w}, \tag{D31}$$

where $\mathbf{w}$ is the array with $4N + 2$ elements given in (D22). We left-multiply this equation by the inverse of the nonsingular matrix $\mathbf{B}$ and solve the resulting standard eigenvalue problem with EISPACK routines.

The stream function formulation presented here can be generalized to all vortex configurations we are considering; however, due to the sensitivity of the corotating vortex pair calculations, it was applied to that system only. It was found to reproduce the Schwarz function shape and stability results for α up to approximately 0.25. Beyond that point, the code exhibited difficulties in obtaining convergence, requiring extremely accurate initial guesses. Due to finite computing resources, this method was not employed in the parameter region of most interest for the corotating pair. It remains, however, a valid formulation in obtaining solutions of problems of uniform vorticity.

Appendix E

Sum Formulae for Infinite Vortex Arrays

In this appendix we derive expressions for the infinite sums used in the expansion of the velocity field for infinite arrays of vortices. We consider the sum

$$\sum_{m=-\infty}^{\infty} \frac{e^{im\lambda}}{(m+s)^n} \tag{E1}$$

for general complex s, real $\lambda \in [0, 2\pi]$, and positive integers n.

First, consider the case $s = 0$. We set $\lambda = \pi t$ and write

$$F_n(t) \equiv \sum_{m=-\infty}^{\infty}{}' \frac{e^{im\pi t}}{m^n}, \tag{E2}$$

where the prime denotes exclusion of the $m = 0$ addend. When $n = 1$, it can be shown by Fourier series expansion that

$$F_1(t) = \begin{cases} -i\pi(t-1), & 0 < t < 2, \\ 0, & t = 0 \text{ or } t = 2, \end{cases} \tag{E3}$$

with period 2 in t. Repeated integration of expression (E2) with respect to t yields the relation

$$F_n(t) = i\pi \int_0^t F_{n-1}(\tau)\, d\tau \; + F_n(0), \qquad n = 2, 3, \ldots, \tag{E4}$$

so from (E3) we obtain the polynomial representation

$$F_n(t) = -(i\pi)^n \sum_{j=0}^{n} \frac{D_{n-j}\, t^j}{j!}. \tag{E5}$$

The constants of integration D_k are chosen so that F_n assumes the correct value at $t = 0$, as follows. From the definition (E2),

$$F_n(0) = \sum_{m=-\infty}^{\infty}{}' \frac{1}{m^n}, \tag{E6}$$

which implies that

$$F_n(0) = -(i\pi)^n D_n = \begin{cases} 0, & \text{if } n \text{ is odd, and} \\ 2\zeta(n), & \text{if } n \text{ is even.} \end{cases} \tag{E7}$$

Using the relationship between the Riemann zeta function and the Bernoulli numbers (Gradshteyn & Ryzhik [1965]), we have that

$$D_k = \frac{2^k}{k!} B_k, \qquad k \in \mathbb{Z}^+, \tag{E8}$$

where B_k denotes the kth Bernoulli number. From the following recurrence relation for Bernoulli numbers (Erdélyi *et al.* [1953]),

$$\sum_{j=0}^{k} \binom{k+1}{j} B_j = 0, \tag{E9}$$

we obtain the following recursive formula for the constants of integration:

$$\begin{aligned} D_0 &= 1, \\ D_k &= -\sum_{j=1}^{k} \frac{2^j}{(j+1)!} D_{k-j}, \qquad k \in \mathbb{Z}^+. \end{aligned} \tag{E10}$$

For nonzero s, let $\lambda = 2\pi p$ and define

$$F_n(p; s) \equiv \sum_{m=-\infty}^{\infty} \frac{e^{2\pi i m p}}{(m+s)^n} \,. \tag{E11}$$

It can be shown directly that

$$F_1(p; s) = \begin{cases} 2\pi i \, \dfrac{e^{2\pi i s(1-p)}}{e^{2\pi i s} - 1}, & 0 < p < 1, \\ \pi \cot \pi s, & p = 0 \ \text{ or } \ p = 1, \end{cases} \tag{E12}$$

where the nonendpoint result is obtained by Fourier series decomposition and the equality for $p = 0$ or $p = 1$ is shown by summation of the residues of F_1. Repeated differentiation of this quantity with respect to s yields the following relation for positive integers n :

$$\begin{aligned} F_n(p; s) &= \frac{1}{(-1)^n (n-1)!} \left(\frac{d}{ds}\right)^{n-1} F_1(p; s) \\ &= \frac{2\pi i}{(-1)^n (n-1)!} \sum_{k=0}^{n-1} \binom{n-1}{k} \left(\frac{d}{ds}\right)^k \left[e^{2\pi i s(1-p)}\right] \left(\frac{d}{ds}\right)^{n-1-k} \left[(e^{2\pi i s} - 1)^{-1}\right]. \end{aligned} \tag{E13}$$

The first differentiated quantity in this expression can be evaluated directly as

$$\left(\frac{d}{ds}\right)^k \left[e^{2\pi i s(1-p)}\right] = (2\pi i)^k (1-p)^k \, e^{2\pi i s(1-p)}. \tag{E14}$$

The second differentiated quantity in (E13) can be written

$$\left(\frac{d}{ds}\right)^k \left[(e^{2\pi i s} - 1)^{-1}\right] = (2\pi i)^k \, f_k(s), \tag{E15}$$

where the function $f_k(s)$ can be shown by induction to obey the recursion relation

$$\begin{aligned} f_0(s) &= \frac{1}{e^{2\pi i s} - 1}, \\ f_k(s) &= -\frac{1}{1 - e^{-2\pi i s}} \sum_{j=1}^{k} \binom{k}{j} f_{k-j}(s), \qquad k \in \mathbb{Z}^+. \end{aligned} \tag{E16}$$

The function $F_n(p; s)$ is discontinuous at the endpoints only for $n = 1$.

Both of these summations were numerically implemented by MSS.

Appendix F

Elliptically Desingularized Double Infinite Array

In analogy with the study of the single array of elliptically desingularized vortices described in §4.3, in this appendix we consider this model for the double array. Specifically, we seek to analytically obtain information about the stability of the street of small vortices of unequal areas; however, the analysis presented herein is incomplete.

As in Chapter 5, we assume that the top row vortices have area A_1 and circulation $\Gamma_1 = \Gamma$, and the bottom row vortices have area A_2 and circulation $\Gamma_2 = -\Gamma$. We denote the position of the centroid of the kth first row elliptical vortex by (x_{k1}, y_{k1}), the ratio of its semimajor to semiminor axes by $\lambda_{k1} = a_{k1}/b_{k1}$, and the angle of orientation of its major axis with respect to the x-axis by ϕ_{k1}. We introduce the quantities δ_{k1}, γ_{k1}, and U_{k1}, defined as

$$\delta_{k1} \equiv \left(\frac{A_1}{8\pi\lambda_{k1}}\right)^{1/2} (\lambda_{k1} - 1)\cos 2\phi_{k1}, \tag{F1}$$

$$\gamma_{k1} \equiv \left(\frac{A_1}{8\pi\lambda_{k1}}\right)^{1/2} (\lambda_{k1} - 1)\sin 2\phi_{k1}, \tag{F2}$$

$$U_{k1} \equiv \left(\delta_{k1}^2 + \gamma_{k1}^2 + \frac{A_1}{2\pi}\right)^{1/2}. \tag{F3}$$

Analogous quantities for the second row vortices are indicated with subscript 2.

For infinite collections of uniform elliptically desingularized vortices, the equations describing the interaction of each pair of vortices are equivalent to those in the case of finitely many vortices. Thus, we infer that the kinetic energy for this system is given by expression (4.3.4), summing instead over all vortices in both

rows; i.e.,

$$
\begin{aligned}
H = \frac{\Gamma_1^2}{8\pi} \sum_{k=-\infty}^{\infty} \Bigg\{ & \log\left[1 + \frac{2\pi}{A_1}\left(\delta_{k1}^2 + \gamma_{k1}^2\right)\right] - \frac{1}{2} + \sum_{j=-\infty}^{\infty}{}' \log\left(R_{kj}^{11}\right)^2 \\
& - 2 \sum_{j=-\infty}^{\infty}{}' \left[\frac{\cos 2\theta_{kj}^{11}}{\left(R_{kj}^{11}\right)^2}(\delta_{j1}U_{j1} + \delta_{k1}U_{k1}) + \frac{\sin 2\theta_{kj}^{11}}{\left(R_{kj}^{11}\right)^2}(\gamma_{j1}U_{j1} + \gamma_{k1}U_{k1}) \right] \Bigg\} \\
& + \frac{\Gamma_2^2}{8\pi} \sum_{k=-\infty}^{\infty} \Bigg\{ \log\left[1 + \frac{2\pi}{A_2}\left(\delta_{k2}^2 + \gamma_{k2}^2\right)\right] - \frac{1}{2} + \sum_{j=-\infty}^{\infty}{}' \log\left(R_{kj}^{22}\right)^2 \\
& - 2 \sum_{j=-\infty}^{\infty}{}' \left[\frac{\cos 2\theta_{kj}^{22}}{\left(R_{kj}^{22}\right)^2}(\delta_{j2}U_{j2} + \delta_{k2}U_{k2}) + \frac{\sin 2\theta_{kj}^{22}}{\left(R_{kj}^{22}\right)^2}(\gamma_{j2}U_{j2} + \gamma_{k2}U_{k2}) \right] \Bigg\} \\
& + \frac{\Gamma_1\Gamma_2}{4\pi} \sum_{k=-\infty}^{\infty} \sum_{j=-\infty}^{\infty} \log\left(R_{kj}^{12}\right)^2 \\
& - \frac{\Gamma_1\Gamma_2}{2\pi} \sum_{k=-\infty}^{\infty} \sum_{j=-\infty}^{\infty} \left[\frac{\cos 2\theta_{kj}^{12}}{\left(R_{kj}^{12}\right)^2}(\delta_{j2}U_{j2} + \delta_{k1}U_{k1}) + \frac{\sin 2\theta_{kj}^{12}}{\left(R_{kj}^{12}\right)^2}(\gamma_{j2}U_{j2} + \gamma_{k1}U_{k1}) \right].
\end{aligned}
\tag{F4}
$$

In the above equality, R_{kj}^{nm} denotes the distance and θ_{kj}^{nm} the angle, relative to the x-axis, between the centers of the kth vortex in the nth row and jth vortex in the mth row.

As in the analysis of §5.2, we consider the vortices uniformly spaced a distance l apart along the x-axis, the rows separated by a distance h, and the centers of the second row vortices horizontally offset a distance $l/2$ from the centers of the first row vortices. Since we seek solutions in which all vortices in a given row are equivalent, we restrict our analysis to the zeroth vortex of each row and use the notation

$$
\begin{gathered}
x_n \equiv x_{0n}, \quad y_n \equiv y_{0n}, \quad n = 1, 2 \qquad \text{and} \\
\delta_n \equiv \delta_{kn}, \quad \gamma_n \equiv \gamma_{kn}, \quad U_n \equiv U_{kn}, \quad n = 1, 2, \; k = \ldots, -1, 0, 1, \ldots .
\end{gathered}
\tag{F5}
$$

We evaluate the derivatives of the Hamiltonian at the assumed x and y centroid

positions to obtain the following equations of motion:

$$\frac{dx_1}{dt} = -\frac{\Gamma_2}{\pi l}\left\{\sum_{j=-\infty}^{\infty}\frac{2\kappa}{(2j+1)^2+(2\kappa)^2} + 16\kappa\,\frac{\delta_1 U_1+\delta_2 U_2}{l^2}\sum_{j=-\infty}^{\infty}\frac{3(2j+1)^2-(2\kappa)^2}{[(2j+1)^2+(2\kappa)^2]^3}\right\}, \tag{F6}$$

$$\frac{dy_1}{dt} = \frac{\Gamma_2}{\pi l}\left\{16\kappa\,\frac{\gamma_1 U_1+\gamma_2 U_2}{l^2}\sum_{j=-\infty}^{\infty}\frac{3(2j+1)^2-(2\kappa)^2}{[(2j+1)^2+(2\kappa)^2]^3}\right\}, \tag{F7}$$

$$\frac{d\delta_1}{dt} = -\frac{\Gamma_2}{\pi l}\left\{\frac{1}{4}\frac{\Gamma_1}{\Gamma_2}\frac{l\gamma_1}{U_1^2} - \frac{\delta_1\gamma_1}{U_1 l}\left[\frac{\pi^2}{6}\frac{\Gamma_1}{\Gamma_2}+A(\kappa)\right]\right\}, \tag{F8}$$

$$\frac{d\gamma_1}{dt} = \frac{\Gamma_2}{\pi l}\left\{\frac{1}{4}\frac{\Gamma_1}{\Gamma_2}\frac{l\delta_1}{U_1^2} - \frac{\delta_1^2+U_1^2}{U_1 l}\left[\frac{\pi^2}{6}\frac{\Gamma_1}{\Gamma_2}+A(\kappa)\right]\right\}, \tag{F9}$$

where

$$A(\kappa) \equiv 2\sum_{j=-\infty}^{\infty}\frac{(2j+1)^2-(2\kappa)^2}{[(2j+1)^2+(2\kappa)^2]^2} = \frac{\pi^2}{2}\left(1-\tanh^2\pi\kappa\right). \tag{F10}$$

Similar equations are found for the variables of the second row vortices.

The equation for the velocity in the x-direction can be simplified to obtain the uniform translation velocity

$$V = \frac{\Gamma}{2l}\tanh\pi\kappa\left(1+2\pi^2\,\frac{\delta_1 U_1+\delta_2 U_2}{l^2}\,\mathrm{sech}^2\,\pi\kappa\right). \tag{F11}$$

As the area of the vortices tends to zero, this velocity approaches the translational velocity of the Kármán point vortex street. Since the street should have no steady velocity component in the y-direction, the time derivatives of y_1 and y_2 should vanish, so from (F7) we expect to find that $\gamma_1 = 0$ and $\gamma_2 = 0$.

Keeping this fact in mind, we now consider the steady-state conditions for δ_n and γ_n. The steady-state equations for these quantities are valid for either row. Expressing these variables in terms of the aspect ratio λ_n, angle of orientation ϕ_n, and rescaled nondimensionalized area $\beta_n \equiv \alpha_n/(2\pi) = A_n/(2\pi l^2)$, for the nth row we obtain the coupled system of equations:

$$\frac{\lambda_n-1}{\lambda_n+1}\sin 2\phi_n\left[1+\frac{\beta_n B(\kappa)}{4}\,\frac{\lambda_n^2-1}{\lambda_n}\cos 2\phi_n\right] = 0, \tag{F12}$$

$$\frac{\lambda_n-1}{\lambda_n+1}\cos 2\phi_n + \frac{\beta_n B(\kappa)}{4}\,\frac{(\lambda_n+1)^2}{\lambda_n}\left[1+\left(\frac{\lambda_n-1}{\lambda_n+1}\right)^2\cos^2 2\phi_n\right] = 0, \tag{F13}$$

where

$$B(\kappa) \equiv 4A(\kappa) - \frac{2\pi^2}{3} = \frac{2\pi^2}{3}\left(2 - 3\tanh^2 \pi\kappa\right). \tag{F14}$$

The valid solution to these equations is found by setting $\sin 2\phi_n = 0$; i.e., $\phi_n = 0$ or $\phi_n = \pi/2$. From (F13) we obtain the following cubic equation for the aspect ratio:

$$\lambda_n^3 + \left(1 \pm \frac{2}{\beta_n B(\kappa)}\right)\lambda_n^2 + \left(1 \mp \frac{2}{\beta_n B(\kappa)}\right)\lambda_n + 1 = 0, \tag{F15}$$

where the $\{+,-\}$ combination corresponds to $\phi_n = 0$, and $\{-,+\}$ to $\phi_n = \pi/2$. As the distance between the rows tends to infinity, this equation reduces to that for the single row aspect ratio given in (4.3.15). Note that if λ_n is a solution for one choice of these angles, then $1/\lambda_n$ is a solution for the the equation corresponding to the other angle. We find a root of the equation for $\phi_n = 0$ (so that $\gamma_n = 0$) which, as expected, is near 1 for small α_n and which increases as α_n does.

To study the linear stability of the double array, we perturb each of the canonical variables and linearize both the Hamiltonian and the equations of motion. With the notation

$$dx_{kj}^{nm} \equiv x_{kn} - x_{jm}, \quad dy_{kj}^{nm} \equiv y_{kn} - y_{jm}, \tag{F16}$$

we find that the first-order Hamiltonian is given by

$$H' = \frac{\Gamma_1^2}{4\pi}\sum_{k=-\infty}^{\infty}\left\{\frac{\delta'_{k1}\delta_{k1} + \gamma'_{k1}\gamma_{k1}}{U_{k1}^2} + {\sum_{j=-\infty}^{\infty}}' \frac{dx'^{11}_{kj}dx^{11}_{kj} + dy'^{11}_{kj}dy^{11}_{kj}}{\left(R^{11}_{kj}\right)^2}\right.$$

$$-2{\sum_{j=-\infty}^{\infty}}' \frac{dx^{11}_{kj}\left[3(dy^{11}_{kj})^2 - (dx^{11}_{kj})^2\right]}{\left(R^{11}_{kj}\right)^6}\left[dx'^{11}_{kj}(\delta_{j1}U_{j1} + \delta_{k1}U_{k1}) - dy'^{11}_{kj}(\gamma_{j1}U_{j1} + \gamma_{k1}U_{k1})\right]$$

$$-2{\sum_{j=-\infty}^{\infty}}' \frac{dy^{11}_{kj}\left[(dy^{11}_{kj})^2 - 3(dx^{11}_{kj})^2\right]}{\left(R^{11}_{kj}\right)^6}\left[dy'^{11}_{kj}(\delta_{j1}U_{j1} + \delta_{k1}U_{k1}) - dx'^{11}_{kj}(\gamma_{j1}U_{j1} + \gamma_{k1}U_{k1})\right]$$

$$\left.-2{\sum_{j=-\infty}^{\infty}}' \frac{\cos 2\theta^{11}_{kj}}{\left(R^{11}_{kj}\right)^2}\left[\frac{\delta_{j1}(\delta'_{j1}\delta_{j1} + \gamma'_{j1}\gamma_{j1})}{U_{j1}} + \frac{\delta_{k1}(\delta'_{k1}\delta_{k1} + \gamma'_{k1}\gamma_{k1})}{U_{k1}} + \delta'_{j1}U_{j1} + \delta'_{k1}U_{k1}\right]\right.$$

$$-2\sum_{j=-\infty}^{\infty}{}'\frac{\sin 2\theta_{kj}^{11}}{\left(R_{kj}^{11}\right)^2}\left[\frac{\gamma_{j1}(\delta'_{j1}\delta_{j1}+\gamma'_{j1}\gamma_{j1})}{U_{j1}}+\frac{\gamma_{k1}(\delta'_{k1}\delta_{k1}+\gamma'_{k1}\gamma_{k1})}{U_{k1}}+\gamma'_{j1}U_{j1}+\gamma'_{k1}U_{k1}\right]\Bigg\}$$

$$+\frac{\Gamma_2^2}{4\pi}\sum_{k=-\infty}^{\infty}\Bigg\{\frac{\delta'_{k2}\delta_{k2}+\gamma'_{k2}\gamma_{k2}}{U_{k2}^2}+\sum_{j=-\infty}^{\infty}{}'\frac{dx'^{22}_{kj}dx^{22}_{kj}+dy'^{22}_{kj}dy^{22}_{kj}}{\left(R_{kj}^{22}\right)^2}$$

$$-2\sum_{j=-\infty}^{\infty}{}'\frac{dx_{kj}^{22}\left[3(dy_{kj}^{22})^2-(dx_{kj}^{22})^2\right]}{\left(R_{kj}^{22}\right)^6}\left[dx'^{22}_{kj}(\delta_{j2}U_{j2}+\delta_{k2}U_{k2})-dy'^{22}_{kj}(\gamma_{j2}U_{j2}+\gamma_{k2}U_{k2})\right]$$

$$-2\sum_{j=-\infty}^{\infty}{}'\frac{dy_{kj}^{22}\left[(dy_{kj}^{22})^2-3(dx_{kj}^{22})^2\right]}{\left(R_{kj}^{22}\right)^6}\left[dy'^{22}_{kj}(\delta_{j2}U_{j2}+\delta_{k2}U_{k2})-dx'^{22}_{kj}(\gamma_{j2}U_{j2}+\gamma_{k2}U_{k2})\right]$$

$$-2\sum_{j=-\infty}^{\infty}{}'\frac{\cos 2\theta_{kj}^{22}}{\left(R_{kj}^{22}\right)^2}\left[\frac{\delta_{j2}(\delta'_{j2}\delta_{j2}+\gamma'_{j2}\gamma_{j2})}{U_{j2}}+\frac{\delta_{k2}(\delta'_{k2}\delta_{k2}+\gamma'_{k2}\gamma_{k2})}{U_{k2}}+\delta'_{j2}U_{j2}+\delta'_{k2}U_{k2}\right]$$

$$-2\sum_{j=-\infty}^{\infty}{}'\frac{\sin 2\theta_{kj}^{22}}{\left(R_{kj}^{22}\right)^2}\left[\frac{\gamma_{j2}(\delta'_{j2}\delta_{j2}+\gamma'_{j2}\gamma_{j2})}{U_{j2}}+\frac{\gamma_{k2}(\delta'_{k2}\delta_{k2}+\gamma'_{k2}\gamma_{k2})}{U_{k2}}+\gamma'_{j2}U_{j2}+\gamma'_{k2}U_{k2}\right]\Bigg\}$$

$$+\frac{\Gamma_1\Gamma_2}{2\pi}\sum_{k=-\infty}^{\infty}\Bigg\{\sum_{j=-\infty}^{\infty}\frac{dx'^{12}_{kj}dx^{12}_{kj}+dy'^{12}_{kj}dy^{12}_{kj}}{\left(R_{kj}^{12}\right)^2}$$

$$-2\sum_{j=-\infty}^{\infty}\frac{dx_{kj}^{12}\left[3(dy_{kj}^{12})^2-(dx_{kj}^{12})^2\right]}{\left(R_{kj}^{12}\right)^6}\left[dx'^{12}_{kj}(\delta_{j2}U_{j2}+\delta_{k1}U_{k1})-dy'^{12}_{kj}(\gamma_{j2}U_{j2}+\gamma_{k1}U_{k1})\right]$$

$$-2\sum_{j=-\infty}^{\infty}\frac{dy_{kj}^{12}\left[(dy_{kj}^{12})^2-3(dx_{kj}^{12})^2\right]}{\left(R_{kj}^{12}\right)^6}\left[\Delta y'^{12}_{kj}(\delta_{j2}U_{j2}+\delta_{k1}U_{k1})-\Delta x'^{12}_{kj}(\gamma_{j2}U_{j2}+\gamma_{k1}U_{k1})\right]$$

$$-2\sum_{j=-\infty}^{\infty}\frac{\cos 2\theta_{kj}^{12}}{\left(R_{kj}^{12}\right)^2}\left[\frac{\delta_{j2}(\delta'_{j2}\delta_{j2}+\gamma'_{j2}\gamma_{j2})}{U_{j2}}+\frac{\delta_{k1}(\delta'_{k1}\delta_{k1}+\gamma'_{k1}\gamma_{k1})}{U_{k1}}+\delta'_{j2}U_{j2}+\delta'_{k1}U_{k1}\right]$$

$$-2\sum_{j=-\infty}^{\infty}\frac{\sin 2\theta_{kj}^{12}}{\left(R_{kj}^{12}\right)^2}\left[\frac{\gamma_{j2}(\delta'_{j2}\delta_{j2}+\gamma'_{j2}\gamma_{j2})}{U_{j2}}+\frac{\gamma_{k1}(\delta'_{k1}\delta_{k1}+\gamma'_{k1}\gamma_{k1})}{U_{k1}}+\gamma'_{j2}U_{j2}+\gamma'_{k1}U_{k1}\right]\Bigg\}. \tag{F17}$$

Linearization of the governing Equations (F6)–(F9) yields the Hamiltonian system

for first-order stability:

$$\Gamma_n \dot{x}'_{kn} = -\frac{\partial H'}{\partial y_{kn}}, \qquad \Gamma_n \dot{\delta}'_{kn} = -\frac{\partial H'}{\partial \gamma_{kn}}, \tag{F18}$$

$$\Gamma_n \dot{y}'_{kn} = \frac{\partial H'}{\partial x_{kn}}, \qquad \Gamma_n \dot{\gamma}'_{kn} = \frac{\partial H'}{\partial \delta_{kn}}. \tag{F19}$$

To study the linear stability of the street of vortices of small unequal area, we write the nondimensional area of the vortices in the nth row as

$$\alpha_n = (1 + q_n)\,\pi\varepsilon^2, \quad n = 1, 2, \tag{F20}$$

where $0 < \varepsilon \ll 1$ and $q_1 = -q_2 = q \in (-1, 1)$, a constant. Using these assumptions, we expand the aspect ratio of the nth row, given by the solution of (F15), as

$$\begin{aligned}\lambda_n = 1 &+ \frac{2}{3}\left(3\tanh^2 \pi\kappa - 2\right)(1 + q_n)\pi^2\varepsilon^2 \\ &+ \frac{2}{9}\left(3\tanh^2 \pi\kappa - 2\right)^2 (1 + q_n)^2 \pi^4 \varepsilon^4 + O(\varepsilon^6),\end{aligned} \tag{F21}$$

with which we expand δ_{kn} and U_{kn} as

$$\frac{\delta^{\pm}_{kn}}{l} = -\frac{\sqrt{2}}{6}(3\tanh^2 \pi\kappa - 2)(1 + q_n^2)^{3/2}\varepsilon^3 + O(\varepsilon^5), \quad \text{and} \tag{F22}$$

$$\frac{U_{kn}}{l} = \frac{1}{\sqrt{2}}(1 + q_n)^{1/2}\varepsilon + O(\varepsilon^5). \tag{F23}$$

Thus, the translation velocity of the street (F11) is given by

$$V = \frac{\Gamma}{2l}\tanh \pi\kappa \left[1 - \pi^2\left(\alpha_1^2 + \alpha_2^2\right)\left(\operatorname{sech}^2 \pi\kappa - \tfrac{1}{3}\right)\operatorname{sech}^2 \pi\kappa\right] + O(\alpha_1^3, \alpha_2^3), \tag{F24}$$

which agrees with the results of Kida [1982] and Jiménez [1986b] to $O(\alpha^2)$, i.e., to $O(\varepsilon^4)$.

Since the variables δ_{kn} and γ_{kn} are of order ε^3 relative to x_{kn} and y_{kn}, we use the following normal mode expansions of the perturbed quantities:

$$x'_{k1} = e^{i2k\pi p}\tilde{x}_1, \qquad x'_{j2} = e^{i(2j+1)\pi p}\tilde{x}_2, \tag{F25}$$

$$y'_{k1} = e^{i2k\pi p}\tilde{y}_1, \qquad y'_{j2} = e^{i(2j+1)\pi p}\tilde{y}_2, \tag{F26}$$

$$\delta'_{k1} = \varepsilon^3 e^{i2k\pi p}\tilde{\delta}_1, \qquad \delta'_{j2} = \varepsilon^3 e^{i(2j+1)\pi p}\tilde{\delta}_2, \tag{F27}$$

$$\gamma'_{k1} = \varepsilon^3 e^{i2k\pi p}\tilde{\gamma}_1, \qquad \gamma'_{j2} = \varepsilon^3 e^{i(2j+1)\pi p}\tilde{\gamma}_2. \tag{F28}$$

The equations governing the linear stability of the elliptical steady states can be written in the form

$$\frac{d\mathbf{v}}{dt} = \frac{\Gamma}{2\pi l^2}\begin{pmatrix}\mathbf{A} & \mathbf{B}\\ \mathbf{C} & \mathbf{D}\end{pmatrix}\mathbf{v}, \tag{F29}$$

where the vector of perturbed quantities $\mathbf{v}$ is given by

$$\mathbf{v} = \begin{bmatrix}\mathbf{x}\\ \mathbf{d}\end{bmatrix}, \quad \text{where} \quad \mathbf{x} = [\,\tilde{x}_1, \tilde{y}_1, \tilde{x}_2, \tilde{y}_2\,]^T \quad \text{and} \quad \mathbf{d} = [\,\tilde{\delta}_1, \tilde{\gamma}_1, \tilde{\delta}_2, \tilde{\gamma}_2\,]^T. \tag{F30}$$

The submatrices are found to have the following structure:

$$\mathbf{A} = \mathbf{A}_0 + \mathbf{A}_2\varepsilon^4 + \cdots, \qquad \mathbf{B} = \mathbf{B}_2\varepsilon^4 + \cdots, \tag{F31}$$

$$\mathbf{C} = \frac{\mathbf{C}_{-1}}{\varepsilon^2} + \mathbf{C}_1\varepsilon^2 + \cdots, \qquad \mathbf{D} = \frac{\mathbf{D}_{-1}}{\varepsilon^2} + \mathbf{D}_1\varepsilon^2 + \cdots. \tag{F32}$$

Attempts to obtain the eigenvalues of this system directly proved unsuccessful, even using symbolic manipulation programs, so we resort to the perturbation method employed by Jiménez [1986b].

Since we are considering the case of small vortices, we restrict our analysis to the neighborhood of the point vortex stability "cross," located at $p = \frac{1}{2}$, $\kappa = \kappa_c \equiv (\sinh^{-1} 1)/\pi$. We take this into account in the perturbation scheme by expanding the matrices in (F31) and (F32) as functions of p and κ about the point $(p, \kappa) = (\frac{1}{2}, \kappa_c)$; as the finite area effects are $O(\varepsilon^4)$ to leading order, in this expansion we assume that $p - \frac{1}{2}$ and $\kappa - \kappa_c$ scale as ε^4. We obtain the expanded matrices

$$\mathbf{A} = \hat{\mathbf{A}}_0 + \hat{\mathbf{A}}_2\varepsilon^4 + \cdots, \qquad \mathbf{B} = \hat{\mathbf{B}}_2\varepsilon^4 + \cdots, \tag{F33}$$

$$\mathbf{C} = \frac{\hat{\mathbf{C}}_{-1}}{\varepsilon^2} + \cdots, \qquad \mathbf{D} = \frac{\hat{\mathbf{D}}_{-1}}{\varepsilon^2} + \cdots, \tag{F34}$$

where

$$\hat{\mathbf{A}}_0 = \mathbf{A}_{0,\times}, \quad \hat{\mathbf{B}}_2 = \mathbf{B}_{2,\times}, \quad \hat{\mathbf{C}}_{-1} = \mathbf{C}_{-1,\times}, \quad \hat{\mathbf{D}}_{-1} = \mathbf{D}_{-1,\times}, \tag{F35}$$

$$\hat{\mathbf{A}}_2 = \mathbf{A}_{2,\times} + \left.\frac{\partial \mathbf{A}_0}{\partial p}\right|_{\times}(p - \frac{1}{2}) + \left.\frac{\partial \mathbf{A}_0}{\partial \kappa}\right|_{\times}(\kappa - \kappa_c), \tag{F36}$$

where the subscript $\times$ denotes evaluation at the location of the point vortex stability cross, $(p, \kappa) = (\frac{1}{2}, \kappa_c)$. We expand the eigenvalues and eigenvectors in the governing equation as follows:

$$\begin{pmatrix} \mathbf{A} & \mathbf{B} \\ \mathbf{C} & \mathbf{D} \end{pmatrix} \begin{bmatrix} \mathbf{x}_0 + \varepsilon^2 \mathbf{x}_1 + \cdots \\ \mathbf{d}_0 + \varepsilon^2 \mathbf{d}_1 + \cdots \end{bmatrix} = \left(\frac{\sigma_{-1}}{\varepsilon^2} + \sigma_0 + \sigma_1 \varepsilon^2 + \cdots \right) \begin{bmatrix} \mathbf{x}_0 + \varepsilon^2 \mathbf{x}_1 + \cdots \\ \mathbf{d}_0 + \varepsilon^2 \mathbf{d}_1 + \cdots \end{bmatrix}. \tag{F37}$$

To $O(1/\varepsilon^2)$, we find the system

$$\sigma_{-1} \mathbf{x}_0 = 0 \quad \text{and} \quad \hat{\mathbf{C}}_{-1} \mathbf{x}_0 + \hat{\mathbf{D}}_{-1} \mathbf{d}_0 = \sigma_{-1} \mathbf{d}_0. \tag{F38}$$

As pointed out by Jiménez, with $\mathbf{x}_0 = \mathbf{0}$ this is the the standard eigenvalue problem for $\hat{\mathbf{D}}_{-1}$, whose eigenvalues correspond to the fast boundary oscillations of the vortex patches.

For the question of the stability of the cooperative modes of the street, we consider the case where $\sigma_{-1} = 0$, i.e., the problems:

$$(\hat{\mathbf{A}}_0 - \sigma_0 \mathbf{I})\, \mathbf{x}_0 = \mathbf{0}, \tag{F39}$$

$$(\hat{\mathbf{A}}_0 - \sigma_0 \mathbf{I})\, \mathbf{x}_1 = \sigma_1 \mathbf{x}_0, \tag{F40}$$

$$(\hat{\mathbf{A}}_0 - \sigma_0 \mathbf{I})\, \mathbf{x}_2 = \sigma_1 \mathbf{x}_1 - (\hat{\mathbf{A}}_2 - \sigma_2 \mathbf{I})\, \mathbf{x}_0 - \hat{\mathbf{B}}_2 \mathbf{d}_0. \tag{F41}$$

Equation (F39) is the point vortex street problem, which can be solved explicitly. The matrix $\hat{\mathbf{A}}_0$ is diagonalizable, so that it has a linearly independent set of left-eigenvectors $\mathbf{y_0}$; left-multiplying (F40) by the adjoint $\mathbf{y}_\mathbf{0}^\dagger$ implies that $\sigma_1 \equiv 0$. Thus, we are led to consider (F41), which can be written

$$-(\hat{\mathbf{A}}_0 - \sigma_0 \mathbf{I})\, \mathbf{x}_2 = (\mathbf{M} - \sigma_2 \mathbf{I})\, \mathbf{x}_0, \tag{F42}$$

where, using (F38), the matrix $\mathbf{M}$ is given by

$$\mathbf{M} = \hat{\mathbf{A}}_2 - \hat{\mathbf{B}}_2 \hat{\mathbf{D}}_{-1}^{-1} \hat{\mathbf{C}}_{-1}. \tag{F43}$$

Since $\hat{\mathbf{A}}_0$ is diagonalizable, we form the matrix $\mathbf{X}$, whose columns are the linearly independent eigenvectors of $\hat{\mathbf{A}}_0$. Defining the vectors $\boldsymbol{\xi}_k = \mathbf{X}^{-1}\,\mathbf{x}_k, k = 0, 2$, such that $\{\boldsymbol{\xi}_0, \sigma_0\}$ are eigensolutions of the diagonal matrix $\boldsymbol{\Sigma}$, Equation (F42) becomes

$$-(\boldsymbol{\Sigma} - \sigma_0 \mathbf{I})\,\boldsymbol{\xi}_2 = (\mathbf{N} - \sigma_2 \mathbf{I})\,\boldsymbol{\xi}_0, \tag{F44}$$

where $\mathbf{N} \equiv \mathbf{X}^{-1}\mathbf{M}\mathbf{X}$, and the matrix $\boldsymbol{\Sigma}$ has the form

$$\boldsymbol{\Sigma} = \frac{i\pi}{2}\begin{pmatrix} -1 & 0 & 0 & 0 \\ 0 & -1 & 0 & 0 \\ 0 & 0 & 1 & 0 \\ 0 & 0 & 0 & 1 \end{pmatrix}. \tag{F45}$$

For the eigenvalue $\sigma_0 = -i\pi/2$, the elements of the matrix $\boldsymbol{\Sigma} - \sigma_0\mathbf{I}$ vanish except for the diagonals of the bottom right 2×2 block. Thus, any vector $\boldsymbol{\xi}_2$ whose last two components are zero is an eigensolution of (F44). Denoting the first two components of this vector by $\mathbf{w}$, the right-hand side of (F44) reduces to the 2×2 eigenvalue problem

$$\begin{pmatrix} N_{11} & N_{12} \\ N_{21} & N_{22} \end{pmatrix} \mathbf{w} = \sigma_2\,\mathbf{w}. \tag{F46}$$

Here, $\mathbf{w}$ is arbitrary, since the eigenvectors corresponding to $\sigma_0 = -i\pi/2$ are $\boldsymbol{\xi}_0^{(1)} = [1, 0, 0, 0]^T$, and $\boldsymbol{\xi}_0^{(2)} = [0, 1, 0, 0]^T$. Thus, we have reduced the problem to that of finding the eigenvectors of (F46). Extensive algebraic manipulations are required to evaluate this matrix and express the condition of linear independence of the eigenvectors. We have been unable, confidently, to evaluate this expression, which nonetheless should provide relationships that determine to leading order the location of the stability cross as a function of the area difference q.

References

1. Aref, H. [1983] Integrable, chaotic, and turbulent vortex motion in two-dimensional flows, *Ann. Rev. Fluid. Mech.* **15**, 345–389.
2. Arnold, V. I. [1978] *Mathematical Methods of Classical Mechanics*, Springer, New York.
3. Baker, G. R., Saffman, P. G. & Sheffield, J. S. [1976] Structure of a linear array of hollow vortices of finite cross-section, *J. Fluid Mech.* **74**, 469–476.
4. Burbea, J. [1982] On patches of uniform vorticity in a plane of irrotational flow, *Arch. Rat. Mech. Anal.* **77**, 349–358.
5. Burbea, J. & Landau, M. [1982] The Kelvin waves in vortex dynamics and their stability, *J. Comput. Phys.* **45**, 127–156.
6. Christiansen, J. P. & Zabusky, N. J. [1973] Instability, coalescence and fission of finite-area vortex structures, *J. Fluid Mech.* **61**, 219–243.
7. Deem, G. S. & Zabusky, N. J. [1978] Vortex waves: stationary "V states," interactions, recurrence, and breaking, *Phys. Rev. Lett.* **40**, 859–862.
8. Dhanak, M. R. [1985] Stability of a regular polygon of finite vortices, preprint.
9. Dongarra, J. J., Bunch, J. R., Moler, C. B. & Stewart, G. W. [1979] *LINPACK Users' Guide*, SIAM, Philadelphia.
10. Domm, U. [1956] Über die Wirbelstraßen von geringster Instabilität, *Z. angew. Math. Mech.* **36**, 367–371.
11. Dritschel, D. G. [1985] The stability and energetics of corotating uniform vortices, *J. Fluid Mech.* **157**, 95–134.
12. Dritschel, D. G. [1986] The nonlinear evolution of rotating configurations of uniform vorticity, preprint.
13. Eckelman, H. [1986] Private communication.

14. Erdélyi, A., Magnus, S., Oberhettinger, F.G. & Tricomi, F. G., eds. [1953] *Higher Transcendental Functions*, McGraw-Hill, New York.

15. Gradshteyn, I. S. & Ryzhik, I. M. [1965] *Table of Integrals, Series, and Products*, Academic Press, New York.

16. Hebert, D. J. [1983] A Hamiltonian-Lagrangian system of vortex boundary curves, *J. Math. Phys.* **24**, 1672–1678.

17. Ho, C.-M. & Huang, L.-S. [1982] Subharmonics and vortex merging in mixing layers, *J. Fluid Mech.* **119**, 443–473.

18. Jiménez, J. [1986a] On the linear stability of the inviscid Kármán vortex street, preprint.

19. Jiménez, J. [1986b] Linear stability of a nonsymmetric Kármán street of small uniform vortices, preprint.

20. Kármán, T. v. [1912] Über den Mechanismus des Widerstandes, den ein bewegter Körper in einer Flüssigkeit erfährt, *Nachr. der K. Gesell. der Wiss. zu Göttingen*, 547–556.

21. Keller, H. B. [1977] Numerical solution of bifurcation and nonlinear eigenvalue problems, in *Applications of Bifurcation Theory* (ed. P. Rabinowitz), Academic Press, New York, pp. 359–384.

22. Kida, S. [1981] Motion of an elliptic vortex in a uniform shear flow, *J. Phys. Soc. Japan* **50**, 3517–3520.

23. Kida, S. [1982] Stabilizing effects of finite core on Kármán vortex streets, *J. Fluid Mech.* **122**, 487–504.

24. Kirchhoff, G. [1877] *Vorlesungen über Mathematische Physik, Vol. IV*, Teubner, Leipzig.

25. Kochin, N. E. [1939] On the instability of Kármán vortex streets, *Dokl. Akad. Nauk SSSR* **24**, 18–22.

26. Lamb, H. [1945] *Hydrodynamics*, Dover, New York.

27. Landau, M. [1981] *The structure and stability of finite area vortex regions of the two-dimensional Euler equations*, Ph. D. thesis, University of Pittsburgh.

28. Leonard, A. [1980] Vortex methods for flow simulation, *J. Comput. Phys.* **37**, 289–335.

29. Love, A. E. H. [1893] On the stability of certain vortex motions, *Proc. Lond. Math. Soc.* **25**, 18–42.

30. MacKay, R. S. [1986] Instability of vortex streets, preprint.

31. Mathlab Group, The [1983] *MACSYMA Reference Manual*, Massachusetts Institute of Technology, Cambridge.

32. Meiron, D. I. , Saffman, P. G. & Schatzman, J. C. [1984] The linear two-dimensional stability of inviscid vortex streets of finite-cored vortices, *J. Fluid Mech.* **147**, 187–212.

33. Melander, M. V. , Styczek, A. S. & Zabusky, N. J. [1984] Elliptically desingularized vortex model for the two-dimensional Euler equations, *Phys. Rev. Lett.* **53**, 1222–1225.

34. Melander, M. V. , Zabusky, N. J. & Styczek, A. S. [1986] A moment model for vortex interactions of the two-dimensional Euler equations. Part1. Computational validation of a Hamiltonian elliptical representation, *J. Fluid Mech.* **167**, 95–115.

35. Moore, D. W. & Saffman, P. G. [1971] Structure of a line vortex in an imposed strain, in *Aircraft Wake Turbulence* (eds. J. Olsen, A. Goldburg, & N. Rogers), Plenum, New York, pp. 339–354.

36. Moore, D. W. & Saffman, P. G. [1975] The density of organized vortices in a turbulent mixing layer, *J. Fluid Mech.* **69**, 465–473.

37. Neu, J. [1984] The dynamics of a columnar vortex in an imposed strain, *Phys.*

Fluids **27**, 2397–2402.

38. Overman, E. A. & Zabusky, N. J. [1982a] Evolution and merger of isolated vortex structures, *Phys. Fluids* **25**,1297–1305.

39. Overman, E. A. & Zabusky, N. J. [1982b] Coaxial scattering of Euler-equation translating V-states via contour dynamics, *J. Fluid Mech.* **125**, 187–202.

40. Overman, E. A. [1986] Steady-state solutions of the Euler equations in two dimensions II. Local analysis of limiting V-states, *SIAM J. Appl. Math.* **46**, 765–800.

41. Pierrehumbert, R. T. [1980] A family of steady translating vortex pairs with distributed vorticity, *J. Fluid Mech.* **99**, 129–144.

42. Pierrehumbert, R. T. & Widnall, S. E. [1981] The structure of organized vortices in a free shear layer, *J. Fluid Mech.* **102**, 301–313.

43. Pierrehumbert, R. T. & Widnall, S. E. [1982] The two- and three-dimensional instabilities of a spatially periodic shear layer, *J. Fluid Mech.* **114**, 59–82.

44. Putterman, S. & Uhlenbeck, G. E. [1969] Thermodynamic equilibrium of rotating superfluids, *Phys. Fluids* **12**, 2229–2236.

45. Rossow, V. J. [1977] Convective merging of vortex cores in lift-generated wakes, *J. Aircraft* **14**, 283–290.

46. Saffman, P. G. [1981] Vortex interactions and coherent structures in turbulence, in *Transition and Turbulence* (ed. R. E. Meyer), Academic Press, New York, pp. 149–166.

47. Saffman, P. G. [1982] Structure and stability of streets of finite vortices, in *Vortex Motion* (eds. H. Hornung & E.-A. Müller), Friedr. Vieweg & Sohn, Braunschweig/Wiesbaden, pp. 142–156.

48. Saffman, P. G. [1984] Vortex Dynamics, Caltech Lecture Course.

49. Saffman, P. G. [1985a] Private communication.

50. Saffman, P. G. [1985b] The superharmonic instability of finite-amplitude water waves, *J. Fluid Mech.* **159**, 169–174.

51. Saffman, P. G. & Baker, G. R. [1979] Vortex interactions, *Ann. Rev. Fluid. Mech.* **11**, 95–122.

52. Saffman, P. G. & Schatzman, J. C. [1981] Properties of a vortex street of finite vortices, *SIAM J. Sci. Stat. Comput.* **2**, 285–295.

53. Saffman, P. G. & Schatzman, J. C. [1982] Stability of a vortex street of finite vortices, *J. Fluid Mech.* **117**, 171–185.

54. Saffman, P. G. & Szeto, R. [1980] Equilibrium shapes of a pair of equal uniform vortices, *Phys. Fluids* **23**, 2339–2342.

55. Saffman, P. G. & Szeto, R. [1981] Structure of a linear array of uniform vortices, *Stud. Appl. Math.* **65**, 223–248.

56. Saffman, P. G. & Tanveer, S. [1982] The touching pair of equal and opposite uniform vortices, *Phys. Fluids* **25**, 1929–1930.

57. Smith, B. T., Boyle, J. M., Dongarra, J. J., Garbow, B. S., Ikebe, Y., Klema, V. C. & Moler, C. B. [1976] *Matrix Eigensystem Routines — EISPACK Guide*, Springer, Berlin.

58. Spreiter, J. R. & Sacks, A. H. [1951] The rolling up of the trailing vortex sheet and its effect on the downwash behind wings, *J. Aero. Sci.* **18**, 21–32.

59. Su, C. H. [1979] Motion of fluid with constant vorticity in a singly-connected fluid, *Phys. Fluids* **22**, 2032–2033.

60. Thomson, W. [1880] Vibrations of a columnar vortex, *Phil. Mag.* **10**, 155–168.

61. Thomson, W. [1887] On the stability of steady and periodic fluid motions, *Phil. Mag.* **23**, 459–464.

62. Widnall, S. E. [1975] The structure and dynamics of vortex filaments, *Ann.*

Rev. Fluid. Mech. **7**, 141–165.

63. Williamson, C. K. [1987] Private communication.

64. Winant, C. D. & Browand, F. K. [1974] Vortex pairing: the mechanism of turbulent mixing layer growth at moderate Reynolds number, *J. Fluid Mech.* **63**, 237–255.

65. Wu, H. M. , Overman, E. A. & Zabusky, N. J. [1984] Steady-state solutions of the Euler equations in two dimensions: rotating and translating V-states with limiting cases, *J. Comput. Phys.* **53**, 42–71.

66. Zabusky, N. J. , Hughes, M. H. & Roberts, K. V. [1979] Contour dynamics for the Euler equations in two dimensions, *J. Comput. Phys.* **30**, 96–106.